Trajectory Exploration and Maneuver Regulation of the Pendubot

by

Robert A. Bailey

B.S., Morehead State University, 1998

B.S., University of Kentucky, 1998

M.S., University of Kentucky, 2001

J.D., University of Denver, 2007

A thesis submitted to the

Faculty of the Graduate School of the

University of Colorado in partial fulfillment

of the requirements for the degree of

Doctor of Philosophy

Department of Electrical, Computer, and Energy Engineering

2012

This thesis entitled:
Trajectory Exploration and Maneuver Regulation of the Pendubot
written by Robert A. Bailey
has been approved for the Department of Electrical, Computer, and Energy Engineering

_____

John Hauser

_____

Youjian (Eugene) Liu

Date _____

The final copy of this thesis has been examined by the signatories, and we find that both the content and the form meet acceptable presentation standards of scholarly work in the above mentioned discipline.

Bailey, Robert A. (Ph.D., Electrical, Computer, and Energy Engineering)

Trajectory Exploration and Maneuver Regulation of the Pendubot

Thesis directed by Prof. John Hauser

The pendulum provides a seemingly inexhaustible source of practical applications and interesting problems which have motivated research in a variety of disciplines. In this thesis, we study equations that described a driven pendulum with odd-periodic driving. The equations also describe the under-actuated, double pendulum system called the pendubot. Techniques for trajectory exploration are developed.

For the inverted pendulum, we first wrote the problem as a two point boundary value problem with Dirichlet boundary conditions. Then, we develop an equivalent linear operator that combines a Nemitski operator (or superposition operator) with the linear operator for the unstable harmonic oscillator. By exploring the properties of the Green's function for the unstable harmonic oscillator with Dirichlet boundary conditions, we developed bounds on various norms that prove useful for determining which parameter values will satisfy invariance and contraction conditions. With a direct application of the Schauder fixed point theorem, we showed that our family of equations representing an inverted pendulum always possessed an odd-periodic solution. Using the Banach fixed point theorem we showed that there is a unique solution within an invariant region of the space of possible solution curves. When there is a unique solution, successive approximations can be used to compute the solution trajectory. To illustrate the power and application of these ideas, we apply them to a pendubot with the inner arm moving at a constant velocity.

For non-inverted trajectories of the pendubot, we presented a necessary condition for trajectories to exist with general periodic forcing. For odd-periodic periodic driving functions this condition is always satisfied. For a driving function of $A\sin(\omega t)$, we found multiple solutions for the outer link. With the trajectories in hand, we demonstrated through simulation and/or physical implementation, the usefulness of maneuver regulation for providing orbital stabilization.

Dedication

I would like to dedicate this thesis to my loving family.

Acknowledgements

I would like to thank my advisor, John Hauser, for his support and patience over the last several years. He was always willing to discuss interesting problems and ideas. He has taught me more than I could have hoped for, and without his guidance and support this thesis would not have been possible.

Contents

Chapter

1 Introduction 1

1.1 Literature Overview 2

1.2 Motivation and Challenges 4

1.3 Organization 5

2 Mathematical Models 7

2.1 Equations of Motion 7

2.2 Parameter ID 11

2.3 Input Transformation 16

2.4 Linear Controllability Singularity 17

2.5 Controllability 18

2.6 Physical Setup 19

2.7 Practical System Brake (L_gV Control) 20

2.7.1 General Theory 21

2.7.2 L_gV Pendubot Design 22

3 Inverted Trajectory Exploration 23

3.1 Constant Velocity Pendubot Equation 23

3.2 General Equation 24

3.3 Trajectory Exploration 25

3.3.1 Operator Equation . . . 26
3.3.2 Green's Functions for Unstable Oscillators . . . 27
3.3.3 Invariance . . . 32
3.3.4 Existence . . . 37
3.3.5 Contraction & Uniqueness . . . 38
3.4 Specialization to the Constant Velocity Pendubot . . . 41
3.4.1 Torque Limits . . . 46
3.5 Contraction Boundary . . . 46
3.5.1 Regions of Unique Solutions Revisited . . . 54
3.6 Continuation . . . 58
3.6.1 Eigenvalues of $D\mathcal{N}_\alpha^\beta(\varphi_\alpha(\cdot))$ . . . 60
3.6.2 Eigenvalues and Conjugate Points . . . 62
3.6.3 Approximating the Eigenvalues of $D\mathcal{N}_\alpha(\varphi_\alpha(\cdot))$ . . . 62
3.7 Example of a Nonconstant Inner Arm Profile . . . 67

4 Non-Inverted Trajectory Exploration 72
4.1 Driven Hanging Pendulum . . . 72
4.2 Existence . . . 73
4.3 Nonlinear Least Squares Trajectory Exploration . . . 75
4.4 Trajectory Exploration Odd-Periodic Driving Function . . . 77

5 Maneuver Regulation 81
5.1 Overview . . . 81
5.2 Longitudinal and transverse coordinates . . . 82
5.3 Transverse Form of the Dynamics . . . 84
5.4 Transverse Linearization . . . 84
5.5 Driven Pendulum Example . . . 85
5.6 Maneuver Regulation Control Law . . . 86

5.7 Maneuver Regulation about Non-Inverted Trajectories 88
5.7.1 Maneuver Regulation 88
5.7.2 One Transverse Coordinate System 89
5.7.3 Regulation of the Transverse Coordinates 93
5.8 Maneuver Regulation about Inverted Trajectories 98

6 Conclusions 103

Bibliography 106

Tables

Table

2.1 Table of identified pendubot parameters ranges for various inputs. 13

Figures

Figure

2.1 Pendubot with inverted outer link. 8

2.2 Plot of an exemplary input torque used for parameter identification. 14

2.3 Plot of θ resulting from the exemplary input torque shown in Figure 2.2. 14

2.4 Plot of φ resulting from the exemplary input torque shown in in Figure 2.2. 15

2.5 Plot of the total energy of the system computed from the angular velocity of θ and the input torque, τ, along with and the estimated total energy based on the identified parameters. The total energy computed from the measured angles agree very closely with the estimated total energy computed using the identified parameters. 15

2.6 The experimental setup for the lab at CU includes a pendubot with an inner link that is approximately six inches and the outer link is approximately nine inches. Only the inner link is connected to a motor, while both links include a quadrature encoder for measuring position with a resolution of $2\pi/5000$. Control designs are implemented using Simulink and a dSpace 1103 PPC controller board with a sampling rate 0f $400Hz$. 20

3.1 Operator norms $\bar{g}(\alpha) = \|\mathcal{A}_\alpha\|$ and $\breve{g}(\alpha) = \|\mathcal{A}_\alpha/\alpha^2\|$ versus α. 31

3.2 The fixed points of $h(\cdot)$ lie within an easily calculated range. 34

3.3 Invariant region estimates: $\alpha \mapsto \delta_0(\alpha, \beta)$ for a selection of β values ranging from 8 up to 46. Note that, for β greater than ≈ 21.7, the associated curve is not continuous at all α; the continuous from the right portion of each of those curves is shown (the other part of each curve lies outside of the chosen δ range). Also depicted on each curve (with a circle) is the value of α above which $\mathcal{N}_\alpha^\beta$ is guaranteed to be a contraction on the corresponding closed ball. 36

3.4 Estimates of Invariant Regions for $\beta \approx 25.6128$ using the smaller of two estimates that both start at β/8. The size of the invariant region is always bounded by a piecewise continuous function $\delta_1(\alpha, \beta) = \min\left\{\frac{\alpha+\beta^2}{8}, \delta_0(\alpha, \beta)\right\}$. 39

3.5 Constant speed pendubot results: invariant region estimate, $\delta_0(\alpha_0 T, \beta)$, and fixed point trajectory norm, $\|\varphi_{\alpha_0 T}(\cdot)\|$, versus T, from 0 to 4 seconds, for the physically chosen $\beta_{\text{CU}} = 8.54$. Also depicted is the time (around 0.31 seconds) above which the nonlinear mapping is known to be a contraction. 42

3.6 Plot of $\varphi_{\max}$ (in degrees) versus T for the constant speed pendubot with α as specified and β varied according to $\beta_{\text{CU}} \cdot 2^{n/2}$ for $n = 0, 1, \ldots, 7$. For a fixed α, the maximum lean angle increases as β is increased. 44

3.7 Plot of $\varphi(t)$ (in degrees) for the constant speed pendubot with T ranging from 0 to 2 in increments of $1/4$ for β_{CU}. 45

3.8 The successive approximations $\varphi_{i+1} = \mathcal{N}_\alpha^\beta$ for the constant speed pendubot with β_{CU} at $T = 0.32$ which is just above the time where the nonlinear mapping is known to be a contraction. 47

3.9 Fixed Point Iteration for $2.5445\beta_{\text{CU}}$ with $T = 0.4$. Here we see that that two convergent subsequences emerge neither of which converge to the solution shown by the dotted line. 48

3.10 Plot of Max/Min torque vs T for inverted trajectories with a constant velocity inner arm. For $T < 0.774$, these trajectories will result in the pivot point of the outer link being pushed and pulled. The torque limits for the pendubot system in the lab at CU easily allow for constant velocity inverted trajectories where the inner arm can be pushed/pulled. 49

3.11 Plot of the curves generated by the left hand side and the right hand side of equation (3.21). These curves can only have one intersection point defining the boundary, $\bar{\delta}(\alpha)$, of the contraction boundary. 51

3.12 Plot of $\delta(\alpha)$ in degrees which defines the boundary of the contraction condition. $\delta(\alpha)$ is independent of β and monotonically decreases as $\alpha \to 0$. 52

3.13 This figure shows (in degrees) that a linear approximation of $\sin(\delta - \pi/4)$ results in an approximation, $\tilde{\delta}(\alpha)$, that is close to the desired curve. 53

3.14 Plot of $\beta(\alpha)$ in degrees. 53

3.15 Plot of various solution regions defined by δ_0, δ_0', and δ_0'' for the β associated with our physical pendubot system, i.e., $\beta_{\text{CU}} = 8.54$. 57

3.16 Plot of solution to the conjugate point problem for the pendubot system when $T = 1.0$ and β_{CU}. The x's show the corresponding values of $\delta_\alpha(\lambda)$ 63

3.17 The maximum and minimum eigenvalues of $D\mathcal{N}_\alpha^\beta$ for pendubot β_{CU} are plotted. For the range of of T shown, the eigenvalues never have a magnitude greater than 1. As a result, the fixed point iteration will have a local convergence for these values of T. 64

3.18 The maximum and minimum eigenvalues of $D\mathcal{N}_\alpha$ for 2.5445β are plotted. For the range shown, the smallest eigenvalue crosses -1 at $T = 0.595$ explaining why the fixed point iteration began to fail for $T < 0.595$. 65

3.19 Plot of a non-constant inner arm velocity profile $\theta(\cdot) = \pi t - a\sin(2\pi t)\theta$ for $T = 1.0$ sec as a varies from 0.0 to 1.0 in increments of 0.05. 68

3.20 Plot of $\varphi(t)$ for a pendubot with a non-constant inner arm velocity profile $\theta(\cdot) = \pi t - a\sin(2\pi t)$ for $T = 1.0$ sec as a varies from 0.0 to 1.0 in increments of 0.05. . 69

3.21 Strobe at twenty equal time intervals of the pendubot maneuver with non-constant inner arm velocity profile $\theta(\cdot) = \pi t - a\sin(2\pi t)$ for $T = 1.0$ sec and $a = 1.0$. . . . 70

3.22 Locus of the Outer Link for $T = 1.0$ sec and $a = 1.0$. 71

4.1 Driven hanging pendulum. 73

4.2 Plot of the maximum angle the outer arm will achieve driven by $\theta(t) = 30\,\pi/180 \sin\,\omega\, t$. We were able to find multiple solutions for the same driving function for various ω. 79

4.3 Plot of multiple, normalized, solutions when $\theta(t) = 30\,\pi/180 \sin\,5.0\, t$. In this case, we found three solutions for the same sinusoidal driving function when $\omega = 5.0$. 79

4.4 Plot of one of the solutions when $\theta(t) = 30\,\pi/180 \sin\,5.0\, t$ along with the first and third fourier components. In this case, the sinusoidal driving function does not result in a pure sinusoid for the outer link. 80

4.5 Plot of multiple, normalized, solutions when $\theta(t) = 30\,\pi/180 \sin\,2.0\, t$. In this case, we found five solutions for the same sinusoidal driving function when $\omega = 2.0$. 80

5.1 Phase plot of θ and $\dot{\theta}/\omega$ along with the local coordinate system (i.e., the transverse coordinate ρ_1 and longitudinal coordinate s). 90

5.2 Plot of desired θ and φ. The driving function, $\theta(t)$, has an amplitude of 40 degrees and a period $T = 0.5$. 94

5.3 Plot of desired τ when a then inner arm of the pendubot is driven by the odd-periodic $\theta(t) = \frac{40\pi}{180}\sin(\frac{2\pi}{0.5}t)$. 95

5.4 Plot of θ vs $\dot{\theta}$ where $\theta(t) = 40\ \pi/180\ \sin 4\pi t$. The circles represent the desired trajectory with solid line representing the data collected from the system. 95

5.5 Plot of φ vs $\dot{\varphi}$ driven by $\theta(t) = 40\ \pi/180\ \sin 4\pi t$. The circles represent the desired trajectory with solid line representing the data collected from the system. 96

5.6 Plot of τ collected from physical system with the maneuver regulation controller. . 96

5.7 Plot of τ vs θ (in degrees). The circles indicate the desired curve while the lines show the τ measured from physical system during the maneuver. 97

5.8 Plot of K(s) used for maneuver regulation about an inverted in inverted trajectory of the constant velocity pendubot with period $T = 1.0$. 98

5.9 Plot of the desired φ and results from a simulation of the inverted trajectory using the maneuver regulation controller with velocity estimation. 99

5.10 Plot of the desired torque and results from a simulation with velocity estimation of an inverted maneuver on the constant velocity pendubot. 100

5.11 Plot of simulation results of θ vs. $d\theta/dt$ of an inverted maneuver on the constant velocity pendubot. The circles show the desired trajectory and the solid line shows the simulation results. 100

5.12 Plot of simulation results of φ vs. $d\varphi/dt$ of an inverted maneuver on the constant velocity pendubot. The circles show the desired trajectory and the solid line shows the simulation results. 101

Chapter 1

Introduction

The pendubot is a two-link planar robot with an actuator only on a fixed pivot. The first link is coupled to the fixed pivot and the second link is connected to the first link opposite the fixed pivot creating the double pendulum system. This system provides a theoretical and experimental setting where aggressive maneuvering, including situations where the pendulum pivot experiences highly variable accelerations, can be explored. The dynamics of the pendubot are closely related to many interesting problems such as the pendulum and cart, a motorcycle, a rocket with vectoring thrust, as well as gaits of robots. The pendubot includes both kinematic and controllability singularities that make the system even more interesting. In addition to modelling uncertainties, measurements of the position and estimates of the velocity at best provide noise-corrupted observations of the system states.

We are particularly interested in understanding how to effectively find and implement aggressive maneuvers in view of uncertainties, disturbances, kinematic singularities, and controllability issues. The dynamics of the pendubot are simple enough to allow for thorough analysis, and complicated enough to provide for some interesting nonlinear behaviors. Moreover, it is not hard to see that the pendubot has four equilibrium points (i.e., when the inner arm is horizontal and the outer arm is vertical) that are not linearly controllable.

Trajectory tracking strategies can be ineffective in tracking aggressive maneuvers of the pendubot. In particular, for many interesting trajectories, such as aggressive periodic orbits, a local degradation in tracking can impact the global performance. Consequently, the practical benefit of

these designs leaves a lot to be desired. For example, the ineffectiveness can be seen when the controllers using these designs are implemented on the physical system as the controllers tend to lack desirable robustness properties. Maneuver regulation provides one scheme for providing stable path following. In particular, maneuver regulation decouples the time index of the motion along the path while regulating the lateral dynamics. This control strategy has proven effective in situations where robustness issues have prevented the use of traditional trajectory tracking controllers.

We divide our study of the pendubot into the following three major parts

(1) Trajectory Exploration;

(2) Maneuver Regulation Design; and

(3) Simulations/Physical Implementation.

1.1 Literature Overview

The pendulum provides what seems to be an inexhaustible source of practical applications and interesting problems which have motivated research in a variety of disciplines. For example, the paper of Mawhin [1] provides an interesting account of how the pendulum has played an important role in the development of nonlinear analysis. The inverted pendulum is a classic experiment that has also been used in control laboratories for several decades to illustrate a variety of concepts in both linear and nonlinear control theory. One finds experiments ranging from the standard inverted pendulum on a cart (or a linear track), to the curved horizontal track (Furuta) [2], to the vertically curved track (pendubot) [3], not mention other systems such as the acrobot [4]. Not only is the inverted pendulum one of the simplest unstable nonlinear systems imaginable, inverted (or nearly inverted) configurations of the pendulum also provide a simple model for rocket dynamics.

Surprisingly, the dynamics of the inverted pendulum continues to appear in numerous other systems of interest. The inverted pendulum driven by a lateral acceleration is clearly present in the dynamic balance of a skier racing down the slope. In much the same way, simple models for exploring bicycle and motorcycle dynamics include the inverted pendulum as a key subsystem,

imposing strong constraints on the system performance—see, e.g., [5, 6], [7], and [8]. These dynamics also show up as internal dynamics in aircraft flight dynamics [11].

Exploration of the driven inverted pendulum with arbitrary bounded lateral acceleration can be found in [12]. In that work, a contraction mapping was used to determine where the solutions lived and also to develop a successive approximations method to find the solution. Similar techniques have been developed by Devasia and Paden [14]. The conditions developed in these previous works are not satisfied for the pendubot with substantial constant inner arm velocity.

A variety of papers have been written discussing swing-up control of the pendubot. Examples include partial feedback linearization techniques [15], an impulse-momentum approach [16], and energy-based approaches [17]-[18]. In [19], a fuzzy logic control strategy is presented for keeping the inner arm and outer arm inverted and with a maximum deviation of approximately .25 rad. [20] uses virtual constraints for their choice of motion planning and for the generation of oscillatory or periodic motions of the not actuated link of the pendubot via output feedback control.

In contrast to these references, we are interested in finding and understanding the types of aggressive trajectories that exist for the pendubot. In particular, we develop techniques for finding periodic trajectories and providing orbital stabilization for aggressive periodic orbits. For the purpose of aggressive trajectory exploration, a logical beginning is with periodic pendubot motions where the outer link is vertical at the top and bottom of its motion. This leads us to consider odd-periodic motions on the pivot of the inverted pendulum and to develop techniques for estimating regions in Banach space where aggressive odd-periodic trajectories of the inverted pendulum exist.

There are a variety of control strategies that can be potentially used to implement aggressive trajectories of the pendubot. Many nonlinear analysis problems of engineering interest can be reduced to a problem of tracking a nominal trajectory. Be it an athletic maneuver, a car changing lanes on an automated highway, an airplane taking a turn, or an idling engine going through a sudden load change, the designer has in mind an appropriate path to be complete in a finite predetermined time and built his control system accordingly. Moreover, many control system objectives

can be obtained by providing a stable motion along a path.

Maneuver regulation provides one scheme for providing stable path following. In particular, maneuver regulation decouples the time index of the motion along the path while regulating the lateral dynamics. (see, e.g., [21] and [22]) In Chapter 5, a more detailed background of maneuver regulation is provided before we finally demonstrate that this type of control strategy can prove effective in implementing aggressive maneuvers of the pendubot.

1.2 Motivation and Challenges

Trajectory exploration, maneuver regulation, and physical implementation each have individual challenges that have to be overcome. With regard to trajectory exploration, aggressive trajectories of the pendubot can result in the outer arm being pushed and pulled by the inner arm. For example, for a constant inner arm velocity it is not hard to see that when that $T < 2\pi/8.11 \approx 0.774sec$ results in the outer arm being pulled down and pushed up. Most of the traditional maneuvers found in the literature of systems, such as the pendulum and cart, do not result in the pivot pulling down on the pendulum. Instead, the pivot on the pendulum is pushing up and gravity will be pulling the link down. With aggressive maneuvers on the pendubot, part of the maneuver can result in the pendulum being thrown up during part of the trajectory. This results in the pivot pulling down on the pendulum and the effects of gravity disappearing.

As a result, it was not clear that trajectories always exist. In fact, we had difficulty finding trajectories when the outer arm began pulling the inner arm. We had used a least squares approach to successfully find trajectories in the hanging down configurations and slower moving inverted maneuvers. However, as the maneuvers became more aggressive, our least squares approached proved unsuccessful. This led to the exploration the existence and uniqueness of inverted trajectories.

As described in more detail below, we began by developing a general form of the inverted pendulum driven by odd periodic and considered the equivalent two point boundary value problem. After development of a Green's function we used the Schauder fixed point theorem to show that

the inverted pendulum with an odd periodic driving acceleration at the pivot always possesses an odd periodic solution. Then, we were able to show that it is sometimes possible to construct a contraction mapping so that the Banach fixed point theorem can be used to ensure that there is a unique solution within an invariant region of the space of possible solution curves. Now we know that trajectories always exist. Moreover, these techniques provide estimates on where the solutions lie. This allows us to more confidently use boundary value solvers and continuation methods to find solution trajectories.

For designing controllers and for successful implementation, the system presents quite a few challenges. The pendubot is an underactuated, non-minimum phase, nonlinear system, without direct control of the outer arm. Due to the non-minimum phase, the inner arm will sometimes need to go in the "wrong" direction. In addition, the system also has kinematic singularities (e.g., inner arm at ninety degrees) which limits our ability to execute nonminimum phase activities. The kinematic singularity results in an effective loss of controllability because the arm can only be moved up and down and not left and right. This is one reason why the controller can have a difficult time when the inner arm is at ninety degrees. We ultimately demonstrate that maneuver regulation can be an effective strategy for this system.

1.3 Organization

This document is organized as follows:

- This chapter discusses the motivation as well as the research goals and contributions of this dissertation.
- **Chapter 2** provides a derivation of a mathematical model of the pendubot is presented. Then, some fundamental limitations of the pendubot are also discussed.
- **Chapter 3** presents an exploration of inverted maneuvers of the pendubot. Odd periodic orbits are closely examined by rewriting and solving a two point boundary value problem.

- **Chapter 4** presents an exploration of maneuvers of the pendubot with the outer link hanging down.

- **Chapter 5** presents an overview and background of maneuver regulation of nonlinear systems. It includes a review of the fundamental definitions and theorems useful to understand the maneuver regulation controllers. Then, physical implementation of trajectories with the outer link hanging down are discussed followed by simulations for a maneuver regulation controller with an inverted outer link.

- **Chapter 6** presents the conclusions based on the above work and discusses future avenues of research.

Chapter 2

Mathematical Models

As with any electro-mechanical system, developing one or more models to understand the behaviors of the system is essential for trajectory exploration, practical control design, and simulation. This chapter starts with the development of a model of the pendubot. We then estimate the parameters for our physical system. An input transformation is presented to write the outer link dynamics which are used later for trajectory exploration. Finally, we discuss some limitations of the physical system including the kinematic and controllability singularities found when the inner arm is horizontal and the outer arm is vertical.

2.1 Equations of Motion

The pendubot as illustrated in Figure 2.1 consists of two links - an inner link and an outer link. A torque can be applied to the inner link via a stationary pivot point providing 360^o of rotation for the inner link. The outer link is connected to the end of the inner link opposite to the stationary pivot point. The outer link can rotate around this moving pivot point in the same plane of motion as the inner link. There is no actuator associated with the moving pivot point to supply a torque to control the outer link. As such, the motion of the outer link is controlled through the movement of the inner link.

For the pendubot in our lab at CU the inner link is approximately six inches and the outer link is approximately nine inches. However different versions of the pendubot exist or can be built. See [10] and [15], for example, where the inner link was approximately eight inches and the outer

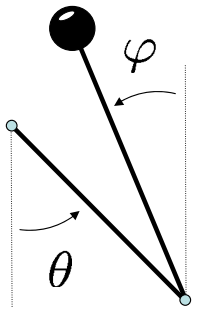


Figure 2.1: Pendubot with inverted outer link.

link was approximately fourteen inches. With this description of the system, we now derive the equations of motion for the pendubot.

For the inner link, let m_1 be the total mass, l_1 be the length, l_{c1} be the distance to the center of mass, and I_1 be the moment of inertia of the inner link about its centroid. Similarly, with regard to the outer link, let m_2 be the total mass, l_2 be the length, l_{c2} be the distance to the center of mass of the outer link, and I_2 be the moment of inertia of the outer link about its centroid. Also, let g be the acceleration of gravity.

The equations of motion can easily be derived using the following Lagrangian dynamics equations:

$$L = T - V$$

$$\frac{d}{dt}\left(\frac{\partial L}{\partial \dot{q}_i}\right) - \frac{\partial L}{\partial q_i} = \tau$$

where T is the kinetic energy and V is the potential energy of the system.

The first step in deriving the equations of motion is to write the position components of the

center of masses of links one and two. Doing this one gets

$$\begin{aligned}
x_1 &= l_{c1}\sin(\theta) \\
y_1 &= -l_{c1}\cos(\theta) = h_1(\theta) \\
x_2 &= l_1\sin(\theta) - l_{c2}\sin(\varphi) \\
y_2 &= -l_1\cos(\theta) + l_{c2}\cos(\varphi) = h_2(\theta,\varphi)
\end{aligned}$$

In order to get the cartesian velocity components, simply take the derivative to get the following

$$\begin{aligned}
\dot{x}_1 &= l_{c1}\cos(\theta)\dot{\theta} \\
\dot{y}_1 &= l_{c1}\sin(\theta)\dot{\theta} \\
\dot{x}_2 &= l_1\cos(\theta)\dot{\theta} - l_{c2}\cos(\varphi)\dot{\varphi} \\
\dot{y}_2 &= l_1\sin(\theta)\dot{\theta} - l_{c2}\sin(\varphi)\dot{\varphi}
\end{aligned}$$

This gives a total velocity of:

$$\begin{aligned}
V_1^2 &= \dot{x}_1^2 + \dot{y}_1^2 \\
&= l_{c1}^2\dot{\theta}^2 \\
V_2^2 &= \dot{x}_2^2 + \dot{y}_2^2 \\
&= l_1^2\dot{\theta}^2 + l_{c2}^2\dot{\varphi}^2 - 2l_1l_{c2}\dot{\theta}\dot{\varphi}\left(\cos\theta\cos\varphi + \sin\theta\sin\varphi\right) \\
&= l_1^2\dot{\theta}^2 - 2l_1l_{c2}\dot{\theta}\dot{\varphi}\cos(\varphi-\theta) + l_{c2}^2\dot{\varphi}^2
\end{aligned}$$

The equations for the kinetic energy, T, and the potential energy, V, can then easily be written as

$$\begin{aligned}
T &= \frac{1}{2}I_1\dot{\theta}^2 + \frac{1}{2}I_2\dot{\varphi}^2 + \frac{1}{2}m_1V_1^2 + \frac{1}{2}m_2V_2^2 \\
&= \frac{1}{2}\begin{bmatrix}\dot{\theta} \\ \dot{\varphi}\end{bmatrix}^T M(\theta,\varphi)\begin{bmatrix}\dot{\theta} \\ \dot{\varphi}\end{bmatrix} \\
V &= -m_1gl_{c1}\cos\theta + m_2g\left[-l_1\cos\theta + l_{c2}\cos\varphi\right]
\end{aligned}$$

where

$$M(\theta,\varphi) = \begin{bmatrix} I_1 + m_1l_{c1}^2 + m_2l_1^2 & -m_2l_1l_{c2}\cos(\varphi-\theta) \\ -m_2l_1l_{c2}\cos(\varphi-\theta) & I_2 + m_2l_{c2}^2 \end{bmatrix}$$

Giving

$$L = T - V = \frac{1}{2}\dot{\theta}^2 d_{11} + \frac{1}{2}\dot{\varphi}^2 d_{22} + \dot{\theta}\dot{\varphi} d_{12} + m_1 g l_{c1} \cos\theta - m_2 g \left[-l_1 \cos\theta + l_{c2} \cos\varphi\right]$$

where

$$\begin{aligned} d_{11} &= I_1 + m_1 l_{c1}^2 + m_2 l_1^2 \\ d_{12} &= -m_2 l_1 l_{c2} \cos(\varphi - \theta) \\ d_{21} &= d_{12} \\ d_{22} &= I_2 + m_2 l_{c2}^2 \end{aligned}$$

So,

$$\begin{aligned} \frac{\partial L}{\partial \theta} &= -\phi_1 - \dot{\theta}\dot{\varphi} h \\ \frac{\partial L}{\partial \dot{\theta}} &= d_{11}\dot{\theta} + \dot{\varphi} d_{12} \\ \frac{d}{dt}\frac{\partial L}{\partial \dot{\theta}} &= d_{11}\ddot{\theta} + \dot{\theta}\dot{d}_{11} + d_{12}\ddot{\varphi} + \dot{\varphi}\dot{d}_{12} \\ \frac{\partial L}{\partial \varphi} &= -\phi_2 + \dot{\theta}\dot{\varphi} h \\ \frac{\partial L}{\partial \dot{\varphi}} &= d_{22}\dot{\varphi} + \dot{\theta} d_{12} \\ \frac{d}{dt}\frac{\partial L}{\partial \dot{\varphi}} &= d_{22}\ddot{\varphi} + \dot{\varphi}\dot{d}_{22} + d_{12}\ddot{\theta} + \dot{\theta}\dot{d}_{12} \\ \frac{d}{dt}\frac{\partial L}{\partial \dot{\theta}} - \frac{\partial L}{\partial \dot{\theta}} &= d_{11}\ddot{\theta} + d_{21}\ddot{\theta} + \phi_1 + h\dot{\theta}\dot{\varphi} = \tau \end{aligned}$$

where

$$\begin{aligned} h &= m_2 l_1 l_{c2} \sin(\varphi - \theta) \\ \phi_1 &= (m_1 g l_{c1} + m_2 g l_1) \sin\theta \\ \phi_2 &= -m_2 g l_{c2} \sin\varphi \end{aligned}$$

The final equations of motion can be written in the following standard matrix form

$$M(\theta, \varphi) \begin{bmatrix} \ddot{\theta} \\ \\ \ddot{\varphi} \end{bmatrix} + C(\theta, \varphi, \dot{\theta}, \dot{\varphi}) + G(\theta, \varphi) = \begin{bmatrix} \tau \\ \\ 0 \end{bmatrix}$$

where

$$M(\theta,\varphi)=\begin{bmatrix} d_{11} & d_{12} \\ d_{21} & d_{22} \end{bmatrix},\ \ C(\theta,\varphi,\dot{\theta},\dot{\varphi})=\begin{bmatrix} h\dot{\varphi}^2 \\ -h\dot{\theta}^2 \end{bmatrix},\ \ G(\theta,\varphi)=\begin{bmatrix} \phi_1 \\ \phi_2 \end{bmatrix}$$

2.2 Parameter ID

Identification of nonlinear systems can be generally divided into model-based techniques and model-less, or black-box techniques. Model-based techniques assume some sort of a priori knowledge about the plant structure and dynamics, while black-box approaches are aimed at plants where little or nothing is known. In this case, we have just developed a model for the pendubot and need to identify the parameters in such a manner that the model response best matches the observed input-output data. There are many options for identifying the parameters for the model we developed. For example, [25] provides an optimization based approach. With this approach, given a choice of parameters ρ and a set of experimental data, a stand optimal control problem is formulated to minimize (in an L^2 sense) the difference between the model response to be the trajectory $(x(\cdot),u(\cdot))$ of the system model $\dot{x}=f(x,u,\rho)$ closest to the given experimental data $(x_d(\cdot),u_d(\cdot))$. We follow [3] and [26] to identify various parameters based on an energy theorem scheme and using a least squares method to estimate the parameters.

For rotational systems, the power, $P(t)$, is related to the torque, τ, and the angular velocity, ω, and can be expressed as

$$P(t)=\omega\,\tau$$

The energy theorem states that the work of forces applied to a system is equal to the change of the total energy of the system. For the pendubot, this can be mathematically written as

$$\int_{t_1}^{t_2}\dot{\theta}^T\tau\;dt=E(t_2)-E(t_1)$$

where the total energy can be written as

$$E = \frac{1}{2}\mu_1\dot{\theta}^2 - \mu_3\dot{\varphi}\dot{\theta}\cos(\varphi-\theta) + \frac{1}{2}\mu_2\dot{\varphi}^2 - \mu_4 g\cos\theta + \mu_5 g\cos\varphi$$

with

$$\begin{aligned}
\mu_1 &= m_1 l_{c1}^2 + m_2 l_1^2 + I_1 = d_{11} \\
\mu_2 &= m_2 l_{c2}^2 + I_2 = d_{22} \\
\mu_3 &= m_2 l_1 l_{c2} \\
\mu_4 &= m_1 l_{c1} + m_2 l_1 \\
\mu_5 &= m_2 l_{c2}
\end{aligned}$$

The energy is a linear combination of these parameters and can be written as

$$E = \begin{bmatrix} \frac{1}{2}\dot{\theta} & \frac{1}{2}\dot{\varphi} & -\dot{\theta}\dot{\varphi}\cos(\varphi-\theta) & -g\cos\theta & g\cos\varphi \end{bmatrix} \begin{bmatrix} \mu_1 \\ \mu_2 \\ \mu_3 \\ \mu_4 \\ \mu_5 \end{bmatrix}$$

This allows us to use a least squares estimation method to identify these parameters giving

$$M(\theta,\varphi)\begin{bmatrix} \ddot{\theta} \\ \ddot{\varphi} \end{bmatrix} + C(\theta,\varphi,\dot{\theta},\dot{\varphi}) + G(\theta,\varphi) = \begin{bmatrix} \tau \\ 0 \end{bmatrix}$$

where

$$M(\theta,\varphi) = \begin{bmatrix} \mu_1 & -\mu_3\cos(\varphi-\theta) \\ -\mu_3\cos(\varphi-\theta) & \mu_2 \end{bmatrix}$$

$$C(\theta,\varphi,\dot{\theta},\dot{\varphi}) = \begin{bmatrix} \mu_3\,\dot{\varphi}^2\sin(\varphi-\theta) \\ -\mu_3\,\dot{\theta}^2\sin(\varphi-\theta) \end{bmatrix}$$

$$G(\theta,\varphi) = \begin{bmatrix} \mu_4\, g\sin\theta \\ -\mu_5\, g\sin\varphi \end{bmatrix}$$

Table 2.1: Table of identified pendubot parameters ranges for various inputs.

μ	Low	High	Selected
μ_1	0.01254052002565	0.01356808738595	0.01302808113329
μ_2	0.00425706510419	0.00468327083910	0.00433245959712
μ_3	0.00367479281471	0.00399861601008	0.00374775571049
μ_4	0.08808765624407	0.08971131877057	0.08948194136085
μ_5	0.02469397236154	0.02791766074388	0.02516833107165

To begin, we first collected several sets of data with various input torques from the pendubot. The torques generated step responses on the inner arm, sinusoidal torques of various frequencies and magnitudes, and a free fall from different initial configurations. All of these data sets contain both useful and irrelevant information, i.e., the signal and the noise. The pendubot has only two encoders to measure the angles of the inner link and the outer link with a resolution of 0.072 degrees. We used a non-causal filter to estimate the velocities and to filter the measured angles. Figures 2.2 - 2.4 illustrate an example of one of the observed input-output data sets.

Using the observed input-output data sets, we identified $\mu = (0.01303, 0.00433, 0.00375, 0.08948, 0.02517)^T$ for our system. Table 2.1 shows the variation in the parameters for the data sets we collected along with our selected parameters. We found the identified parameters we selected generally allowed total energy of the model to match the total energy of the observed data on the order of 10^{-3}. Figure 2.5 is a plot of the total energy of the system computed from the angular velocity of θ and the input torque, τ, along with and the estimated total energy based on the identified parameters.

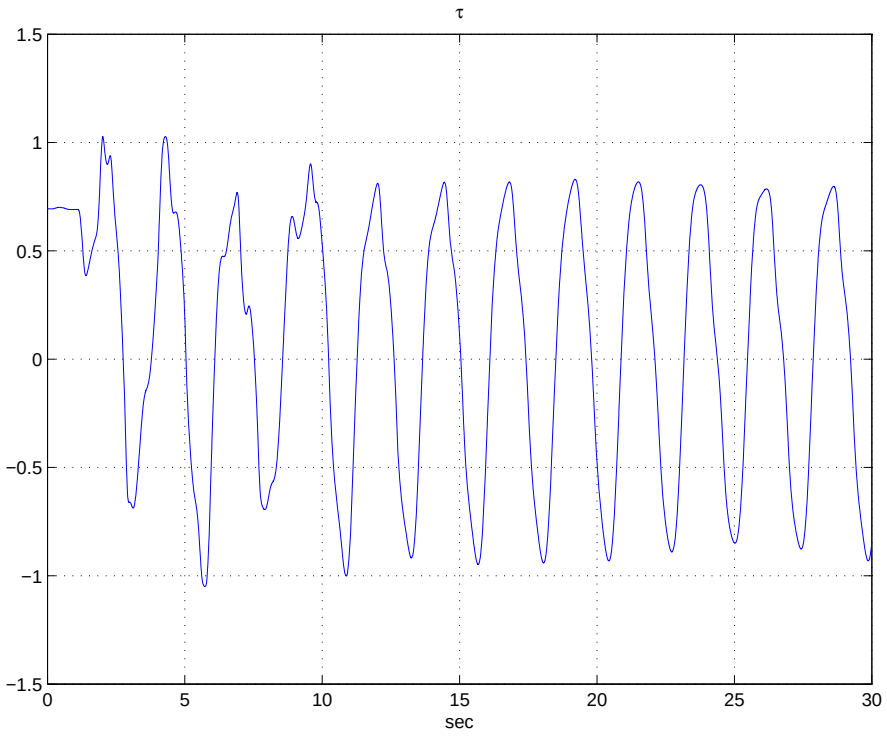


Figure 2.2: Plot of an exemplary input torque used for parameter identification.

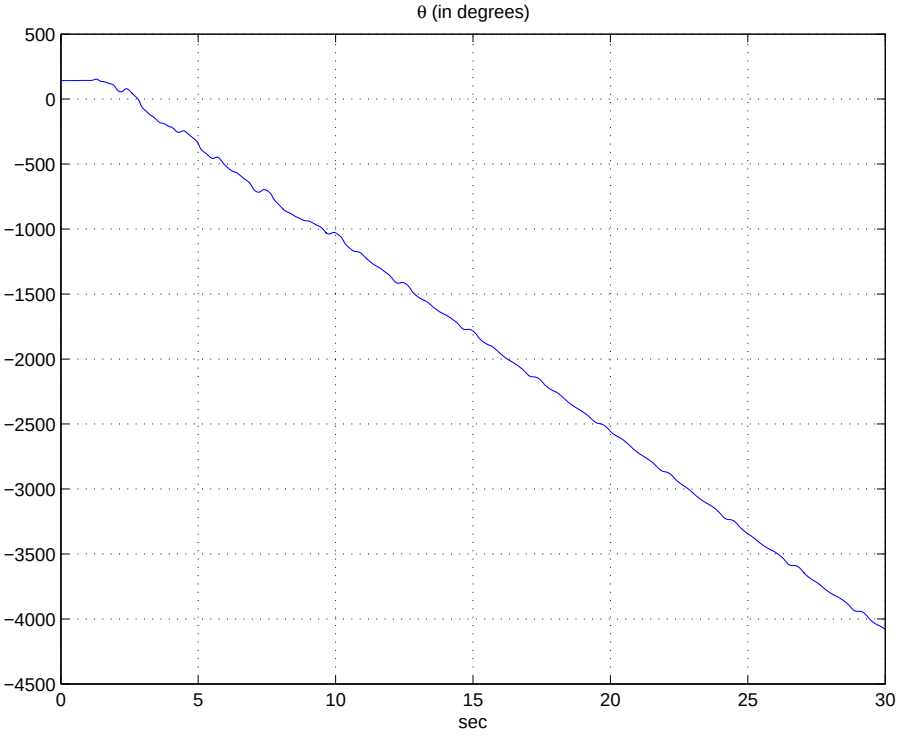


Figure 2.3: Plot of θ resulting from the exemplary input torque shown in Figure 2.2.

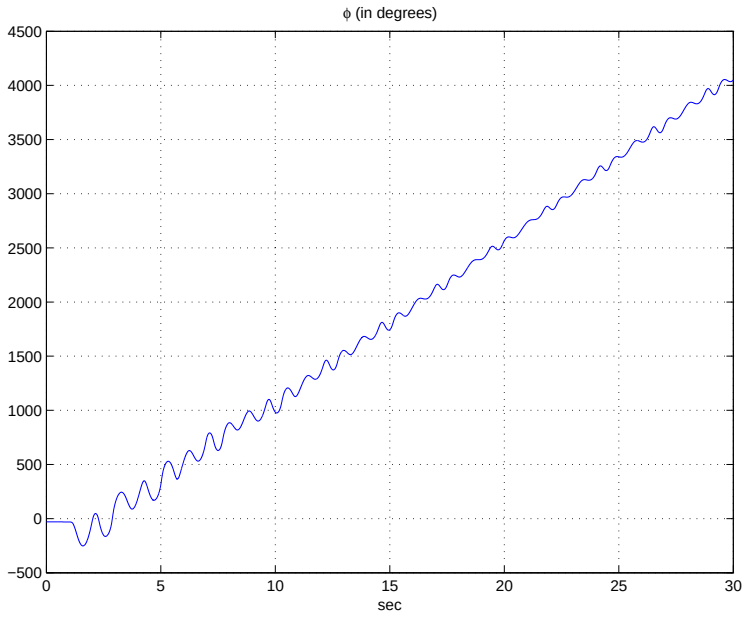


Figure 2.4: Plot of φ resulting from the exemplary input torque shown in in Figure 2.2.

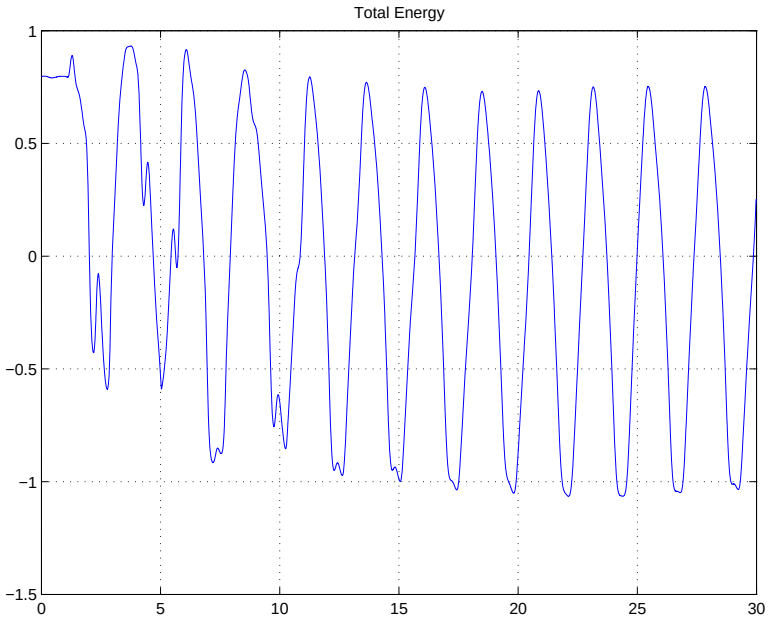


Figure 2.5: Plot of the total energy of the system computed from the angular velocity of θ and the input torque, τ, along with and the estimated total energy based on the identified parameters. The total energy computed from the measured angles agree very closely with the estimated total energy computed using the identified parameters.

2.3 Input Transformation

The full equations can be written as

$$\begin{bmatrix} \mu_1 & -\mu_3\cos(\varphi-\theta) \\ -\mu_3\cos(\varphi-\theta) & \mu_2 \end{bmatrix} \begin{bmatrix} \ddot{\theta} \\ \ddot{\varphi} \end{bmatrix} + \begin{bmatrix} \mu_3\,\dot{\varphi}^2\sin(\varphi-\theta) \\ -\mu_3\,\dot{\theta}^2\sin(\varphi-\theta) \end{bmatrix} + \begin{bmatrix} \mu_4\,g\sin\theta \\ -\mu_5\,g\sin\varphi \end{bmatrix} = \begin{bmatrix} \tau \\ 0 \end{bmatrix}$$

To decouple the accelerations, we multiply on the left by the adjugate matrix (from Cramer's rule) to obtain

$$\begin{aligned} (\mu_1\mu_2 - \mu_3^2\cos^2(\varphi-\theta))\,\ddot{\theta} &= (\mu_3^2\,\dot{\theta}^2\cos(\varphi-\theta) - \mu_2\mu_3\,\dot{\varphi}^2)\sin(\varphi-\theta) \\ &\quad + \mu_3\mu_5\,g\sin\varphi\cos(\varphi-\theta) - \mu_2\mu_4\,g\sin\theta + \mu_2\,\tau \\ (\mu_1\mu_2 - \mu_3^2\cos^2(\varphi-\theta))\,\ddot{\varphi} &= (\mu_1\mu_3\,\dot{\theta}^2 - \mu_3^2\,\dot{\varphi}^2\cos(\varphi-\theta))\sin(\varphi-\theta) \\ &\quad + \mu_1\mu_5\,g\sin\varphi - \mu_3\mu_4\,g\sin\theta\cos(\varphi-\theta) + \mu_3\cos(\varphi-\theta)\,\tau \end{aligned}$$

Feedback transformations may be used for a number of theoretical and practical purposes. From a theoretical point of view, the simplest model is obtained by taking the control input u to be the inner arm acceleration $\ddot{\theta}$. Indeed, the feedback transformation

$$\begin{aligned} \tau = \;& \mu_4\,g\sin\theta - (\mu_3\mu_5/\mu_2)\,g\sin\varphi\cos(\varphi-\theta) + (\mu_1 - (\mu_3^2/\mu_2)\cos^2(\varphi-\theta))u \\ & +(\mu_3\dot{\varphi}^2 - (\mu_3^2/\mu_2)\dot{\theta}^2\cos(\varphi-\theta))\sin(\varphi-\theta) \end{aligned}$$

can be used to transform the system into

$$\begin{aligned} \ddot{\theta} &= u \\ \ddot{\varphi} &= (\mu_5 g/\mu_2)\,\sin\varphi + (\mu_3/\mu_2)\,(\dot{\theta}^2\sin(\varphi-\theta) + u\cos(\varphi-\theta)) \\ &= g/l\,\sin\varphi + (l_1/l)\,(\dot{\theta}^2\sin(\varphi-\theta) + u\cos(\varphi-\theta)) \end{aligned}$$

where $l_1 = \mu_3/\mu_5$ is the length of the inner link and $l = \mu_2/\mu_5$ is the inertial length of the outer link. This form can also be obtained by simply using the second equation of the Lagrangian form above with $\ddot{\theta} = u$.

As a result of the feedback transformation above, the outer link dynamics can be written as

$$\ddot{\varphi} = \frac{g}{l}\sin\varphi + \frac{l_1}{l}\dot{\theta}^2(t)\sin\left(\varphi - \theta(t)\right) + \frac{l_1}{l}\ddot{\theta}(t)\cos\left(\varphi - \theta(t)\right) \tag{2.1}$$

Here, the C^2 inner arm trajectory $\theta(\cdot)$ may be chosen arbitrarily and imposed by an appropriate (state dependent) choice of $\tau(\cdot)$. We use this time-varying nonlinear equation for trajectory exploration in Chapter 3. Also, we immediately see that when $(\varphi - \theta(t)) = \pm\pi/2$ that no control action can be directly applied.

From an experimental point of view, the above feedback transformation is not practical since the velocities $\dot{\varphi}$ and $\dot{\theta}$ cannot be directly measured. However, since the angles φ and θ are accurately measured (using optical encoders), we can use the position dependent portion

$$\tau = \mu_4\, g \sin\theta - (\mu_3\mu_5/\mu_2)\, g \sin\varphi \cos(\varphi - \theta) + (\mu_1 - (\mu_3^2/\mu_2)\cos^2(\varphi - \theta))u$$

to compensate for gravity to obtain

$$\begin{aligned} \ddot{\theta} &= u + \sin(\varphi - \theta)[-\mu_2 a_2(\varphi - \theta)\dot{\varphi}^2 + a_1(\varphi - \theta)\dot{\theta}^2] \\ \ddot{\varphi} &= (g/l)\,\sin\varphi + (l_1/l)\,\cos(\varphi - \theta)\quad u + \sin(\varphi - \theta)[-a_1(\varphi - \theta)\dot{\varphi}^2 + \mu_1 a_2(\varphi - \theta)\dot{\theta}^2] \end{aligned}$$

where $a_2(\varphi - \theta) = \mu_3/(\mu_1\mu_2 - \mu_3^2\cos^2(\varphi - \theta))$ and $a_1(\varphi - \theta) = \mu_3\cos(\varphi - \theta)a_2(\varphi - \theta)$.

2.4 Linear Controllability Singularity

The pendubot has a continuum of equilibrium points with the outer arm in a vertical position. The linearization around four of these equilibrium points (i.e., for the inner link horizontal and the outer link vertical) result in a linear controllability singularity. The dynamics for the pendubot can be written as

$$\begin{bmatrix} \ddot{\theta} \\ \ddot{\varphi} \end{bmatrix} = M^{-1}(\theta, \varphi)\left\{ \begin{bmatrix} \tau \\ 0 \end{bmatrix} - C(\theta, \varphi, \dot{\theta}, \dot{\varphi}) - G(\theta, \varphi) \right\}$$

Let $x = (\theta, \dot{\theta}, \varphi, \dot{\varphi})$ and linearize $\dot{x} = f(x, u)$ about x_0 and u_0 to get a linear system of the form

$$\begin{aligned} \dot{x} &= Ax + Bu \\ y &= Cx + Du \end{aligned} \tag{2.2}$$

with state $x \in \mathbb{R}^n$, $u \in \mathbb{R}$.

Definition 2.4.1. *A linear system is controllable if for any x_0, $x_f \in \mathbb{R}^n$ and any time $T > 0$ there exists an input $u : [0, T] \in \mathbb{R}$ such that the solution of the dynamics starting from $x(0) = x_0$ and applying input $u(\cdot)$ gives $x(T) = x_f$.*

Note that x_0 and x_f do not have to be equilibrium points. However, when x_f is not an equilibrium point, the system will not stay at x_f after time T. The following theorem provides a simple test for controllability.

Theorem 1. *A linear system is controllable if and only if the $n \times n$ controllability matrix*

$$[B \;\; AB \;\; A^2B \;\; ... \;\; A^{n-1}B]$$

has full rank.

As an example, the linearization of $\dot{x} = f(x, u)$ about $x_0 = (\pi/2, 0, 0, 0)$, $\tau = \mu_4 g$ gives

$$A = \begin{bmatrix} 0 & 1 & 0 & 0 \\ 0 & 0 & 0 & 0 \\ 0 & 0 & 0 & 1 \\ 0 & 0 & \mu_5 g/\mu_2 & 0 \end{bmatrix} \quad B = \begin{bmatrix} 0 \\ 1/\mu 1 \\ 0 \\ 0 \end{bmatrix}$$

The controllability matrix, $C = [B \quad AB \quad A^2B \quad A^3B]$ has a rank of 2. In addition, the controllability matrix becomes ill-conditioned as the equilibrium points approach one of theses four points where linear controllability is lost. However, the failure to find controllability from the linearization does not allow us to conclude that the nonlinear system is not controllable.

2.5 Controllability

Consider the nonlinear system

$$\begin{aligned} \dot{x} &= f(x, u) \\ y &= g(x, u) \end{aligned} \tag{2.3}$$

with state $x \in \mathbb{R}^n$, $u \in \mathbb{R}$.

Definition 2.5.1. *A nonlinear system is controllable if for any* x_0, $x_f \in \mathbb{R}^n$ *and any time* $T > 0$ *there exists an input* $u : [0, T] \in \mathbb{R}$ *such that the solution of the dynamics starting from* $x(0) = x_0$ *and applying input* $u(\cdot)$ *gives* $x(T) = x_f$.

Many nonlinear controllability results arise from the consideration of the controllability of the time-varying linearization about a trajectory of the nonlinear system

$$(L) \quad \dot{z} = A(t)z + B(t)v, \quad A(t), B(t) \in \mathcal{C}^\infty$$

Define $\mathcal{A} : C(\cdot) \mapsto \dot{C}(\cdot) - A(\cdot)C(\cdot)$

Theorem 2. *If span*$\{B(\cdot) \quad (\mathcal{A}B))(\cdot) \quad (\mathcal{A}^2B))(\cdot) \quad \cdots\}(t_0) = \mathbb{R}^n$, *then (L) is controllable on* $[t_0, t_0 + \delta]$ *for every* $\delta > 0$.

To use this test on a nonlinear system at a point (NOT an equilibrium) on a trajectory, it is helpful for the control to be constant on $[t_0, t_0 + \epsilon]$, avoiding the differentiating of $u(\cdot)$. For the pendubot at $\theta = \pi/2$ and $\varphi = 0$ configuration, we are not able to conclude controllability nor a lack of controllability.

2.6 Physical Setup

Figure 2.6 is a block diagram illustrating our experimental setup. To control the pendubot, we used a dSpace 1103 PPC controller board with the sampling rate set at 400Hz. The implementation of most of our control laws required velocity feedback. The pendubot currently is not equipped with a sensor, e.g., a tachometer, for measuring the velocity of the inner and outer links. Instead, the pendubot only has two rotary encoders for the measurement of the position of the inner and outer links. These encoders have a resolution of $2\pi/5000 = 0.072$ degrees.

The pendubot is a nonlinear system and therefore the separation principle will not apply in general. That is, an observer that asymptotically reconstructs the state of the pendubot will not guarantee that a given stabilizing state-feedback controller will remain stable when using the

estimated state instead of the actual state. To estimate the velocity we used the following dirty differentiator:

$$V(s) = \frac{50s}{s + 50}$$

This adds time delay to the velocity estimation and additional dynamics which can be included within the simulations.

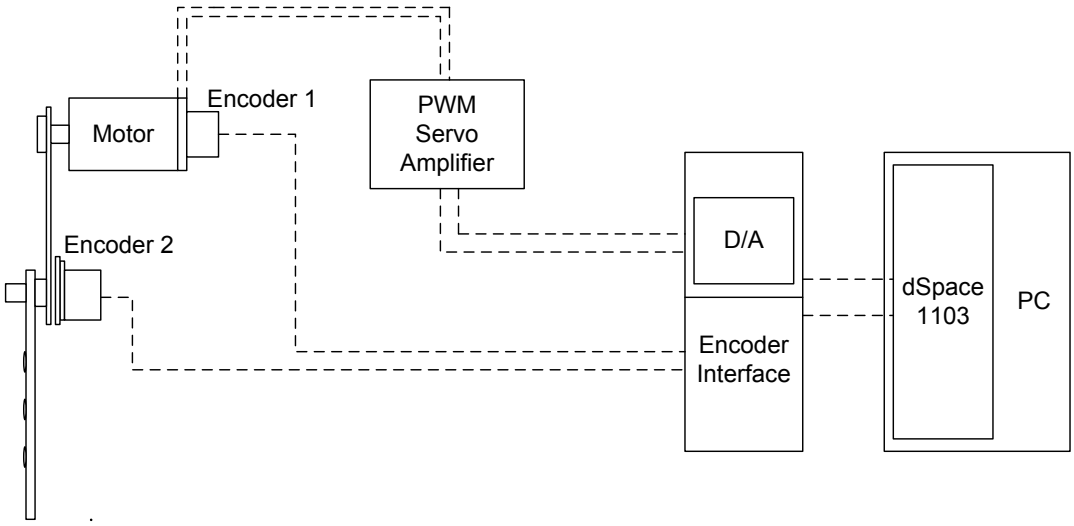


Figure 2.6: The experimental setup for the lab at CU includes a pendubot with an inner link that is approximately six inches and the outer link is approximately nine inches. Only the inner link is connected to a motor, while both links include a quadrature encoder for measuring position with a resolution of $2\pi/5000$. Control designs are implemented using Simulink and a dSpace 1103 PPC controller board with a sampling rate 0f $400Hz$.

2.7 Practical System Brake (L_gV Control)

The pendubot in the inverted position is unstable system and can quickly pump unwanted amounts of energy into the system that could be potentially damaging. In this section, we design a braking mechanism which will dampen the energy out of the system, as quickly as possible, when either of the pendubot links exceed a predetermined threshold. To this end, we have developed an L_gV controller which will be activated when either of the links exceed some predetermined velocity.

2.7.1 General Theory

Given a function $h : \mathbb{R}^n \to \mathbb{R}$ and a vector field $f : \mathbb{R}^n \to \mathbb{R}$ the Lie derivative of h with respect to f as:

$$L_f h(x) \equiv Dh(x) \cdot f(x) = \sum_i \frac{\partial h(x)}{\partial x_i} \cdot f_i(x)$$

Assume we had the following affine single input system

$$\dot{x} = f(x) + g(x)u$$

In this case, we would like to dampen the energy, h, out of the system. So,

$$h(x) = T + V$$

$$\begin{aligned}
\dot{h}(x,u) &= Dh(x)\ \dot{x} \\
&= L_f h(x) + L_g h(x)\ u \\
&= Dh(x) \cdot f(x) + L_g h(x)\ u \\
&= 0 + L_g h(x)\ u \quad \text{(since energy is conserved)} \\
&= L_g h(x)\ u
\end{aligned}$$

The $L_g V$ control is given by

$$u = -k\ L_g h(x)$$

which gives

$$\frac{d}{dt}\{h(x(t))\} = -k\ \left(L_g h(x)\right)^2 \leq 0$$

Note that u is evaluated and applied pointwise.

2.7.2 L_gV Pendubot Design

For the pendubot, the total energy can be written as

$$h = T + V \;=\; \frac{1}{2}\dot{q}^T M(q)\dot{q} + V(q)$$

where $q = (\theta, \varphi)$. The time derivative of the energy can be written as

$$\frac{d}{dt}\{h(x(t)\} = \dot{q}^T M(q)\ddot{q} + \sum_i \frac{\partial}{\partial q_i}\left\{\frac{1}{2}\dot{q}^T M(q)\dot{q} + V(q)\right\}\dot{q}_i$$

(conservation of energy then gives)

$$= \dot{q}^T M(q) M^{-1}(q)\tau$$

$$= \dot{q}^T \tau \qquad \text{(which is power)}$$

Therefore,

$$L_g h(x) = \dot{q}^T \tau$$

$$= \dot{q}_1$$

$$u = -k_p \; L_g h(x)$$

$$= -k_p \dot{q}_1 = -k_p \dot{\theta}$$

After a little experimentation, we found that $k_p = 0.5$ to be an effective value for damping the energy out of our system. In order to determine when to apply the brake we developed a set of simple switching logic which had values that were typically dependent on the desired maneuver. For example, when either link exceeds some predetermined velocity (e.g., based on the maximum velocities of the desired trajectory), then switching logic can be used to switch to this controller to dampen out the energy of the system.

Chapter 3

Inverted Trajectory Exploration

This chapter starts with the development of a general form of the inverted pendulum driven by odd-periodic forcing. Then, we rewrite the problem as a two point boundary value problem and develop a Green's function for an unstable harmonic oscillator with Dirichlet boundary conditions. Using the Schauder fixed point theorem, we then show that the inverted pendulum with an odd periodic driving acceleration at the pivot **always** possesses an odd periodic solution. We also show it is sometimes possible to construct contraction mapping so that the Banach fixed point theorem can be used to ensure that there is a unique solution within an invariant region of the space of possible solution curves before searching for trajectories (e.g. using bvp4c and continuation).

3.1 Constant Velocity Pendubot Equation

As discussed in section 2.3, the outer link dynamics can be written as

$$\ddot{\varphi} = \frac{g}{l}\sin\varphi + \frac{l_1}{l}\dot{\theta}^2(t)\sin\left(\varphi - \theta(t)\right) + \frac{l_1}{l}\ddot{\theta}(t)\cos\left(\varphi - \theta(t)\right)$$

where $l_1 = \mu_3/\mu_5$ is the length of the inner link and $l = \mu_2/\mu_5$ is the inertial length of the outer link. Here, the C^2 inner arm trajectory $\theta(\cdot)$ may be chosen arbitrarily and imposed by an appropriate (state dependent) choice of $\tau(\cdot)$. The motion $\theta(\cdot)$ is odd-periodic if $\theta(t)$ is odd and there is a $T > 0$ such that $\theta(t+T) = \theta(t) \mod 2\pi$ for all t, e.g., $\theta(t+T) = \theta(t) + 2\pi$ for all t. In the case of constant inner arm velocity $\dot{\theta} = 2\pi/T$, we have

$$\ddot{\varphi} = \frac{g}{l}\sin\varphi + \frac{l_1}{l}\left(\frac{2\pi}{T}\right)^2\sin\left(\varphi - (2\pi/T)t\right) \ .$$

Rescaling time, we obtain the normalized, period 2, constant inner arm speed pendubot dynamics

$$\ddot{\varphi} = \alpha^2 \sin\varphi + \beta \sin(\varphi - \pi t) \tag{3.1}$$

where $\alpha = \sqrt{g/l}\ T/2$ and $\beta = \pi^2\, l_1/l$. We will refer to the system (3.1) as the constant velocity pendubot.

3.2 General Equation

The general form of the (unnormalized) inverted pendulum driven by odd periodic forcing is given by

$$l\ddot{\varphi} = g\sin\varphi + a_y(t)\sin\varphi + a_x(t)\cos\varphi \tag{3.2}$$

where the continuous acceleration functions, $a_x(t)$ and $a_y(t)$, are periodic (with common period T) and odd and even, respectively. Defining $a(t) = (a_x^2(t) + a_y^2(t))^{1/2}$, we see that (3.2) is of the form

$$l\ddot{\varphi} = g\sin\varphi + a(t)\sin(\varphi - \psi(t)) \tag{3.3}$$

where $\psi(t)$ satisfies $a_x(t) = -a(t)\sin\psi(t)$ and $a_y(t) = a(t)\cos\psi(t)$. We will restrict our attention to the case where $\psi(t)$ can be chosen to be continuous which occurs, e.g., when $a(t) > 0$ for all t. Clearly, $a(t)$ and $\psi(t)$ are even and odd periodic, respectively, in the sense described above.

Rescaling time so that the system has period 2, we see that the inverted pendulum with odd period forcing has the form

$$\ddot{\varphi} = \alpha^2 \sin\varphi + \beta\,\eta(t)\sin(\varphi - \theta(t)) \tag{3.4}$$

where $\eta(t)$ and $\theta(t)$ are continuous functions that are even and (generalized) odd periodic of period 2, respectively, $|\eta(t)| \le 1$ for $t \in [0,1]$, and $\alpha = \sqrt{g/l}\ T/2$. For the sake of brevity, we will write the general form as

$$\ddot{\varphi} = \alpha^2 \sin\varphi + \beta\, f(\varphi, t) \tag{3.5}$$

where the function $f(\varphi, t) = \eta(t)\sin(\varphi - \theta(t))$ is

- continuously differentiable in φ and continuous in t,
- odd in both arguments: $f(-\varphi, -t) = -f(\varphi, t)$,
- periodic in t with period 2: $f(\varphi, t+2) = f(\varphi, t)$,
- 2π-cyclic in φ: $f(\varphi + 2\pi, t) = f(\varphi, t)$,
- normalized: $|f(\varphi, t)| \leq 1$ for all φ and t,
- bounded derivative: $|\frac{\partial f}{\partial \varphi}(\varphi, t)| \leq 1$ for all φ and t.

Note that (4.4) and hence, (3.5), describes a general driven inverted pendulum and not just the pendubot. Moreover, equation (3.5) parameterizes a family of equations based on two variables, α and β which covers a very general acceleration profile. Important properties of the system are thus characterized by the two numbers: α and β. For the pendubot in our lab at CU the inner link is approximately six inches and the outer link is approximately nine inches. However different versions of the pendubot exist or can be built. See [15], for example, where the inner link was approximately eight inches and the outer link was approximately fourteen inches. The physical pendubot in our lab at CU is characterized by the (identified) parameters $l_1 = 0.149\,m$ and $l = 0.172\,m$ (with $g = 9.81\,m/s^2$) so that $\beta_{\text{CU}} \approx 8.54$ and $\alpha = \alpha_0 T$ with $\alpha_0 \approx 3.78$. In the next sections, we will explore properties of solutions of the inverted pendulum with odd periodic forcing as these parameters vary.

3.3 Trajectory Exploration

In this section we study the solution properties of a family of inverted pendulum systems driven by odd periodic forcing. Using the Schauder fixed point theorem, we show that the inverted pendulum with an odd periodic driving acceleration at the pivot always possesses an odd periodic solution. Fundamental to the production of good estimates is the development of a Green's function for an unstable harmonic oscillator with Dirichlet boundary conditions. We also show that

it is sometimes possible to use the Banach fixed point theorem to ensure that there is a unique solution within an invariant region of the space of possible solution curves. Using these results, we characterize the solutions of periodically driven inverted pendulum systems such as that given by $\ddot{\varphi} = \alpha^2 \sin\varphi + \beta \sin(\varphi - \pi t)$, which describes a pendubot with constant inner arm velocity.

The nonlinear analysis techniques explored include topological [13] as well as analytic techniques (e.g., contraction mapping) that are more commonly known to control engineers. From the topological point of view, we use the Schauder fixed point theorem to show that the inverted pendulum with an odd periodic driving acceleration at the pivot always possesses an odd periodic solution. With an eye toward the development of good estimates, we provide a careful development of a Green's function for an unstable harmonic oscillator with Dirichlet boundary conditions. From the analytic point of view, we show that it is sometimes possible to construct a contraction mapping so that the Banach fixed point theorem can be used to ensure that there is a unique solution within an invariant region of the space of possible solution curves.

Using these techniques we are able to provide insights into the types of trajectories of the inverted pendulum, and hence the trajectories of the pendubot, that are possible with odd periodic forcing. In fact, we are able to show that inverted trajectories exist as the period, T, of the odd periodic forcing term approaches zero.

3.3.1 Operator Equation

We seek an odd periodic solution $\varphi(\cdot)$ with period 2 of (3.5). Since the right hand side of (3.5) is odd with respect to (φ, t), the desired curve may be found by solving the two point boundary value problem

$$\ddot{\varphi} = \alpha^2 \sin\varphi + \beta\, f(\varphi, t)\,, \quad \varphi(0) = 0 = \varphi(1) \tag{3.6}$$

for $\varphi(t)$, $t \in [0,1]$. That is, the curve $\varphi(t)$, $t \in [0,1]$, can be extended (in the obvious way) to an odd periodic solution of (3.5). Now, writing the dynamics as

$$\ddot{\varphi} = \alpha^2\varphi - \alpha^2 \left[(\varphi - \sin\varphi) - \beta/\alpha^2\, f(\varphi, t)\right]\,, \tag{3.7}$$

we see that $\varphi(\cdot)$ is a solution to the boundary value problem if and only if it is a fixed point of the nonlinear operator

$$\mathcal{N}_\alpha^\beta[\varphi(\cdot)] = \mathcal{A}_\alpha[\,\mathcal{M}(\varphi(\cdot),\cdot)\,]$$

where $\mathcal{M}[\,\cdot\,]$ is the superposition (or Nemitski) operator

$$\mathcal{M}[\varphi(\cdot)](t) = \varphi(t) - \sin\varphi(t) - \beta/\alpha^2\, f(\varphi(t), t)$$

and $\mathcal{A}_\alpha[\,\cdot\,]$ is the linear operator $\mu(\cdot) \mapsto \gamma(\cdot)$ given by the linear boundary value problem

$$\ddot{\gamma} - \alpha^2\gamma = -\alpha^2\mu(t)\,, \quad \gamma(0) = 0 = \gamma(1)\,. \tag{3.8}$$

Thus, the two point boundary value problem (3.6) is equivalent to the operator equation $\varphi(\cdot) = \mathcal{N}_\alpha^\beta[\varphi(\cdot)]$. For brevity, we will sometimes fix β and write $\varphi = \mathcal{N}_\alpha[\,\varphi\,]$.

3.3.2 Green's Functions for Unstable Oscillators

The linear differential operator $\mathcal{A}_\alpha[\,\cdot\,]$ can be rewritten as an integral operator whose kernel is called a Green's function of the differential operator. As we will see, the integral operator is a bounded operator which we can use to study the properties of the unbounded differential operator $\mathcal{A}_\alpha[\,\cdot\,]$. In this section, we explore the properties of the Green's function for the unstable harmonic oscillator with Dirichlet boundary conditions and show that the operator $\mathcal{A}_\alpha[\,\cdot\,]$ is a compact operator.

Consider the family of linear systems,

$$\ddot{\gamma} - \alpha^2\gamma = -\alpha^2\mu(t)\,, \tag{3.9}$$

parameterized by $\alpha > 0$ and driven by a bounded input $\mu(\cdot)$. Let $\mathcal{A}_\alpha$ be the operator that maps a bounded $\mu(\cdot)$ to the solution curve $\gamma(\cdot)$ of the linear two point boundary value problem

$$\ddot{\gamma} - \alpha^2\gamma = -\alpha^2\mu(t)\,, \quad \gamma(0) = 0 = \gamma(1)\,. \tag{3.10}$$

To see that, for each $\alpha > 0$, the operator $\mathcal{A}_\alpha$ is well defined, note that the solution of (3.9) with initial values $\gamma(0) = 0$, $\dot\gamma(0) = \dot\gamma_0$ is given by

$$\begin{aligned}\gamma(t) \;=\; & \tfrac{1}{2\alpha}\left(e^{\alpha t} - e^{-\alpha t}\right)\dot\gamma_0 \\ & - \int_0^t \tfrac{\alpha}{2}\left(e^{\alpha(t-s)} - e^{-\alpha(t-s)}\right)\mu(s)\,ds\,.\end{aligned} \tag{3.11}$$

Since $\alpha > 0$, the system (3.9) is hyperbolic so that the map $\dot\gamma_0 \mapsto \gamma(1)$ is onto, and $\gamma(1) = 0$ is obtained using

$$\dot\gamma_0 = \tfrac{\alpha^2}{e^\alpha - e^{-\alpha}} \int_0^1 \left(e^{\alpha(1-s)} - e^{-\alpha(1-s)}\right)\mu(s)\,ds\,.$$

Substituting $\dot\gamma_0$ into (3.11), we see that the desired map $\mathcal{A}_\alpha : \mu(\cdot) \mapsto \gamma(\cdot)$ is well defined and given by

$$\gamma(t) = \int_0^1 g_\alpha(t,s)\mu(s)\,ds\,, \quad t \in [0,1]\,, \tag{3.12}$$

where

$$g_\alpha(t,s) := \begin{cases} \alpha\left[\frac{\sinh \alpha t}{\sinh \alpha}\sinh\alpha(1-s) - \sinh\alpha(t-s)\right], & s \le t, \\ \alpha\left[\frac{\sinh \alpha t}{\sinh \alpha}\sinh\alpha(1-s)\right], & t < s. \end{cases}$$

Simplifying the $s \le t$ expression, we find that the Green's function is, as expected, symmetric, $g_\alpha(t,s) = g_\alpha(s,t)$, with

$$g_\alpha(t,s) = \begin{cases} \frac{\alpha}{\sinh\alpha}\sinh\alpha s\,\sinh\alpha(1-t)\,, & s \le t\,, \\ \frac{\alpha}{\sinh\alpha}\sinh\alpha t\,\sinh\alpha(1-s)\,, & t < s\,. \end{cases}$$

Lemma 3. *The Green's function $g_\alpha(t,s)$ is continuous and nonnegative on the square $[0,1]\times[0,1]$ for each $\alpha > 0$.*

Proof. Fix $\alpha > 0$ and note that $g_\alpha(t,s)$ is continuous on the line $s = t$ and thus continuous on the square. Clearly, $g_\alpha(t,s) \ge 0$ for $t \le s$. For the other case, define $r_s(t) = \sinh\alpha(t-s)\,/\,\sinh\alpha t$ and note that $g_\alpha(t,s) \ge 0$, $t \ge s > 0$, is equivalent to $r_s(t) \le r_s(1)$, $t \ge s > 0$. The result follows since $r_s'(t) = 2\alpha\sinh\alpha s\,/\,\sinh^2\alpha t > 0$ for all $t \ge s > 0$. □

Since $g_\alpha(t,s)$ is nonnegative on the square $[0,1]^2$, we find that

$$|\gamma(t)| \le \tilde{g}_\alpha(t)\,\|\mu(\cdot)\|$$

so that

$$\tilde{g}_\alpha(t) := \int_0^1 g_\alpha(t,s)\,ds = 1 - \frac{\sinh\alpha t + \sinh\alpha(1-t)}{\sinh\alpha}$$

provides a pointwise upper bound on the response. Furthermore, since $\tilde{g}'_\alpha(1/2) = 0$ and $\tilde{g}''_\alpha(t) < 0$, $t \in [0,1]$, the maximum value of $\tilde{g}_\alpha(\cdot)$ occurs at $t = 1/2$. Defining $\bar{g}(\alpha) := \max_{t\in[0,1]} \tilde{g}_\alpha(t)$, we see that the norm (or gain) of the operator $\mathcal{A}_\alpha$ is given by

$$\|\mathcal{A}_\alpha\| = \bar{g}(\alpha) = 1 - 1\,/\cosh\alpha/2$$

where the valid input $\mu(t) = 1$, $t \in [0,1]$, achieves the bound. The bound $\bar{g}(\cdot)$ is monotonically increasing with $\lim_{\alpha\to\infty}\bar{g}(\alpha) = 1$. Also, it is little surprise that $\bar{g}(0) = 0$, since no input comes into the system in the limit $\alpha = 0$.

Now, using (3.11), it is easy to see that, for each bounded $\mu(\cdot)$, the resulting $\gamma(\cdot)$ is continuously differentiable on the open interval $(0,1)$. Indeed, differentiating (3.11) and collecting terms and simplifying, we find that the operator $\dot{\mathcal{A}}_\alpha$ mapping $\mu(\cdot)$ to $\dot{\gamma}(\cdot)$ is given by

$$\dot{\gamma}(t) = \int_0^1 \dot{g}_\alpha(t,s)\mu(s)\,ds\,, \quad t \in [0,1]\,,$$

where

$$\dot{g}_\alpha(t,s) := \begin{cases} -\frac{\alpha^2}{\sinh\alpha}\sinh\alpha s\,\cosh\alpha(1-t)\,, & s \le t\,, \\ \\ \frac{\alpha^2}{\sinh\alpha}\cosh\alpha t\,\sinh\alpha(1-s)\,, & t < s\,. \end{cases}$$

Note that $\dot{g}_\alpha(t,s) = \frac{\partial}{\partial t}g(t,s)$ for $t \neq s$ and that the value of $\dot{g}_\alpha(t,s)$ at $t = s$ where $t \mapsto g_\alpha(t,s)$ is **not** differentiable is immaterial.

Clearly, $\dot{\mathcal{A}}_\alpha$ is a bounded linear operator. To develop explicit bounds, note that

$$|\dot{\gamma}(t)| \le \dot{\tilde{g}}_\alpha(t)\|\mu(\cdot)\|$$

where $\dot{\tilde{g}}_\alpha(t) := \int_0^1 |\dot{g}_\alpha(t,s)|\, ds$ is given by

$$\dot{\tilde{g}}_\alpha(t) = \alpha \frac{\cosh\alpha - \cosh\alpha t - \cosh\alpha(1-t) + \cosh\alpha(1-2t)}{\sinh\alpha}$$

Lemma 4. $\dot{\tilde{g}}_\alpha(t) \le \alpha \tanh\alpha/2$ *for all* $t \in [0,1]$ *with equality holding at* $t = 0$ *and* $t = 1$.

Proof. Equality at $t = 0$ and $t = 1$ is easily verified. The inequality is equivalent to

$$1 + \cosh\alpha(2t-1) \le 2\cosh\alpha/2 \;\cosh\alpha(2t-1)/2\,.$$

The result follows easily by noting that hyperbolic cosine curves $\tau \mapsto 1 + \cosh\tau$ and $\tau \mapsto b\cosh\tau/2$ can intersect in at most two places, $\tau = \pm\tau_0$ for some $\tau_0 \ge 0$. □

Thus, defining $\dot{\bar{g}}(\alpha) := \max_{t\in[0,1]} \dot{\tilde{g}}_\alpha(t)$, we find that

$$\|\dot{\mathcal{A}}_\alpha\| = \dot{\bar{g}}(\alpha) = \alpha\tanh\alpha/2\,.$$

Note that the dots in $\dot{\bar{g}}(\alpha)$ and $\dot{\tilde{g}}_\alpha(t)$ indicate that these are bounds for $\dot{\gamma}(t)$—they are suggestive rather than operational.

Since $\mathcal{A}_\alpha$ maps bounded functions on $[0,1]$ into continuously differentiable functions on $[0,1]$ in a uniform manner, we obtain the well known result:

Proposition 5. $\mathcal{A}_\alpha$ *is a compact linear operator.*

The operator $\mathcal{A}_\alpha/\alpha^2$ maps bounded $\mu(\cdot)$ to $\gamma(\cdot)$ satisfying the related linear boundary value problem,

$$\ddot{\gamma} - \alpha^2\gamma = -\mu(t)\,, \quad \gamma(0) = 0 = \gamma(1)\,, \tag{3.13}$$

and has norm (or gain)

$$\left\|\mathcal{A}_\alpha/\alpha^2\right\| = \bar{g}(\alpha)/\alpha^2 =: \breve{g}(\alpha)\,.$$

Lemma 6. *The function* $\breve{g}(\cdot)$ *is strictly decreasing on* $[0,\infty)$*, and satisfies* $\lim_{\alpha\to 0}\breve{g}(\alpha) = 1/8$ *and* $\breve{g}(\alpha) \to 0$ *as* $\alpha \to \infty$.

Proof. $\breve{g}'(\alpha) < 0$, $\alpha > 0$, follows from the fact that

$$(\alpha/4)\tanh\alpha/2 < \alpha^2/8 < \cosh\alpha/2 - 1\,, \quad \alpha \neq 0.$$

The limit $\breve{g}(0) = 1/8$ is easily derived using the L'Hôpital rule and the limit $g(+\infty) = 0$ is immediate. □

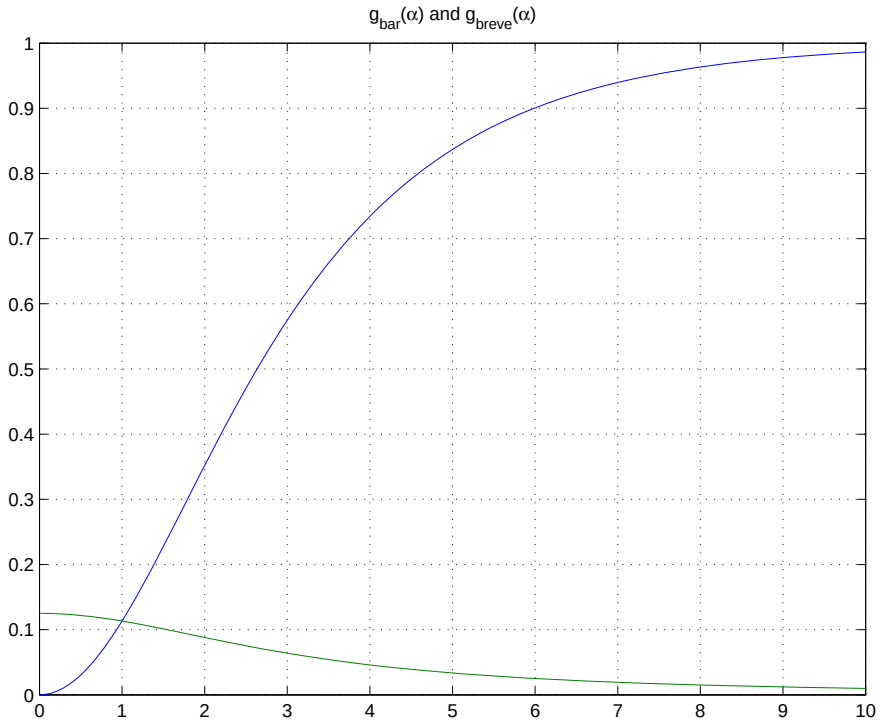


Figure 3.1: Operator norms $\bar{g}(\alpha) = \|\mathcal{A}_\alpha\|$ and $\breve{g}(\alpha) = \|\mathcal{A}_\alpha/\alpha^2\|$ versus α.

We can go one step further and see that the Green's function for $\mathcal{A}_\alpha/\alpha^2$ given by $h_\alpha(t,s) := g_\alpha(t,s)/\alpha^2$ converges (as $\alpha \to 0$) to the Green's function for $\ddot{\gamma} = -\mu(t)$, $\gamma(0) = 0 = \gamma(1)$, given by

$$h_0(t,s) = \begin{cases} s(1-t)\,, & s \leq t\,, \\ t(1-s)\,, & t \leq s\,. \end{cases}$$

Here, as with $g_\alpha(t,s)$, $h_0(t,s) \geq 0$ so that

$$|\gamma(t)| \leq \tilde{h}_0(t)\|\mu(\cdot)\|$$

where

$$\tilde{h}_0(t) := \int_0^1 h_0(t,s)\,ds = t(1-t)/2\,.$$

Defining $\bar{h}(\alpha) = \max_{t\in[0,1]} \tilde{h}_\alpha(t)$, we see that the norm of this operator is $\bar{h}(0) = 1/8 = \breve{g}(0)$.

3.3.3 Invariance

In the search for periodic solutions or, equivalently, fixed points of $\mathcal{N}_\alpha^\beta[\,\cdot\,]$, we begin by describing invariant sets of $\mathcal{N}_\alpha^\beta[\,\cdot\,]$.

Proposition 7. *The set*

$$\bar{B}_\delta = \{\varphi(\cdot) \in L_\infty : \|\varphi(\cdot)\| \le \delta\}$$

is invariant under $\mathcal{N}_\alpha^\beta[\,\cdot\,]$, $\mathcal{N}_\alpha^\beta[\,\bar{B}_\delta\,] \subset \bar{B}_\delta$, if

$$\bar{g}(\alpha)\,(\delta - \sin\delta) + \breve{g}(\alpha)\,\beta \le \delta\,. \tag{3.14}$$

Proof. Let $\|\varphi(\cdot)\| \le \delta$ and note that

$$\begin{aligned}
\|\,\mathcal{N}_\alpha^\beta[\varphi(\cdot)]\,\| &= \|\,\mathcal{A}_\alpha[\,\varphi(\cdot) - \sin\varphi(\cdot) - \beta/\alpha^2\, f(\varphi(\cdot),\cdot)\,]\,\| \\
&\le \bar{g}(\alpha)\,\|\varphi(\cdot) - \sin\varphi(\cdot)\| + \beta\bar{g}(\alpha)/\alpha^2 \\
&= \bar{g}(\alpha)\,\|\varphi(\cdot) - \sin\varphi(\cdot)\| + \breve{g}(\alpha)\,\beta \\
&\le \bar{g}(\alpha)\,(\delta - \sin\delta) + \breve{g}(\alpha)\,\beta
\end{aligned}$$

since $\delta \mapsto \delta - \sin\delta$ is a strictly increasing function. □

This leads us to the consideration of the fixed points of the scalar operator $\delta \mapsto h(\delta) = h(\delta;\alpha,\beta)$ where

$$h(\delta;\alpha,\beta) := \bar{g}(\alpha)\,(\delta - \sin\delta) + \breve{g}(\alpha)\,\beta \tag{3.15}$$

is defined for $\delta \in [0,\infty)$. We denote the first positive fixed point by

$$\delta_0(\alpha,\beta) := \min\{\delta > 0 : h(\delta;\alpha,\beta) = \delta\}\,. \tag{3.16}$$

The fixed points of (3.15), such as the smallest fixed point, $\delta_0(\alpha, \beta)$, are important and will resurface in many of the following sections.

Facts:

- For all $\alpha > 0$ and all $\beta > 0$, $h(\cdot)$ has at least one fixed point.

  Noting, as shown in figure 3.2, that $\epsilon = h(\delta)$ is bounded above and below by $\epsilon = \bar{g}(\alpha)(\delta + 1) + \beta\breve{g}(\alpha)$ and $\epsilon = \max\{\bar{g}(\alpha)(\delta - 1) + \beta\breve{g}(\alpha), \beta\breve{g}(\alpha)\}$, respectively, we see that every fixed point of $h(\cdot)$ lies in $[\delta_-, \delta_+]$ with

  $$\delta_+ = (\beta\breve{g}(\alpha) + \bar{g}(\alpha))/(1 - \bar{g}(\alpha)),$$
  $$\delta_- = \max\{(\beta\breve{g}(\alpha) - \bar{g}(\alpha))/(1 - \bar{g}(\alpha)), \beta\breve{g}(\alpha)\},$$

  and that, since $h(\cdot)$ is continuous, there is at least one fixed point.

- For each $\alpha > 0$, the function $\beta \mapsto \delta_0(\alpha, \beta)$ is strictly increasing.

- The set $[0, \delta_0(\alpha, \beta)]$ is invariant under $h(\cdot)$.

- If there is only one fixed point, then $[0, \delta]$ is invariant for every $\delta \geq \delta_0(\alpha, \beta)$, and the iteration $\delta^{k+1} = h(\delta^k)$ converges to $\delta_0(\alpha, \beta)$ from every $\delta^0 \geq 0$.

- If there is more than one fixed point and $\bar{g}(\alpha)(1 - \cos\delta_0(\alpha, \beta)) < 1$, then the set $[0, \delta]$ is invariant for each $\delta \in [\delta_0(\alpha, \beta), \delta_1(\alpha, \beta))$, where $\delta_1(\alpha, \beta)$ denotes the second positive fixed point. Moreover, $\delta^k \to \delta_0(\alpha, \beta)$ for each $\delta^0 \in [0, \delta_1(\alpha, \beta))$ so that $\delta_0(\alpha, \beta)$ is a stable fixed point of the discrete time system $\delta^{k+1} = h(\delta^k)$.

- Independent of the number of fixed points, the sequence $\{\delta^k\}_{k=0}^{\infty}$ starting from $\delta^0 = 0$ converges to $\delta_0(\alpha, \beta)$. That is, $\delta_0(\alpha, \beta)$ is always attractive from the left. This will be shown below.

Lemma 8. *Suppose that $h : \mathbb{R}_+ \to \mathbb{R}_+$ is C^1 with $h'(\delta) > 0$ for almost all $\delta \in \mathbb{R}_+$. Then $h(\delta) > \delta$ implies that $h(\epsilon) > \epsilon$ for all $\epsilon \in [\delta, h(\delta)]$. For the weaker case with $h'(\delta) \geq 0$, $\delta \in \mathbb{R}_+$, $h(\delta) \geq \delta$ implies that $h(\epsilon) \geq \epsilon$ for all $\epsilon \in [\delta, h(\delta)]$. Similar results are obtain for $<$ and $\leq$.*

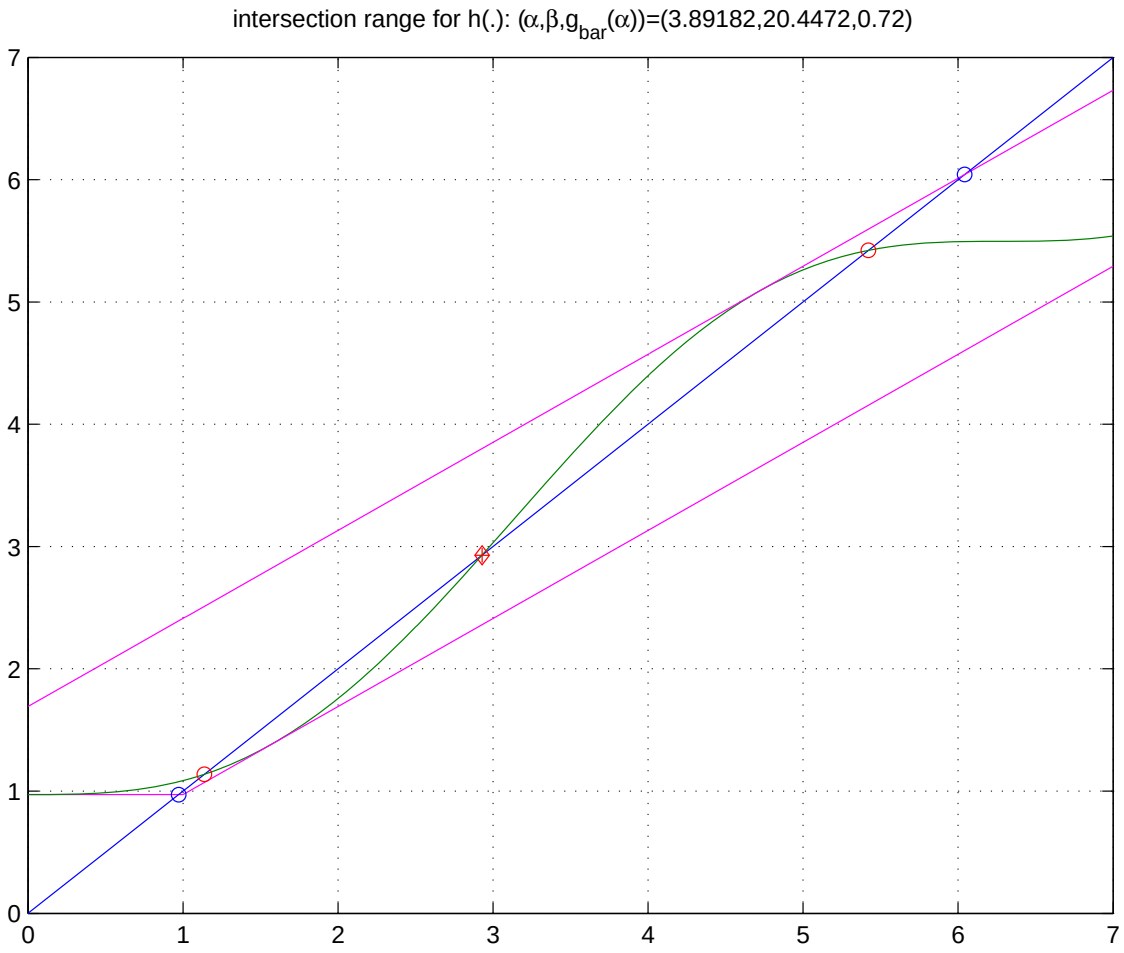


Figure 3.2: The fixed points of $h(\cdot)$ lie within an easily calculated range.

Proof. Set $g(\delta, \epsilon) = \int_0^1 h'(\delta + s(\epsilon - \delta))\, ds$ and note that, by the fundamental theorem of calculus,

$$h(\epsilon) = h(\delta) + g(\delta, \epsilon) \cdot (\epsilon - \delta)\,.$$

Thus, when $h'(\delta) > 0$ almost everywhere, we see that $\epsilon > \delta$ implies that $g(\delta, \epsilon) \cdot (\epsilon - \delta) > 0$ and $h(\epsilon) > h(\delta)$ so that $h(\cdot)$ is strictly increasing. Thus, for $\epsilon \in (\delta, h(\delta)]$,

$$h(\epsilon) > h(\delta) \geq \epsilon$$

so that $h(\epsilon) > \epsilon$ as desired. The weaker case follows directly. □

Proposition 9. *Suppose that $h : \mathbb{R}_+ \to \mathbb{R}_+$ is C^1, strictly increasing ($h'(\delta) > 0$ for almost all $\delta \in \mathbb{R}_+$), and such that $h(0) > 0$ and $h(\gamma) \leq \gamma$ for some $\gamma > 0$. Then the sequence $\{\delta^k\}_{k=0}^{\infty}$ obtained using*

$$\delta^{k+1} = h(\delta^k), \quad \delta^0 = 0,$$

is strictly increasing and converges to δ^*, the smallest (positive) fixed point of $h(\cdot)$. If the hypothesis on $h(\cdot)$ is weakened to $h'(\delta) \geq 0$, $\delta \in \mathbb{R}_+$, the sequence $\{\delta^k\}$ is nonincreasing and again converges to δ^*. If there is an $\epsilon > 0$ such that $h'(\delta) = 0$ for $\delta \in (\epsilon, \delta^*)$, then $\delta^k \to \delta^*$ in a finite number of steps.

Proof. Since $h(\delta^0) > \delta^0$, we see, by Lemma 8, that $\delta^{k+1} = h(\delta^k) > \delta^k$ for all $k \geq 0$ and, furthermore, that $h(\delta) > \delta$ for $\delta \in [0, \delta^k]$ for every $k \geq 0$. Thus, since $\delta^k < \gamma$ for all k, we see $\delta^k \to \delta^*$ for some $\delta^* \leq \gamma$. Since $\epsilon^k = h(\delta^k)$ also converges to δ^* and $h(\cdot)$ is continuous, we conclude that δ^* is a fixed point, $\delta^* = h(\delta^*)$. Furthermore, δ^* is the smallest positive fixed point since $h(\delta) > \delta$ for all $\delta < \delta^*$.

Under the weaker hypothesis, it is clear that $\{\delta^k\}$ is either strictly increasing or converges in finite steps and that, if it converges, then it must converge to a fixed point. Letting δ^* be the smallest positive fixed point, we claim that $\delta^k \leq \delta^*$ for all k. If not, there is a k_0 such that $\delta^{k_0} < \delta^* < \delta^{k_0+1} = h(\delta^{k_0})$. In that case, we see that $\delta^* > \delta^{k_0}$ and $h(\delta^*) < h(\delta^{k_0})$ which contradicts the fact that $h(\cdot)$ is nondecreasing. The result follows. □

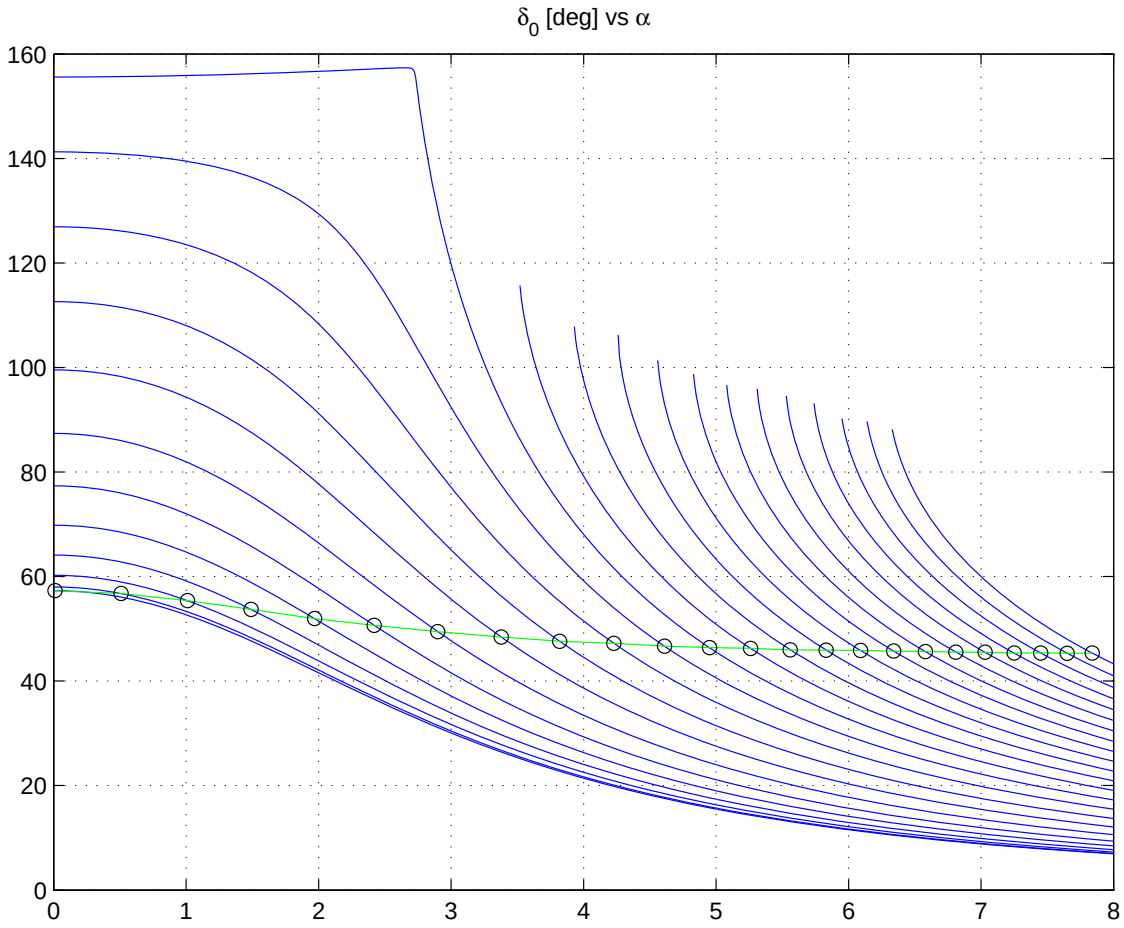


Figure 3.3: Invariant region estimates: $\alpha \mapsto \delta_0(\alpha, \beta)$ for a selection of β values ranging from 8 up to 46. Note that, for β greater than ≈ 21.7, the associated curve is not continuous at all α; the continuous from the right portion of each of those curves is shown (the other part of each curve lies outside of the chosen δ range). Also depicted on each curve (with a circle) is the value of α above which $\mathcal{N}_\alpha^\beta$ is guaranteed to be a contraction on the corresponding closed ball.

Thus, since $\delta \mapsto h(\delta;\alpha,\beta)$ is strictly increasing and satisfies the other conditions of Proposition 9, we see that $\delta_0(\alpha,\beta)$ is easily computed by successive approximation using $\delta^{k+1} = h(\delta^k)$ with $\delta^0 = 0$. Furthermore, the set $\bar{B}_\delta$ with $\delta = \delta_0(\alpha,\beta)$ is invariant under the corresponding operator $\mathcal{N}_\alpha^\beta[\,\cdot\,]$. Note that the mapping $(\alpha,\beta) \mapsto \delta_0(\alpha,\beta)$ is not continuous at every (α,β). In fact, $\beta = 4\pi(\cosh^{-1}(2))^2 \approx 21.7948$ is a critical value above which the curve associated with $\alpha \mapsto \delta_0(\alpha,\beta)$ will not be continuous. Figure 3.3 depicts the function $\alpha \mapsto \delta_0(\alpha,\beta)$ for a number of different β values.

3.3.4 Existence

Now that we have invariant sets of $\mathcal{N}_\alpha^\beta$, we can use the Schauder fixed point theorem to show that the two point boundary value problem (3.6) possesses a C^2 solution for all α and β and that $\mathcal{N}_\alpha^\beta$ always has a fixed point.

Proposition 10. *Given $\alpha > 0$ and $\beta > 0$, the two point boundary value problem (3.6) possesses a C^2 solution satisfying $|\varphi(t)| \le \delta_0(\alpha,\beta)$, $t \in [0,1]$.*

Proof. Let $\delta = \delta_0(\alpha,\beta)$ and note that, by proposition 7, the convex closed set $\mathcal{B} = \bar{B}_\delta$ is invariant under $\mathcal{N}_\alpha^\beta$. Now, the functions $\psi \in \mathcal{N}_\alpha^\beta[\mathcal{B}]$ are all such that $|\dot{\psi}(t)| \le \dot{\bar{g}}(\alpha)\,(\delta - \sin\delta + \beta/\alpha^2)$ so that $\mathcal{N}_\alpha^\beta[\mathcal{B}]$ is an equicontinuous family and $\mathcal{N}_\alpha^\beta : \mathcal{B} \to \mathcal{B}$ is a compact map. Thus, by the Schauder fixed point theorem, there is a $\varphi(\cdot) \in \mathcal{B}$ such that $\varphi = \mathcal{N}_\alpha^\beta[\,\varphi\,]$, so that $\varphi(\cdot)$ is a solution of (3.6). That $\varphi(\cdot)$ is C^2 follows immediately. □

We saw that $\varphi(\cdot)$ is a solution to the boundary value problem if and only if it is a fixed point of the nonlinear operator $\mathcal{N}_\alpha^\beta[\varphi(\cdot)] = \mathcal{A}_\alpha[\,\mathcal{M}((\cdot),\cdot)\,]$ and hence, the two point boundary value problem (3.6) was equivalent to $\varphi(\cdot) = \mathcal{N}_\alpha[\varphi(\cdot)]$. However, we can define a different nonlinear operator

$$\bar{\mathcal{N}}_\alpha[\varphi(\cdot)] = \mathcal{B}[\,\mathcal{M}_1\,]$$

where $\mathcal{M}_1[\varphi(\cdot)](t) = \alpha^2 \sin\varphi(t) - \beta\, f(\varphi(t),t)$ and $\mathcal{B}$ is the linear operator $\mu(\cdot) \mapsto \gamma(\cdot)$ given by

the linear boundary value problem

$$\ddot{\gamma} = \mu(t), \;\; \gamma(0) = 0 = \gamma(1).$$

It is not hard to show that $\|\mathcal{B}\| = 1/8$. Hence, $\bar{B}_{\frac{\alpha^2+\beta}{8}}$ is invariant under $\bar{\mathcal{N}}$.

It is clear that $\delta_0(\alpha, \beta)$ is piecewise continuous in α for a fixed β. In addition, $\delta_0(\alpha, \beta)$ will only have downward jumps. For some choices of α and β, $\bar{B}_{\frac{\alpha^2+\beta}{8}}$ will be a better estimate of the invariant region.

Combining the two estimates, we see that for a given β, there exists an α such that $\mathcal{N}_\alpha^\beta$ or $\bar{\mathcal{N}}$ is invariant on $\bar{B}_{\delta_1(\alpha,\beta)}$. The size of the invariant region is always bounded by a piecewise continuous function $\delta_1(\alpha, \beta) = \min\left\{\frac{\alpha+\beta^2}{8}, \delta_0(\alpha, \beta)\right\}$. The invariant region for both estimates start at β/8 and, as a function of α, the estimate from $\bar{\mathcal{N}}$ increases while the estimate from $\mathcal{N}_\alpha$ goes to 0 asymptotically. In particular, for $\beta > 4\pi(cosh^{-1}(2))^2 \approx 21.7948$, the bound on the invariant region will result in the $\frac{\alpha+\beta^2}{8}$ being smaller for some α. Figure 3.4 shows the estimates of the invariant regions when $\beta \approx 25.6128$.

3.3.5 Contraction & Uniqueness

In the dual interests of obtaining an algorithm for computing a periodic solution $\varphi(\cdot)$ and determining when it is unique, we now seek conditions under which $\mathcal{N}_\alpha^\beta$ is a contraction.

Define $p(\delta) := \delta - \sin\delta$ and

$$q(\delta) := \max_{|\epsilon|\le\delta} |p'(\epsilon)| = \begin{cases} 1 - \cos\delta\,, & \delta \le \pi \\ 2\,, & \delta > \pi \end{cases} \tag{3.17}$$

and note that

$$|(\varphi_1 - \sin\varphi_1) - (\varphi_2 - \sin\varphi_2)| \le q(\delta)\,|\varphi_1 - \varphi_2|$$

for all φ_1, φ_2 such that $|\varphi_1| \le \delta$ and $|\varphi_2| \le \delta$. Note also that $|f(\varphi_1, t) - f(\varphi_2, t)| \le |\varphi_1 - \varphi_2|$ for all φ_1, φ_2 and for all t. We have the following result.

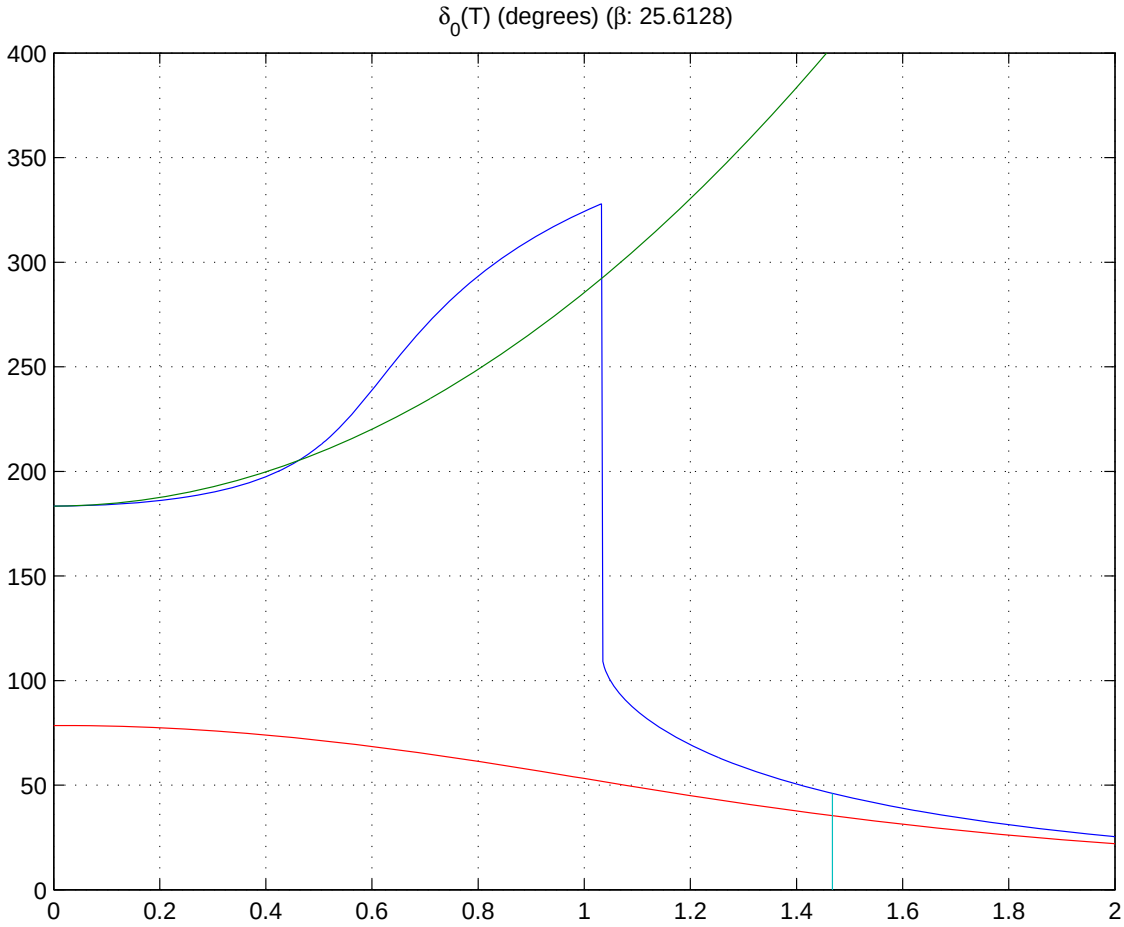


Figure 3.4: Estimates of Invariant Regions for $\beta \approx 25.6128$ using the smaller of two estimates that both start at $\beta/8$. The size of the invariant region is always bounded by a piecewise continuous function $\delta_1(\alpha, \beta) = \min\left\{\frac{\alpha+\beta^2}{8}, \delta_0(\alpha, \beta)\right\}$.

Proposition 11. *Let $\alpha > 0$ and $\beta > 0$ be given and suppose that $\delta > 0$ is such that $\mathcal{B} = \bar{B}_\delta$ is invariant under $\mathcal{N}_\alpha^\beta$. If*

$$\bar{g}(\alpha)\, q(\delta) + \breve{g}(\alpha)\, \beta < 1 \tag{3.18}$$

then $\mathcal{N}_\alpha^\beta : \mathcal{B} \to \mathcal{B}$ is a contraction and the nonlinear boundary value problem (3.6) possesses a unique solution $\varphi(\cdot)$ in $\mathcal{B}$.

Proof. Let $\varphi_1(\cdot), \varphi_2(\cdot) \in \mathcal{B}$ and note that

$$\begin{aligned}
&\| \mathcal{N}_\alpha^\beta[\varphi_1(\cdot)] - \mathcal{N}_\alpha^\beta[\varphi_2(\cdot)] \| \\
&\quad = \| \mathcal{A}_\alpha[(\varphi_1(\cdot) - \sin\varphi_1(\cdot)) - (\varphi_2(\cdot) - \sin\varphi_2(\cdot))] \\
&\qquad\qquad - \beta\mathcal{A}/\alpha^2[f(\varphi_1(\cdot),\cdot) - f(\varphi_2(\cdot),\cdot)] \| \\
&\quad \leq (\bar{g}(\alpha)\, q(\delta) + \breve{g}(\alpha)\, \beta) \| \varphi_1(\cdot) - \varphi_2(\cdot) \|
\end{aligned}$$

so that $\mathcal{N}_\alpha^\beta$ is contractive on the closed invariant set $\mathcal{B}$. Uniqueness (and existence) follows from the Banach fixed point theorem. □

When the contraction property holds for $\mathcal{N}_\alpha^\beta$ on an invariant set $\bar{B}_\delta$, the (unique) solution trajectory $\varphi(\cdot)$ may be computed using successive approximations $\varphi_{i+1} = \mathcal{N}_\alpha^\beta[\varphi_i(\cdot)]$ starting from, e.g., $\varphi_0(\cdot) \equiv 0$. Note that the contractive condition (3.18) is rather restrictive and is only satisfied on a subset of possible values of α and β.

Figure 3.3 illustrates the nature of the condition for contraction. In that figure, circles are used to depict, for each of the selected β s, the value of α (and the corresponding δ_0) above which the contractive condition (3.18) is satisfied. Indeed, it appears that

- For each $\alpha > 0$, there is a $\beta_0 = \beta_0(\alpha) > 0$ such that

  $$\bar{g}(\alpha)\, q(\delta_0(\alpha,\beta)) + \breve{g}(\alpha)\, \beta < 1$$

  for all $\beta \in (0, \beta_0(\alpha))$.

- Given $\alpha_0 > 0$ and setting $\beta_0 = \beta_0(\alpha_0)$,

$$\bar{g}(\alpha)\, q(\delta_0(\alpha, \beta_0)) + \breve{g}(\alpha)\, \beta_0 < 1$$

  for all $\alpha > \alpha_0$.

- $\alpha \mapsto \beta_0(\alpha)$ is strictly increasing, and $\beta_0(\alpha) > 8$ for all $\alpha > 0$.

- $\delta_0(\alpha, \beta_0(\alpha)) < 1$ for all $\alpha > 0$.

3.4 Specialization to the Constant Velocity Pendubot

Remember from (3.1), that the dynamics for a constant inner arm velocity can be written as

$$\ddot{\varphi} = \alpha^2 \sin\varphi + \beta \sin(\varphi - \pi t) \tag{3.19}$$

where $\alpha = \sqrt{g/l}\; T/2$ and $\beta = \pi^2\, l_1/l$. The physical pendubot in our lab at CU is characterized by the (identified) parameters $l_1 = 0.149\, m$ and $l = 0.172\, m$ (with $g = 9.81\, m/s^2$) so that $\beta_{\text{CU}} \approx 8.54$ and $\alpha = \alpha_0 T$ with $\alpha_0 \approx 3.78$.

Intuitively, it is clear that, when the period T is large so that the inner arm moves slowly, there will be a pendubot trajectory in which the outer link trajectory $\varphi(\cdot)$ remains very close to zero at all times. This is due to the fact that the primary acceleration seen at the pivot will be gravity, pushing up on the inverted pendulum. On the other hand, when the period T is very short (even approaching zero), a substantial centripetal acceleration will be present at the pivot, more than overcoming gravity resulting in the pendulum being pulled down (rather than pushed up) at the top of the inner arm cycle. Intuition for this case is somewhat hard to come by.

Figure 3.5 helps us to develop our intuition for what the periodic trajectories look like as the motion becomes faster and faster. First, note that we are guaranteed that, even as T goes to zero, there will be a periodic trajectory that does not exceed 62 degrees for β_{CU}. Furthermore, provided we choose $T > 0.31$ and β_{CU}, we can use the successive approximation approach to compute the **unique** periodic trajectory.

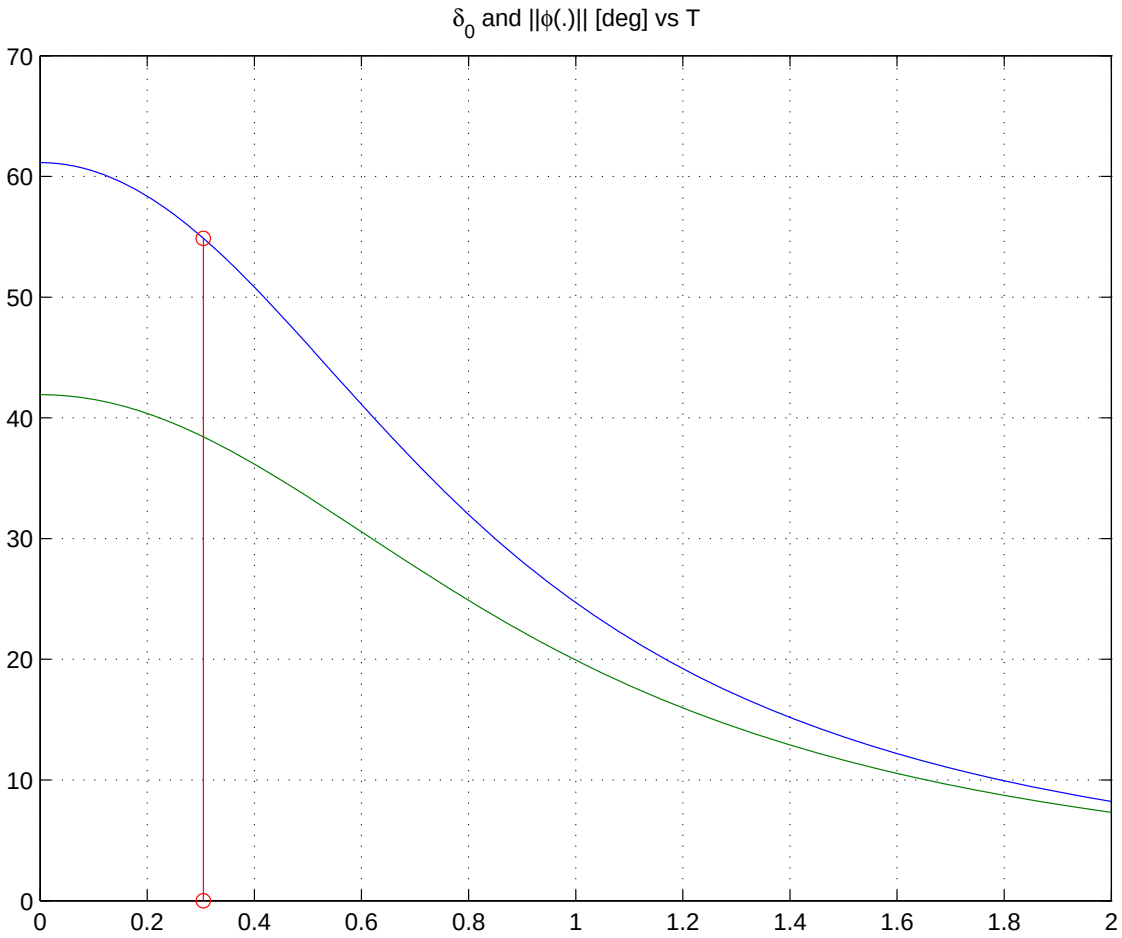


Figure 3.5: Constant speed pendubot results: invariant region estimate, $\delta_0(\alpha_0 T, \beta)$, and fixed point trajectory norm, $\|\varphi_{\alpha_0 T}(\cdot)\|$, versus T, from 0 to 4 seconds, for the physically chosen $\beta_{\text{CU}} = 8.54$. Also depicted is the time (around 0.31 seconds) above which the nonlinear mapping is known to be a contraction.

By adjusting the β we can explore trajectories of a pendubot that has a different inner arm length. As β is increased, the maximum angle of the outer arm, $\varphi(\cdot)_{\max}$, increases. Figure 3.6 illustrates $\varphi_{\max}$ (in degrees) versus T for the constant speed pendubot with α as specified and β varied according to $\beta_{\text{CU}} \cdot 2^{n/2}$ for $n = 0, 1, \ldots, 7$.

Figure 3.7 shows what half a period of the actual trajectories look like as the period T is varied in the constant velocity pendubot case for β_{CU}. Even as the period T approaches zero the maximum lean angle for the outer arm stayed within 42 degrees! At this point in our development, in order to ensure the application of a successive approximation approach will converge to solutions to the operator $\mathcal{N}_\alpha^\beta[\varphi(\cdot)] = \mathcal{A}_\alpha[\,\mathcal{M}(\varphi(\cdot), \cdot)\,]$, the contraction property must be satisfied. Figure 3.8, shows the successive approximations $\varphi_{i+1} = \mathcal{N}_\alpha^\beta[\varphi_i(\cdot)]$ starting with $\varphi_0(\cdot) \equiv 0$ for $T = 0.32$ for the pendubot in our lab at CU with $\beta_{\text{CU}} = 8.54$. We see that, within ten iterations we start to approximate the solution very well.

In our experience, for $\beta_{\text{CU}} = 8.54$ and for α in the specified range, the successive approximation algorithm always converged to the desired trajectory, even for $T < 0.31$. Note that this is **not** what happens when β is increased to, say, 25. In situations where the successive approximation approach is ineffective, one may attempt to use Newton's method to develop a continuation strategy for determining solutions as α (or β) is varied. One may, for instance, use the Matlab two point boundary value solver `bvp4c` as part of such a continuation strategy. This approach will be locally effective so long as 1 is not an eigenvalue of $D\mathcal{N}_\alpha^\beta[\varphi_\alpha(\cdot)]$.

For a constant velocity pendubot with a β of 2.5445 times that of the pendubot in our lab we found the fixed point iteration of the map starting with $\varphi(\cdot) \equiv 0$ actually converges for $T > 0.595$. For $T < .595$, the infinite sequence generated by the fixed point map resulted in convergent subsequences for all choices of α and β. However, none of the convergent subsequences when $T < .595$ were solutions. Note that the infinite sequence generated by the successive approximations forms an equicontinuous family since every element of the sequence lies in the invariant region and all the elements of the sequence have the same bounded derivative. Therefore, the infinite sequence generated by the fixed point map will have some convergent subsequences for **all** choices of α and

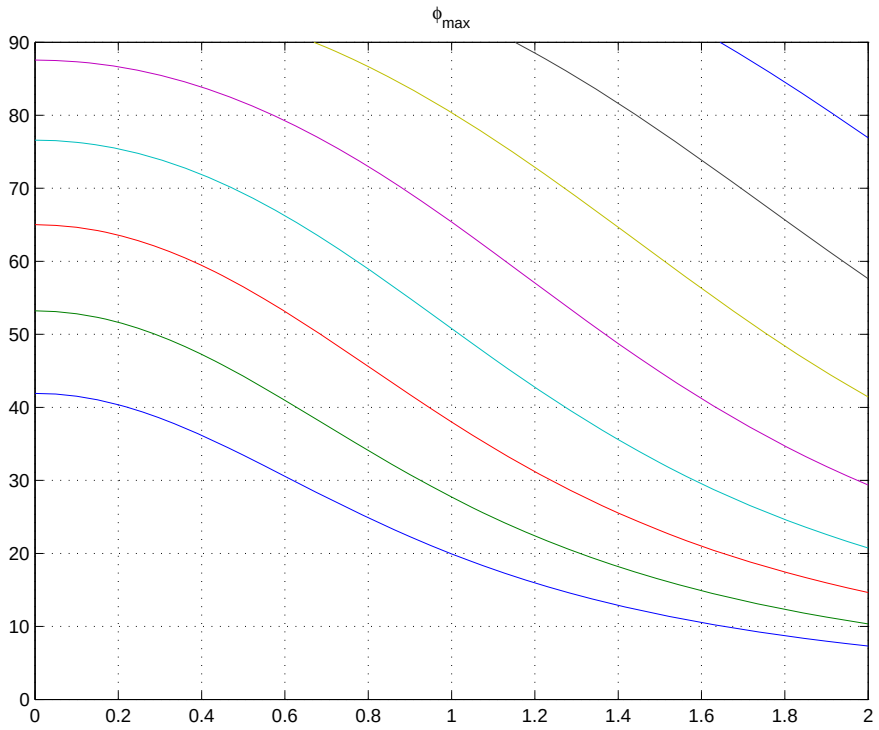


Figure 3.6: Plot of $\varphi_{\max}$ (in degrees) versus T for the constant speed pendubot with α as specified and β varied according to $\beta_{\text{CU}} \cdot 2^{n/2}$ for $n = 0, 1, \ldots, 7$. For a fixed α, the maximum lean angle increases as β is increased.

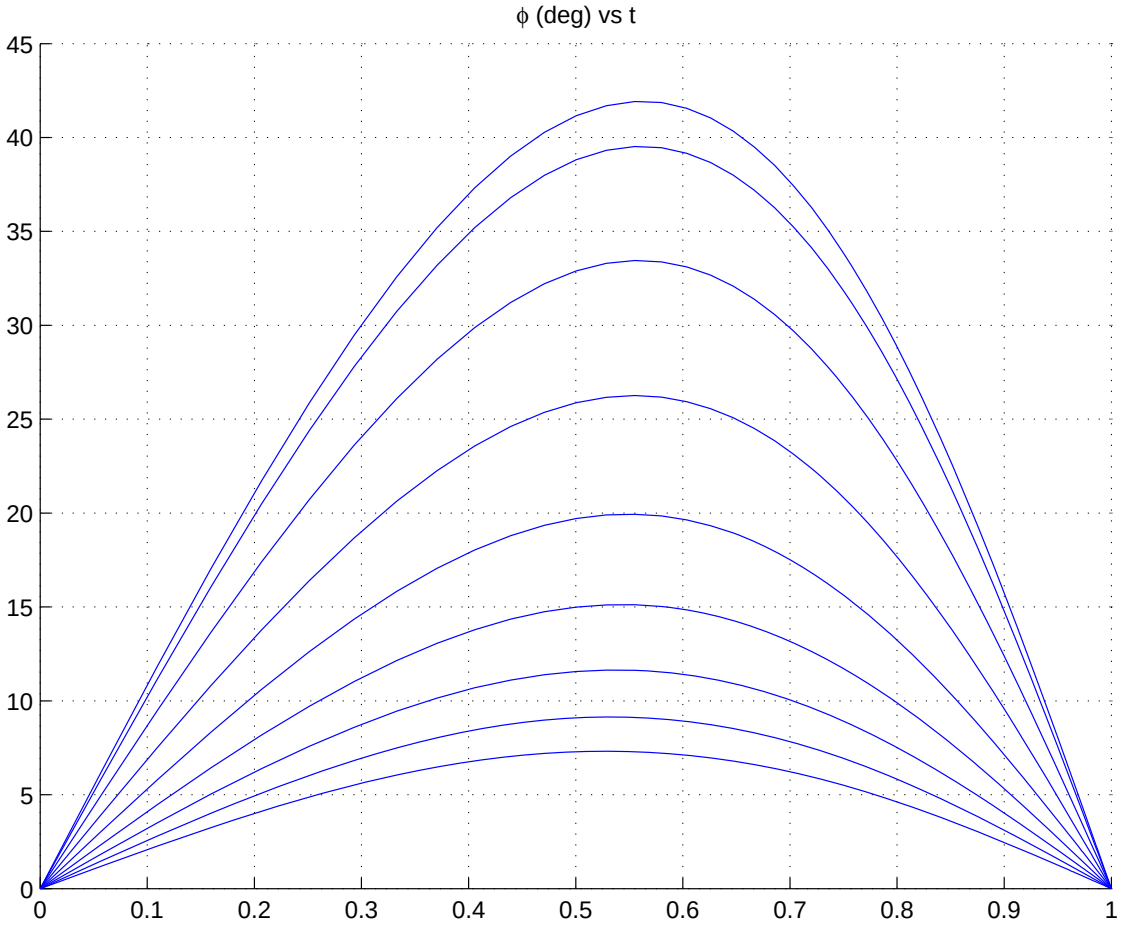


Figure 3.7: Plot of $\varphi(t)$ (in degrees) for the constant speed pendubot with T ranging from 0 to 2 in increments of $1/4$ for β_{CU}.

β.

However, we do not know that these convergent subsequences will be fixed points of the operator $\mathcal{N}_\alpha^\beta[\,\cdot\,]$ unless we are in a region where the contraction property holds. Figure 3.9 shows the successive approximations for the constant velocity pendubot when the chosen $\beta = 2.5445\beta_{\text{CU}}$ and $T = 0.4$. In this case, there are two convergent subsequences neither of which converge to the solution (shown by the dotted line). As we will discuss below in our use of continuation methods, the eigenvalues of the operator $D\mathcal{N}_\alpha^\beta$ determine the change in the successfulness of the successive approximation approach.

3.4.1 Torque Limits

The pendubot in the lab at CU has limited torque of 2.4 N-m. Trajectories with an inverted outer arm can end up pushing or pulling the inner arm. Consider the following

$$V^2/R = l_1\dot{\theta} = g$$

$$\Rightarrow \dot{\theta} = \sqrt{g/l_1} \approx 8.11 rad/sec$$

$$\Rightarrow T \approx 2\pi/8.11 \approx 0.774 sec$$

Figure 3.10 shows the maximum and minimum torque requirements for a range of periods, T, in the constant inner arm velocity case.

In particular, we see that we are within the torque limits for a variety of constant velocity inner arm trajectories that result in the outer arm being pushed and pulled along the trajectory (i.e., $T < .774$).

3.5 Contraction Boundary

In this section, we are interested in finding the set of (α, β, δ) that satisfy the invariance condition (3.14) and the boundary of the contraction condition (3.18). That is, we would like to

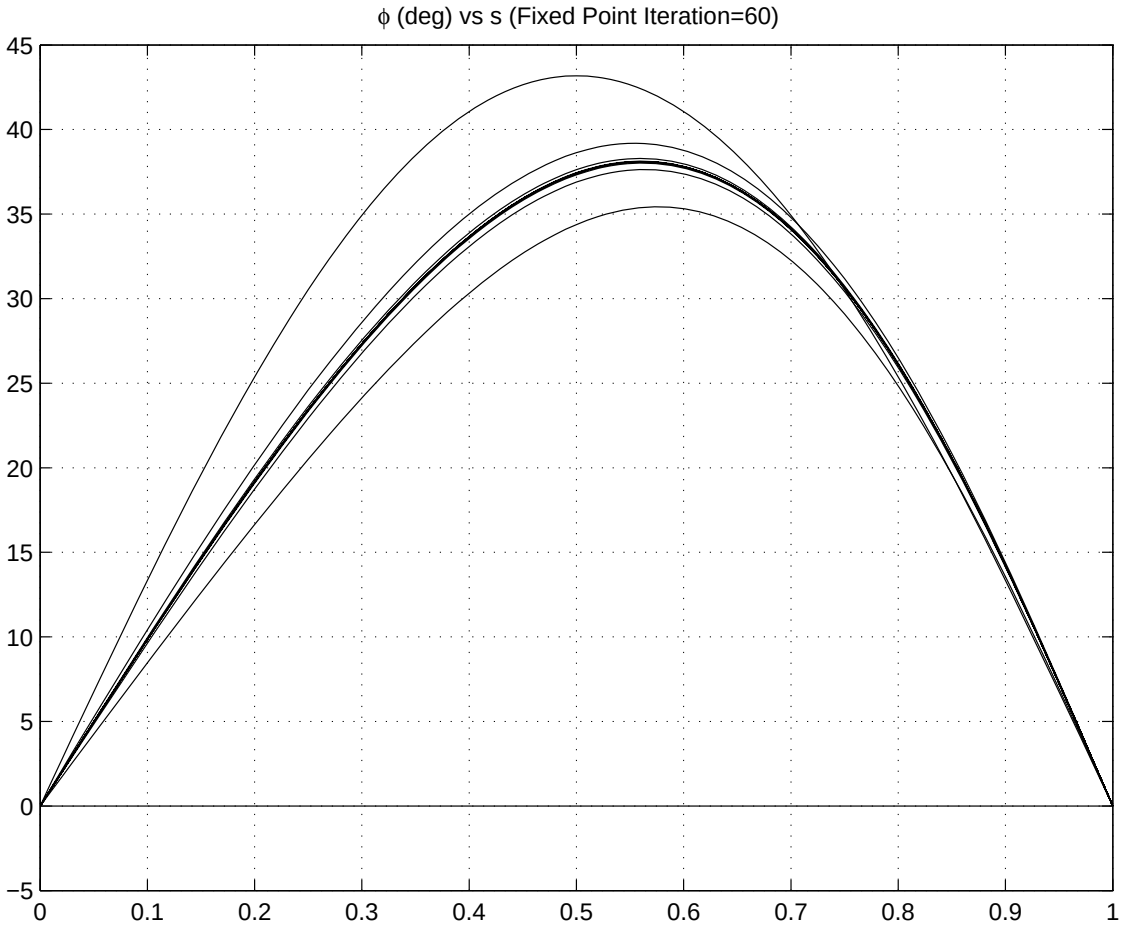


Figure 3.8: The successive approximations $\varphi_{i+1} = \mathcal{N}_\alpha^\beta$ for the constant speed pendubot with β_{CU} at $T = 0.32$ which is just above the time where the nonlinear mapping is known to be a contraction.

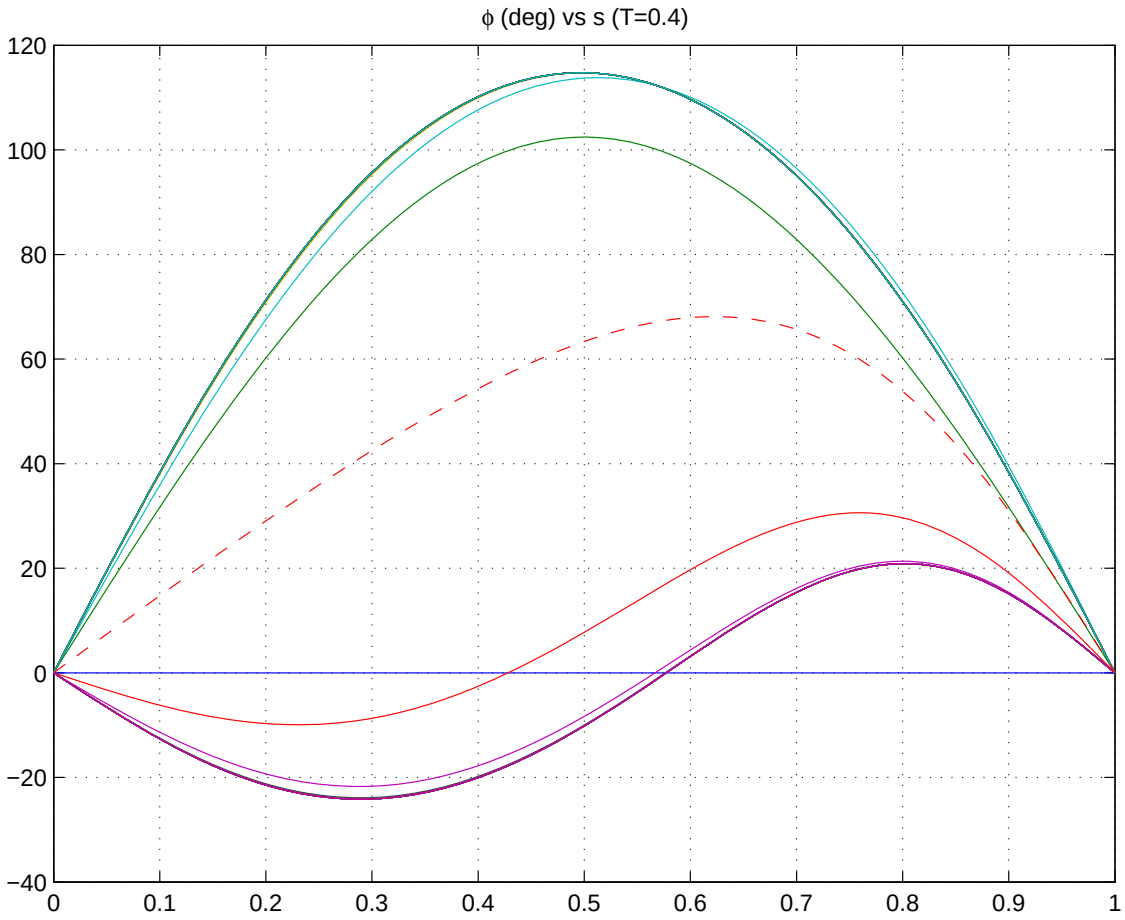


Figure 3.9: Fixed Point Iteration for $2.5445\beta_{\mathrm{CU}}$ with $T = 0.4$. Here we see that that two convergent subsequences emerge neither of which converge to the solution shown by the dotted line.

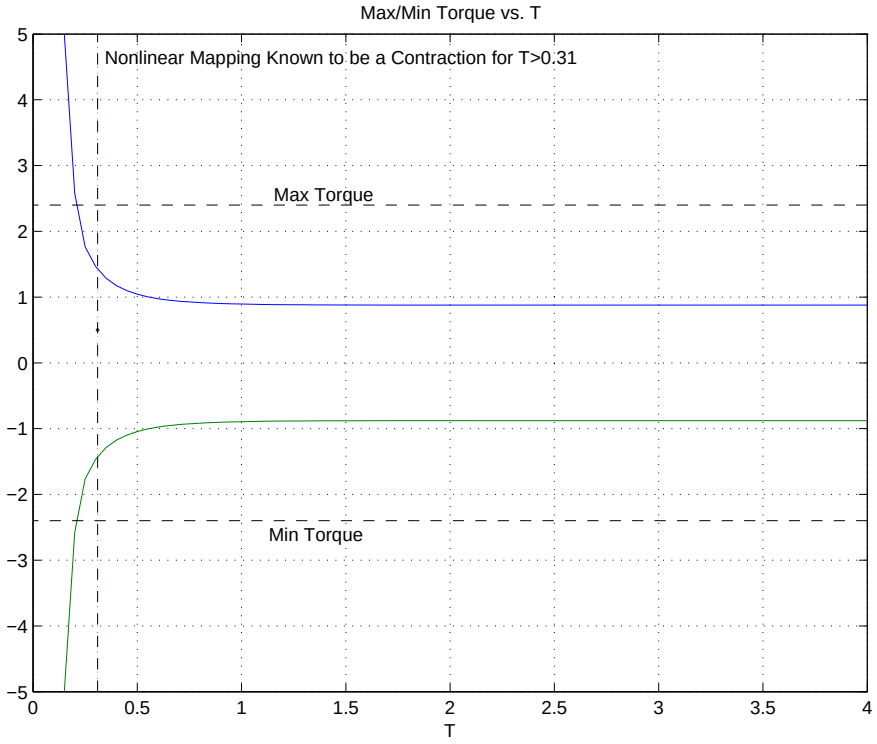


Figure 3.10: Plot of Max/Min torque vs T for inverted trajectories with a constant velocity inner arm. For $T < 0.774$, these trajectories will result in the pivot point of the outer link being pushed and pulled. The torque limits for the pendubot system in the lab at CU easily allow for constant velocity inverted trajectories where the inner arm can be pushed/pulled.

characterize the set that describes the inverse image of the zero set, i.e., the set $F^{-1}((0,0))$ where

$$F(\alpha,\beta,\delta)=\begin{bmatrix}\bar{g}(\alpha)(\delta-\sin\delta)+\breve{g}(\alpha)\beta-\delta\\ \bar{g}(\alpha)q(\delta)+\breve{g}(\alpha)\beta-1\end{bmatrix}$$

and $q(\delta)$ defined in (3.17). Equating the components of F we can eliminate β from consideration to obtain

$$\bar{g}(\alpha)(\delta-\sin\delta)-\delta=\bar{g}(\alpha)(1+r(\delta))-1 \tag{3.20}$$

where

$$r(\delta)=q(\delta)-1=\begin{cases}-\cos\delta, & \delta\le\pi\\ 1, & \delta>\pi\end{cases}$$

Rewriting equation (3.20) we get

$$\sin\delta+r(\delta)=\frac{(1-\bar{g}(\alpha))}{\bar{g}(\alpha)}(1-\delta) \tag{3.21}$$

which gives, by a simple trigonometric identity, for $\delta\le\pi$

$$\sqrt{2}\sin(\delta-\pi/4)=\frac{1-\bar{g}(\alpha)}{\bar{g}(\alpha)}(1-\delta)$$

and for $\delta>\pi$

$$1+\sin\delta=\frac{1-\bar{g}(\alpha)}{\bar{g}(\alpha)}(1-\delta).$$

Hence, the left hand side of equation (3.21) is equal to

$$\sin\delta+r(\delta)=\begin{cases}\sqrt{2}\sin(\delta-\pi/4), & \delta\le\pi\\ 1+\sin\delta, & \delta>\pi.\end{cases}$$

Note that the curves generated by the left hand side and the right hand side of equation (3.21), as functions of δ, can only intersect at one point defining $\delta=\bar{\delta}(\alpha)$. Figure 3.11 shows a plot of the left hand side and the right hand side with only one intersection point. Note that $\sqrt{2}\sin(\delta-\pi/4)$ starts at -1 when $\delta=0$ and increases to $\sqrt{2}$ when $\delta=3\pi/4$ with a zero crossing at $\pi/4$. In addition, $\frac{1-\bar{g}(\alpha)}{\bar{g}(\alpha)}(1-\delta)$ starts at $\frac{1-\bar{g}(\alpha)}{\bar{g}(\alpha)}$ when $\delta=0$ and decreases with a zero crossing at $\delta=1$. Indeed, it is

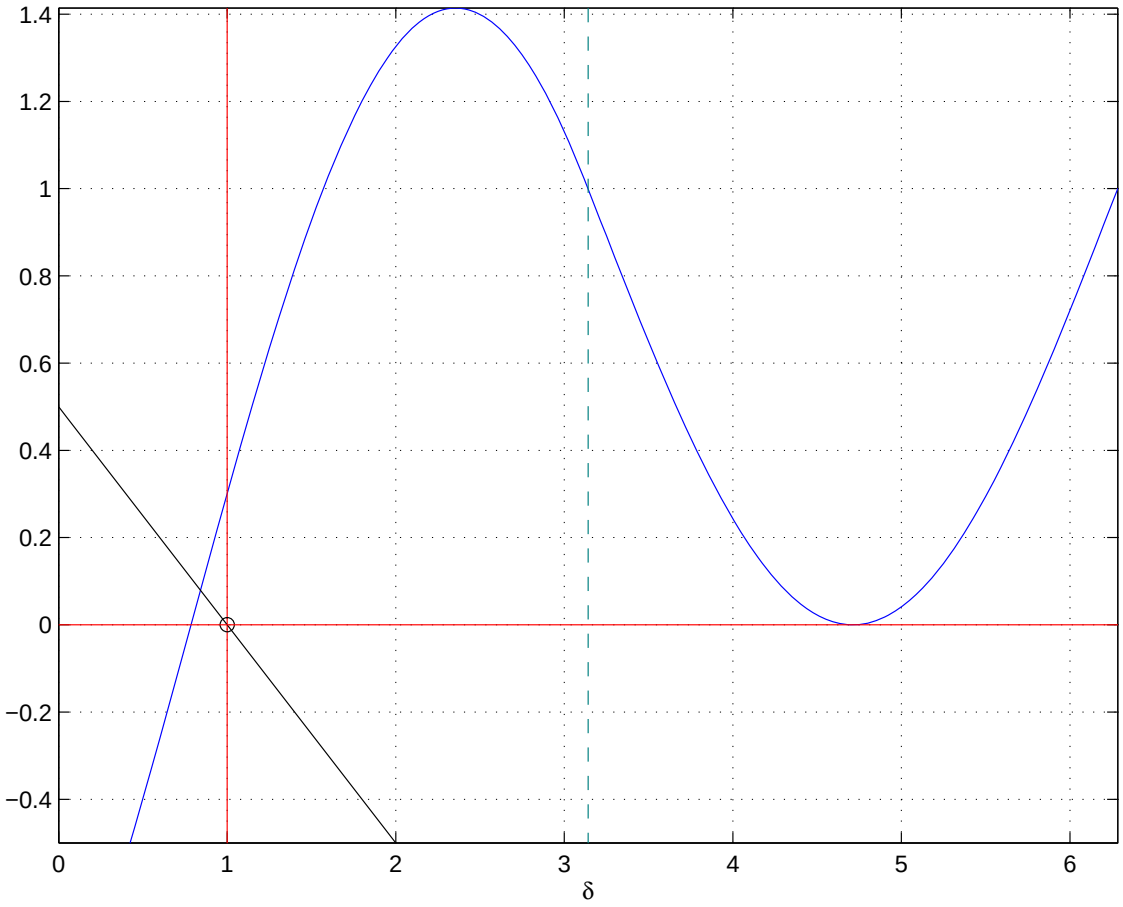


Figure 3.11: Plot of the curves generated by the left hand side and the right hand side of equation (3.21). These curves can only have one intersection point defining the boundary, $\bar{\delta}(\alpha)$, of the contraction boundary.

clear that for each α there can be only one crossing which which lies in $\delta \in (\pi/4, 1)$. Moreover, the solution will start at $\delta = 1$ when $\alpha = 0$ and monotonically decrease approaching $\pi/4$ as $\alpha \to \infty$. Figure 3.12 is plot of $\delta(\alpha)$. Since $\delta \in (\pi/4, 1)$ is only varying by about twelve degrees,

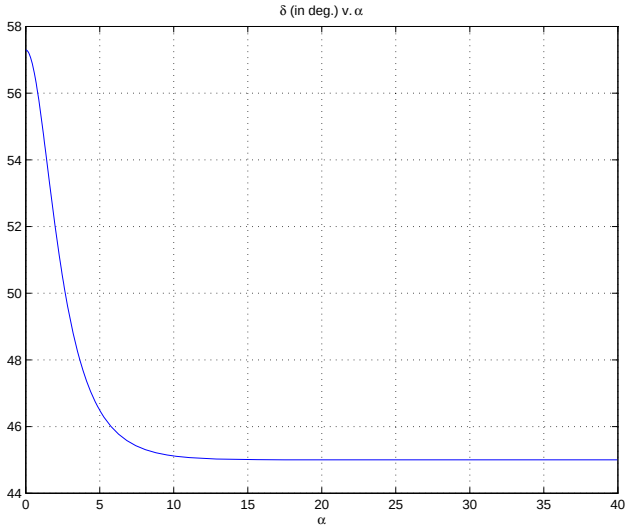


Figure 3.12: Plot of $\delta(\alpha)$ in degrees which defines the boundary of the contraction condition. $\delta(\alpha)$ is independent of β and monotonically decreases as $\alpha \to 0$.

$\sin(\delta - \pi/4)$ can be approximated effectively by a linear approximation. A simple substitution of the linear approximation for $\sin(\delta - \pi/4)$ results in $\tilde{\delta}(\alpha) \approx \delta(\alpha)$ given by

$$\tilde{\delta}(\alpha) = \frac{\pi}{4} + \frac{1 - \bar{g}(\alpha)}{1 + (\sqrt{2} - 1)\bar{g}(\alpha)} \left(1 - \frac{\pi}{4}\right)$$

Figure 3.13 is a plot, in degrees, of the difference between the approximation $\tilde{\delta}(\alpha)$ and $\delta(\alpha)$. As can be seen from Figure 3.13, $\tilde{\delta}(\alpha)$ is a very good approximation of $\delta(\alpha)$. Note that $\tilde{\delta}(\alpha)$ and $\delta(\alpha)$ agree at $\alpha = 0$ and as $\alpha \to \infty$. The $\delta(\alpha)$ which defines the boundary of the contraction condition is independent of β. Once we have $\delta(\alpha)$ we can compute $\beta(\alpha)$ by

$$\beta(\alpha) = \frac{\delta(\alpha) - \bar{g}(\alpha)(\delta(\alpha) - \sin\delta(\alpha))}{\breve{g}(\alpha)}$$

Figure 3.14 shows a plot of $\beta(\alpha)$.

Proposition 12. *For each $\alpha > 0$, there is a $\beta_0 = \beta_0(\alpha)$ such that*

$$\bar{g}(\alpha)q(\delta_0(\alpha, \beta)) + \breve{g}(\alpha)\beta < 1$$

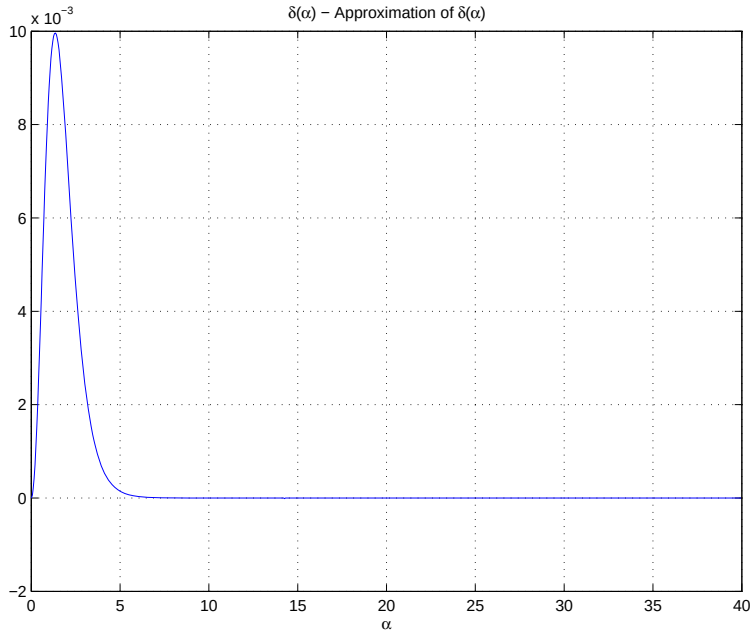


Figure 3.13: This figure shows (in degrees) that a linear approximation of $\sin(\delta - \pi/4)$ results in an approximation, $\tilde{\delta}(\alpha)$, that is close to the desired curve.

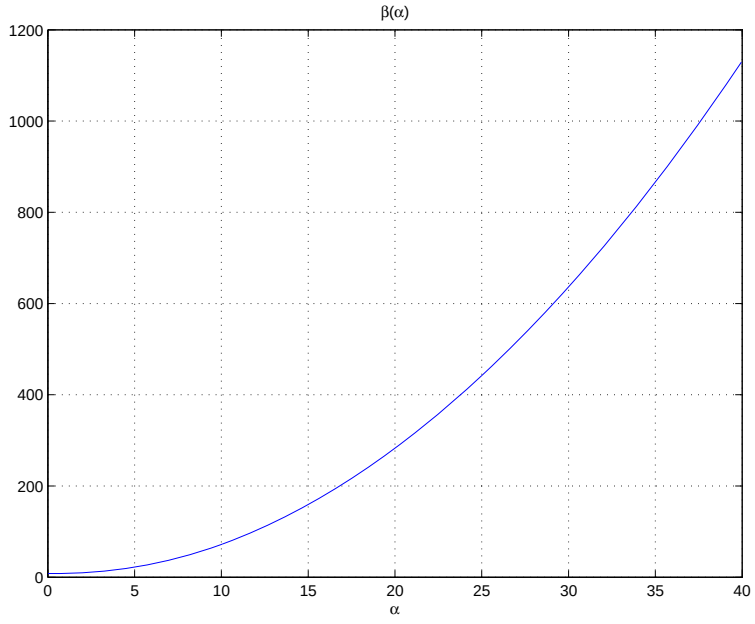


Figure 3.14: Plot of $\beta(\alpha)$ in degrees.

Proposition 13. *$\alpha \mapsto \bar{\beta}(\alpha)$ is strictly increasing, and $\bar{\beta}(\alpha) > 8$ for all $\alpha > 0$.*

Remember, $\delta_0(\alpha, \beta) = min\{\delta > 0 : h(\delta; \alpha, \beta) = \delta\}$ where $h(\delta; \alpha, \beta) := \bar{g}(\alpha)(\delta - \sin\delta) + \breve{g}(\alpha)\beta$ is the first positive fixed point of $h(\delta; \alpha, \beta)$.

Proposition 14. *For each $\alpha > 0$, $\beta \mapsto \delta_0(\alpha, \beta)$ is strictly increasing.*

Proof. Fix $\alpha > 0$ and let $\beta_2 > \beta_1 > 0$ be arbitrary. Set $\delta_1 = \delta_0(\alpha, \beta_1)$ and $\delta_2 = \delta_0(\alpha, \beta_2)$. Clearly, $h(\delta; \alpha, \beta_2) > h(\delta; \alpha, \beta_1)$ for all α and $\delta > 0$. In addition, $h(\delta; \alpha, \beta_1) > \delta_1$ for $\delta \in (0, \delta_1]$ since $h(\delta_1; \alpha, \beta_1) = \delta_1$ is the first intersection. Thus, $h(\delta; \alpha, \beta_2) > \delta$ for all $\delta \in (0, \delta_1]$. Therefore, $\delta_2 > \delta_1$. Hence, $h(\delta; \alpha, \beta_2) > h(\delta; \alpha, \beta_1) > \delta$ on $[0, \delta)$ and $h(\delta_1; \alpha, \beta_2) > h(\delta_1; \alpha, \beta_1) = \delta_1$ so that $h(\delta; \alpha, \beta_2) > \delta$ for all $\delta \in (0, \delta_1]$. □

3.5.1 Regions of Unique Solutions Revisited

We previously provided conditions on α and β that ensure guarantee the existence of a set $\mathcal{B}$ for which $\mathcal{N}_\alpha^\beta : \mathcal{B} \to \mathcal{B}$ is a contraction. When $\mathcal{N}_\alpha^\beta$ is a contraction, we showed that there will be a unique fixed point within the closed invariant set $\mathcal{B}$ so that the nonlinear boundary value problem possesses a unique solution $\varphi(\cdot)$ in $\mathcal{B}$. Recall that various properties of $\mathcal{N}_\alpha^\beta$ are parameterized by (α, β, δ). In particular, for each (α, β), with $\beta < \bar{\beta}(\alpha)$, there exists a set $\mathcal{B} = \bar{\mathcal{B}}_{\delta_0(\alpha,\beta)}$, with $\delta_0 < \bar{\delta}(\alpha)$, such that $\mathcal{N}_\alpha^\beta : \mathcal{B} \to \mathcal{B}$ is a contraction. In this section we expand our consideration to regions of α and β where $\mathcal{N}_\alpha^\beta$ is not guaranteed to be a contraction. During this consideration we are able to find unique solutions on sets larger than $\mathcal{B}$ where our estimates of $\mathcal{N}_\alpha^\beta$ being a contraction do not hold. To this end, we show that $\mathcal{N}_\alpha^\beta$ is a set contractive map on certain sets allowing us to describe larger invariance regions on which there is a unique solution and regions for which no solutions exist.

Let δ_0 be the first positive fixed points of the comparison function $h : \mathbb{R}^+ \to \mathbb{R}^+$. Define δ_1 to be the minimum of the second positive fixed point of h and $+\infty$. When $h'(\delta_0) < 1$, the comparison function h is strictly increasing and will be a monotonically decreasing map on $[\delta_0, \delta_1)$. Then, for

any $\delta \in (\delta_0, \delta_1)$, we have $\delta_0 < h(\delta) < \delta$ so that $\mathcal{N}_\alpha^\beta[\bar{\mathcal{B}}_\delta] \subset \bar{\mathcal{B}}_{h(\delta)}$. Also, for some $\delta < \delta_1$ and $\delta \in [\delta_0, \delta_2)$ $\mathcal{N}_\alpha^\beta$ will be a contraction on $\bar{\mathcal{B}}_\delta$.

Fix $\alpha > 0$ and let $\beta < \bar{\beta}(\alpha)$. Then, $\delta = \delta_0(\alpha, \beta)$ defines a set, $\bar{B}_{\delta_0(\alpha,\beta)}$, on which $\mathcal{N}_\alpha^\beta$ is a contraction. That is, for all $\delta \leq \delta_0$, $\mathcal{N}_\alpha^\beta$ satisfies the invariance condition

$$\bar{g}(\alpha)(\delta - \sin\delta) + \breve{g}(\alpha)\beta \leq \delta$$

and the contraction condition

$$\bar{g}(\alpha)(1 - \cos\delta) + \breve{g}(\alpha)\beta < 1.$$

Hence, there will be a unique fixed point on $\bar{B}_{\delta_0}$.

Theorem 15. *There exists*

(1) A $\delta_0' > \delta_0$ such that $\mathcal{N}_\alpha^\beta$ is a contraction on $\bar{B}_\delta$, for each $\delta \in [\delta_0, \delta_0')$; and

(2) There exists a $\delta_0'' > \delta_0$ such that $\mathcal{N}_\alpha^\beta$ has a unique fixed point in $\bar{B}_\delta$, for each $\delta \in [\delta_0, \delta_0'')$.

Proof. To see there always exists a $\delta_0' > \delta_0$ such that $\mathcal{N}_\alpha^\beta$ is a contraction on $\bar{B}_\delta$, for all $\delta \in [\delta_0, \delta_0')$, we need $\cos\delta > \frac{\beta}{\alpha^2} - \frac{1-\bar{g}(\alpha)}{\bar{g}(\alpha)} = \delta_0 \sin\delta_0 - (1-\delta_0)\frac{1-\bar{g}(\alpha)}{\bar{g}(\alpha)}$. Clearly, $\delta_0' = \delta_0 + \epsilon$ will satisfy

$$\bar{g}(\alpha)(1 - \cos\delta) + \breve{g}(\alpha)\beta \leq 1.$$

for small $\epsilon > 0$. It is also clear that the invariance condition,

$$\bar{g}(\alpha)(\delta - \sin\delta) + \breve{g}(\alpha)\beta \leq \delta$$

will also hold for small $\epsilon > 0$ with $\delta \in [0, \delta_0']$.

Now, note that there exists a δ_0'' such that for all $\delta \in [\delta_0, \delta_0']$, $\mathcal{N}_\alpha^k[\bar{B}_\delta] \mapsto \bar{B}_\delta$. □

Note that δ_0'' may be large enough that $\mathcal{N}_\alpha^\beta$ might not be a contraction on $\bar{B}_{\delta_0''}$.

Fix $\beta > 0$, then $\delta_0(\alpha, \beta)$ provides the smallest estimate of a region $\bar{B}_{\delta_0(\alpha,\beta)}$ that is invariant under $\mathcal{N}_\alpha^\beta$, and is defined to be the smallest fixed point of $h(\cdot; \alpha, \beta)$ so that

$$\delta_0 = \min\{\delta : h(\delta; \alpha, \beta) = \delta\}$$

$\delta_0(\alpha,\beta)$ is always well defined, and in $(0,\infty)$. $\delta_0' : \mathbb{R}^2_+(\alpha,\beta)$ is given by $\min\{\delta > 0 : h_{cr}(\delta;\alpha,\beta) = 1\}$ where $h_{cr}(\delta;\alpha,\beta) = \bar{g}(\alpha)(1 - cos(\delta)) + \breve{g}(\alpha)\beta$. Thus, for $\alpha > 0$ such that $\delta_0(\alpha) \leq \delta_0'(\alpha)$, it is clear that the two point boundary value problem (parameterized by α,β) has a unique solution within $\bar{B}_{\delta_0(\alpha,\beta)}$ since, on (or restricted to) that closed set, $\mathcal{N}_\alpha^\beta$ is a contraction.

The mapping

$$\delta_0'' : \mathbb{R}^2_+ \to \mathbb{R}_+ \cup \{+\infty\}$$

provides (or defines) the boundary for the domain of attraction for the fixed point

$$\delta_0(\alpha,\beta) = h(\delta_0(\alpha,\beta);\alpha,\beta).$$

This is computed by finding the second largest fixed point, if it exists, of $h(\delta)$.

Proposition 16. *Fix $\alpha \geq 0$ and $\beta > 0$, then $\delta_0'' > \delta_0'$.*

Proposition 17. *Let $h'(\delta_0(\alpha,\beta);\alpha,\beta) \leq 1$ for all $(\alpha,\beta) \in \mathbb{R}^2_+$. Then, $\delta_0(\alpha,\beta)$ is an asymptotically stable fixed point if and only if $h'(\delta_0(\alpha,\beta);\alpha,\beta) < 1$.*

Thus, $\delta_0''(\alpha,\beta)$ is greater than or equal to $\delta_0(\alpha,\beta)$, including possibly $+\infty$, with the inequality being strict if and only if

$$h'(\delta_0(\alpha,\beta);\alpha,\beta) = \bar{g}(\alpha)(1 - \cos\delta_0(\alpha,\beta)) < 1$$

When $h' < 1$ and there are multiple solutions to $h(\delta;\alpha,\beta) = \delta$, $\delta_0''(\alpha,\beta)$ is given by the second smallest solution. Figure 3.15 shows a plot of δ_0, δ_0', and δ_0'' for the β associated with our physical pendubot system, i.e., $\beta_{\text{CU}} = 8.54$.

Region I is the region where $\delta_0(\alpha) \leq \delta_0'(\alpha)$. Therefore, it is clear that the two point boundary value problem (parameterized by (α,β)) has a unique solution within $\bar{B}_{\delta_0(\alpha,\beta)}$ since, in region I, $\mathcal{N}_\alpha^\beta$ is a contraction. In region II, we know that the invariance condition is satisfied and hence there will be a solution within $B_{\delta_0(\alpha,\beta)}$. In addition, we see that to the left of $\alpha \approx 4.14$, i.e., region III, the domain of attraction is infinite and there will no solutions where $\varphi(0) = \varphi(1) = 0$ within this region. We know that $\delta_0(\alpha,\beta)$ is attractive from the left, converging monotonically from initial

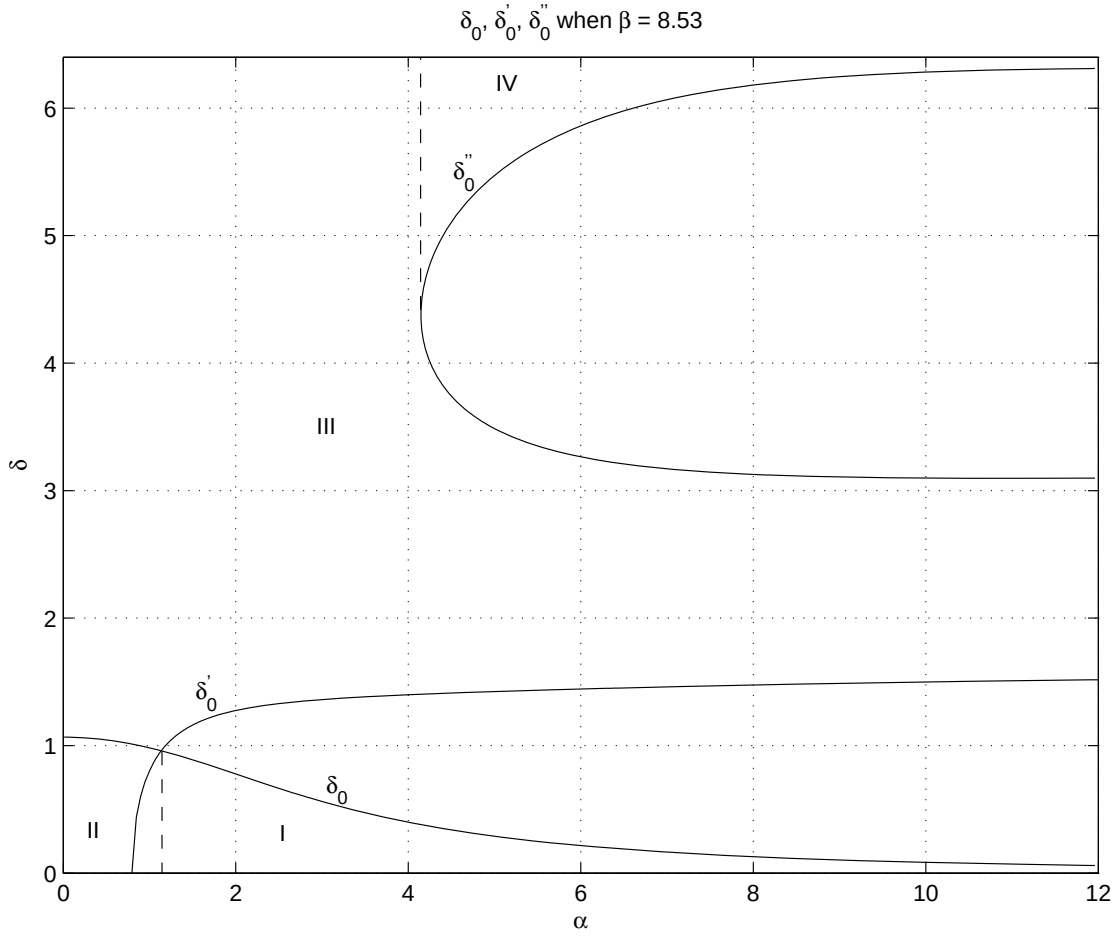


Figure 3.15: Plot of various solution regions defined by δ_0, δ_0', and δ_0'' for the β associated with our physical pendubot system, i.e., $\beta_{\text{CU}} = 8.54$.

conditions in the set $[0, \delta_0(\alpha, \beta)]$. Moreover, Figure 3.15 shows that there is a (globally!) unique solution when $\beta = 8.54$ and $\alpha \in (1.2, 4.14)$.

Also,

$$\delta_0''(\alpha, \beta) = \min\{\delta > \delta_0(\alpha, \beta) : \delta = h(\delta; \alpha, \beta)\}$$

To the left of $\alpha \approx 4.14$ we see that the domain of attraction is unbounded and there will be only one solution where $\varphi(0) = \varphi(1) = 0$. When $h' < 1$, then, we have a guaranteed region where δ_0 will be a stable fixed point of $\delta^{k+1} = h(\delta^k)$. In the region where $\delta : h' > 1$ and less than δ_0'', there can be no solutions as the sets of δ will be shrunk or contracted into sets where we know there is a unique solution. Hence in this region, there are no solutions.

Also, for $\beta_{\text{CU}} = 8.54$, δ_0'' has a minimum of approximately 3.09 when $\alpha = 11.01$. As a result, we can conclude that there is only one solution with $\varphi(0) = \varphi(1) = 0$ that is less than ≈ 177 degrees when $\alpha > 1.2$. To this end, we use the fact that if $\delta_0(\alpha, \beta)$ is an asymptotically stable fixed point of $h(\cdot; \alpha, \beta)$, then $\mathcal{B}_{\delta_0(\alpha,\beta)}$ is an asymptotically attractive invariant set of $\mathcal{N}_\alpha^\beta$, and $\mathcal{B}_{\delta_1}$ is contained in the region of attraction of $\bar{\mathcal{B}}_{\delta_0}$.

3.6 Continuation

Using the Schauder fixed point theorem, we have proven the existence of solutions of the two point boundary value problem

$$\ddot{\varphi} = \alpha^2 \sin\varphi + \beta\, f(\varphi, t)\,, \quad \varphi(0) = 0 = \varphi(1)$$

for all $\alpha > 0$ and $\beta > 0$. In addition, we found a conservative condition which ensures that $\mathcal{N}_\alpha^\beta[\cdot]$ is a contraction on the invariant set $\bar{B}_\delta$ so that there will be a unique solution within the set $\bar{B}_\delta$. Moreover, when the contraction property holds, the fixed point of $\mathcal{N}_\alpha^\beta[\cdot]$ for a particular α, $\varphi_\alpha(\cdot)$, is a well defined function of α giving a curve $\alpha \mapsto \varphi_\alpha$ in $\mathcal{C}_0^2[0, 1]$.

We have found, experimentally at least, that we could trace the curve $\alpha \mapsto \varphi_\alpha$ using the boundary value solver all the way to α equals zero for each of the $\beta' s$ that we tried. Since our condition on when $\mathcal{N}_\alpha^\beta[\cdot]$ is conservative, we suspect that a local, or isolated, solution should

continue to exist for parameters outside of those that satisfy the contraction condition. In this section, we explore the use of continuation methods to find solutions outside of the parameters in which our conservative condition guarantees $\mathcal{N}_\alpha^\beta[\cdot]$ is a contraction.

Recall that

$$\mathcal{N}_\alpha^\beta[\varphi] = \mathcal{A}_\alpha\left[\mathcal{M}(\varphi(\cdot),\cdot)\right]$$

where $\mathcal{M}[\varphi(\cdot)](t) = \varphi(t) - \sin\varphi(t) - \beta/\alpha^2\, f(\varphi(t),t)$. Hence,

$$D\mathcal{N}_\alpha^\beta[\varphi_\alpha]\cdot\psi = \mathcal{A}_\alpha\left[\mathcal{M}'(\varphi(\cdot),\cdot)\psi(\cdot)\right]$$

where $\mathcal{M}'(\varphi(\cdot),\cdot))(t) = 1 - \cos\varphi(t) - \beta/\alpha^2 f'(\varphi(t),t)$.

The contraction condition (3.18) provides a conservative estimate on the norm of $D\mathcal{N}_\alpha^\beta[\varphi_\alpha]$.

Proposition 18. *Given β, if α is in the range on which $\mathcal{N}_\alpha^\beta$ is a contraction with fixed point φ_α, then $\|D\mathcal{N}_\alpha^\beta[\varphi_\alpha]\| < 1$.*

Proof. Pick α so that $\mathcal{N}_\alpha^\beta$ is a contraction $\bar{B}_\delta$ with $\delta = \delta_0(\alpha,\beta)$. Suppose $\|\psi\| \le 1$, i.e., $(|\psi(t)| \le 1 \forall t \in [0,T])$, then

$$\begin{aligned}
\|D\mathcal{N}_\alpha^\beta[\varphi_\alpha]\cdot\psi\| &= \|\mathcal{A}_\alpha\left[\mathcal{M}'(\varphi_\alpha(\cdot),\cdot)\psi\right]\| \\
&\le \|\mathcal{A}_\alpha\|\,\|\mathcal{M}'\psi\| \\
&= \|\mathcal{A}_\alpha\| \max_{t\in[0,T]}\left|1 - \cos\varphi_\alpha(\cdot) - \frac{\beta}{\alpha^2}f'(\varphi_\alpha(t),t)\right|\ |\psi(t)| \\
&\le \bar{g}(\alpha)\,\|1-\cos\varphi_\alpha(\cdot)\| + \beta\frac{\bar{g}(\alpha)}{\alpha^2}\,\|f'(\varphi_\alpha(\cdot),\cdot)\| \\
&\le \bar{g}(\alpha)\,\|1-\cos\varphi_\alpha(\cdot)\| + \beta\breve{g}(\alpha)\,\|f'(\varphi_\alpha(\cdot),\cdot)\| \\
&\le \bar{g}(\alpha)q(\delta) + \beta\breve{g}(\alpha) < 1.
\end{aligned}$$

□

Since the $\rho(\mathcal{A}) \le \|\mathcal{A}\|$ for a bounded linear operator, the spectrum does not contain 1 when the contraction condition is satisfied. If we are at a fixed point and $D\mathcal{N}_\alpha^\beta - I$ is an invertible

operator, then the implicit function theorem applies. By starting with a $\varphi_\alpha(\cdot)$, with α in the region where the contraction condition is satisfied, a direct application of the implicit function theorem states that a solution exists for some nontrivial interval around α. As long as the largest real eigenvalue for $D\mathcal{N}_\alpha^\beta[\varphi_\alpha]$ is less than 1, we can repeat the process and find fixed points, $\varphi_\alpha(\cdot)$, outside of our original region of contraction. Next we show that the eigenvalues of $D\mathcal{N}_\alpha^\beta(\varphi_\alpha(\cdot))$, i.e., $D\mathcal{N}_\alpha^\beta(\varphi_\alpha(\cdot))\psi = \lambda\psi$ are real and use conjugate point theory to find the eignevalues.

3.6.1 Eigenvalues of $D\mathcal{N}_\alpha^\beta(\varphi_\alpha(\cdot))$

In Section 3.3.2, we developed the Green's function $g_\alpha(t,s)$ for the unstable harmonic oscillator so that we could study the integral operator

$$\mathcal{G}[\psi(\cdot)](t) = \int_0^1 g_\alpha(t,s)\psi(s)ds$$

that corresponds to the linear differential operator $\mathcal{A}_\alpha$. $\mathcal{G}[\cdot]$ is a compact, self-adjoint operator on $L^2[0,1]$ and therefore has an infinite sequence of real eigenvalues which converge to zero. [35] In fact, $\mathcal{G}$ is a positive operator since all of the eigenvalues are positive and converge to zero. This can be seen by writing the following second order ordinary differential equation with constant coefficients that corresponds to the linear operator

$$\ddot{\gamma} - \alpha^2\gamma = -\alpha^2\lambda_n\gamma, \;\; \gamma(0) = 0 = \gamma(1).$$

Then, solving for the eigenvalues, λ_n, one gets

$$\lambda_n = \frac{\alpha^2}{\alpha^2 + n^2\pi^2}, \;\; n = 1, 2, ... \tag{3.22}$$

with eigenvectors $\phi_n(t) = \sin n\pi t$.

A trace class operator is an operator whose trace norm $\|\mathcal{G}\|_{tr} = \sum_1^\infty |\lambda_n|$ is finite. [36] Clearly, $\mathcal{G}$ is a trace class operator. Moreover, from [36], any positive trace class operator $\mathcal{G}$ has a unique positive square root $\mathcal{J}$ where $\mathcal{G} = \mathcal{J}\mathcal{J}$. In fact, the kernel $g_\alpha(t,s)$ can be written with an eigenfunction expansion

$$g_\alpha(t,s) = \sum_1^\infty \lambda_n\phi_n(t)\overline{\phi_n(s)}$$

and $\mathcal{J}$ must have a kernel $j_\alpha(t,s)$ given by

$$j_\alpha(t,s) = \sum_1^\infty \lambda_n^{1/2} \phi_n(t) \overline{\phi_n(s)}.$$

By defining a multiplication operator

$$\mathcal{H}[\psi(\cdot)](t) = h_\alpha^\beta(t)\psi(t)$$

where $h_\alpha^\beta(t) = 1 - \cos\varphi_\alpha(t) - \beta/\alpha^2 f'(\varphi_\alpha(t),t)$ we can write $D\mathcal{N}_\alpha^\beta(\varphi_\alpha(\cdot))\psi = GH\psi$. The multiplication operator, $\mathcal{H}$, is not compact and has no eigenvalues.

Proposition 19. *Suppose $h_\alpha(\cdot)$ not constant for any open interval of $[0,1]$. Then, $\mathcal{H}$ has no eigenvalues.*

Proof. Suppose λ is an eigenvalue of $\mathcal{H}$ with eigenvector $\psi(t)$ so that $h_\alpha^\beta(t)\psi(t) = \lambda\psi(t)$. Suppose that $t_0 \in (0,1)$ is such that $\psi(t_0) \neq 0$. Then there is an open interval $(t_1,t_2) \subset [0,1]$ with $t_0 \in (t_1,t_2)$ such that $\psi(t) \neq 0$ for $t \in (t_1,t_2)$ which implies that $h_\alpha^\beta(t) = \lambda$ for each $t \in (t_1,t_2)$. □

Theorem 20. *The composition $\mathcal{GH} : X \to X$ is a compact operator with the spectrum being only a countable set of nonzero real eigenvalues with the only possible accumulation point being at zero.*

Proof. First, note that the composition $\mathcal{GH}$ is compact since $\mathcal{G}$ is compact and $\mathcal{H}$ is bounded. Now, consider $\mathcal{GH} = \mathcal{JJH}$. The operator $\mathcal{JHJ}$ is a compact, self-adjoint, linear operator. Suppose this operator has an eigenstructure $\mathcal{JHJ}\varphi_n = \lambda_n\varphi_n$, then $\psi_n = \mathcal{J}\varphi_n$ is an eigenvector with eigenvalue λ_n of $\mathcal{GH}$ because $\mathcal{GHJ}\varphi_n = \mathcal{JJHJ}\varphi_n = \mathcal{J}(\lambda_n\varphi_n) = \lambda_n\mathcal{J}\varphi_n$.

Suppose that λ, ψ is an eigenvalue, eigenvector pair of $\mathcal{GH}$ so that $\mathcal{GH}\psi = \lambda\psi = \mathcal{JJH}\psi$. If $\lambda \neq 0$, set $\varphi = \mathcal{JH}\psi/\lambda$. Then, $\mathcal{J}\varphi = \mathcal{JJH}\psi/\lambda = \lambda\psi/\lambda = \psi$ and $\mathcal{JHJ}\varphi = \mathcal{JHGH}\psi/\lambda = \mathcal{JH}\psi = \lambda\varphi$ so that λ is a non-zero eignevalue of $\mathcal{JHJ}$, i.e., $\lambda = \lambda_n$ for some $n = 1,2,....$ If $\mathcal{GH}\psi = 0\psi$, then $(\mathcal{H}\psi)(\cdot) \in ker\mathcal{G}$. This implies that $(\mathcal{H}\psi)(t) = 0$ for almost all t (i.e., $\mathcal{H}\psi = 0\psi$) which contradicts the fact that $\mathcal{H}$ has no eigenvalues. □

3.6.2 Eigenvalues and Conjugate Points

Since the eigenvalues of $D\mathcal{N}_\alpha^\beta[\varphi_\alpha(\cdot)]$ are real, we can study a conjugate point problem. In particular, we are interested in finding for what values of λ is the solution of

$$\ddot{\gamma} - \alpha^2 \left(1 - \frac{1}{\lambda} h_\alpha^\beta(t)\right) \gamma = 0, \;\; \gamma(0) = 0, \; \dot{\gamma}(0) = 1. \tag{3.23}$$

such that $\gamma(1) = 0$. Define $\delta_\alpha^\beta(\lambda)$ that maps to the solution of the differential equation (3.23) with $\gamma(0) = 0$ and $\dot{\gamma}(0) = 1$ at $t = 1$, i.e., $\delta_\alpha^\beta(\lambda) : \lambda \mapsto \gamma(1)$. For a given α and β, the values of $\delta_\alpha^\beta(\lambda) = 0$ are the eigenvalues of $D\mathcal{N}_\alpha^\beta[\varphi_\alpha(\cdot)]$. Note that the solution of the differential equation (3.23) will depend continuously the parameters.

Given α and β, we can solve the differential equation of the conjugate point problem for a family of λ. Figure 3.16 shows the solution of the conjugate point problem when $T = 1.0$ and β_{CU}. There is a largest and smallest zero crossing and the only accumulation point is at zero. So, we can plot the smallest and largest eigenvalue for our system which $\delta_\alpha(\lambda) = 0$ as seen in figure 3.17.

Note however, that the smallest and largest eigenvalues change as β changes. For our configuration of the pendubot, the eigenvalues never have a magnitude greater than one. This, however, is not always the case. For example, figure 3.18 shows the smallest eigenvalues when $\beta = 21.72 \approx 2.544\beta_{\text{CU}}$ crosses -1.0. Since $\mathcal{GH}$ is a compact linear operator, we can use a sequence of finite rank operators (e.g., by using numerical integration with a quadrature formula) to get a very good estimate of the eigenvalues of $\mathcal{GH}$. [37]

3.6.3 Approximating the Eigenvalues of $D\mathcal{N}_\alpha(\varphi_\alpha(\cdot))$

As discussed above, the linear operator $D\mathcal{N}_\alpha^\beta[\varphi_\alpha(\cdot)]$ is a compact linear operator. Therefore, the spectrum of $D\mathcal{N}_\alpha^\beta[\varphi_\alpha(\cdot)]$ is a countable set of eigenvalues, with zero being the only accumulation point. Moreover, since $D\mathcal{N}_\alpha^\beta[\varphi_\alpha(\cdot)]$ is a compact linear operator, we can approximate $D\mathcal{N}_\alpha^\beta[\varphi_\alpha(\cdot)]$ by a sequence of finite rank operators using numerical integration with a quadrature formula. [37]

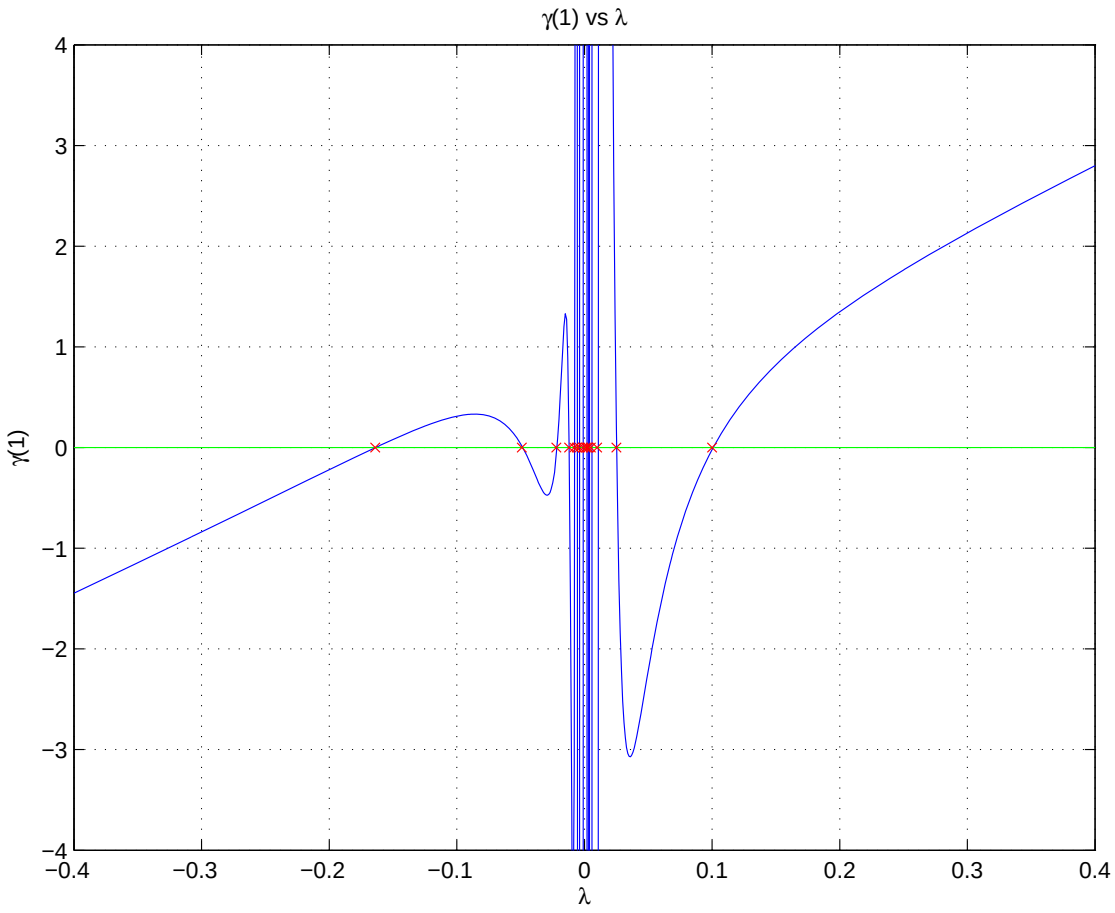


Figure 3.16: Plot of solution to the conjugate point problem for the pendubot system when $T = 1.0$ and β_{CU}. The x's show the corresponding values of $\delta_\alpha(\lambda)$

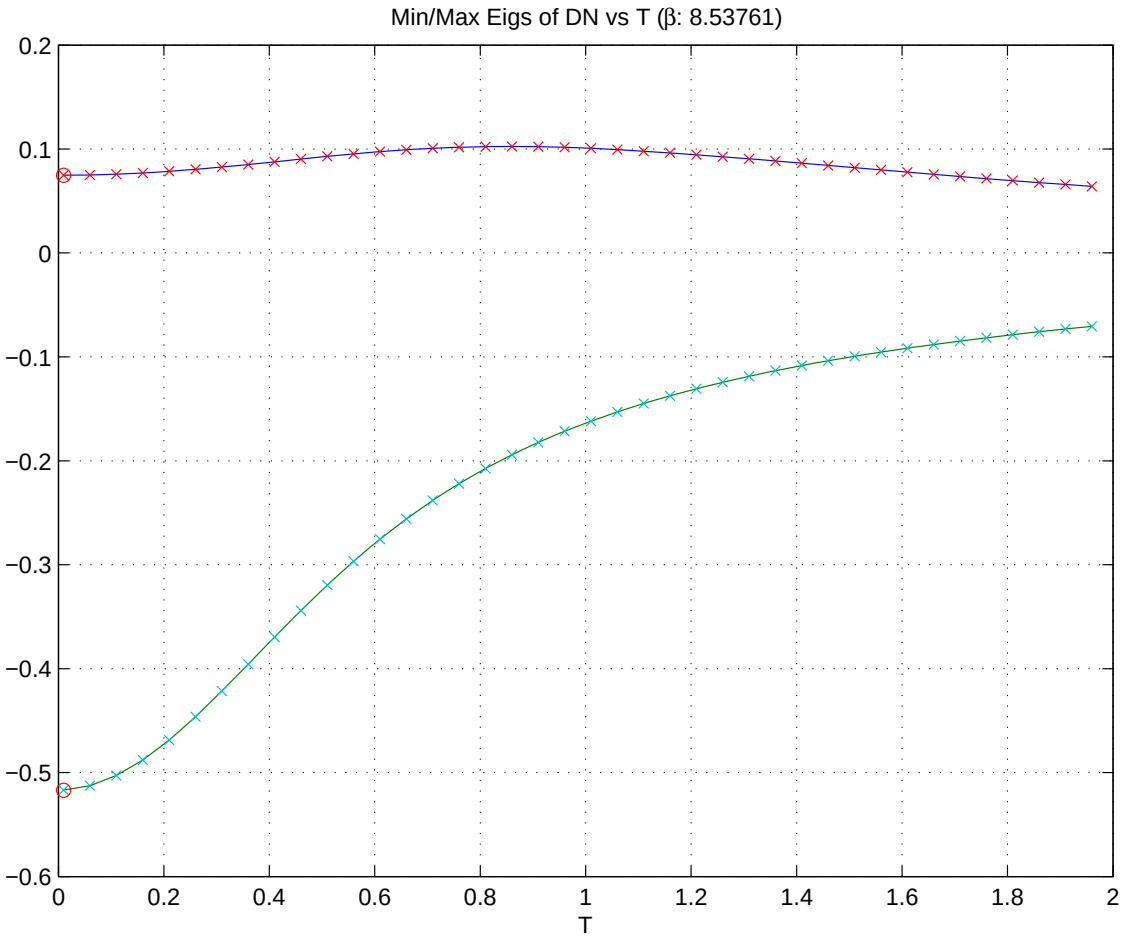


Figure 3.17: The maximum and minimum eigenvalues of $D\mathcal{N}_\alpha^\beta$ for pendubot β_{CU} are plotted. For the range of of T shown, the eigenvalues never have a magnitude greater than 1. As a result, the fixed point iteration will have a local convergence for these values of T.

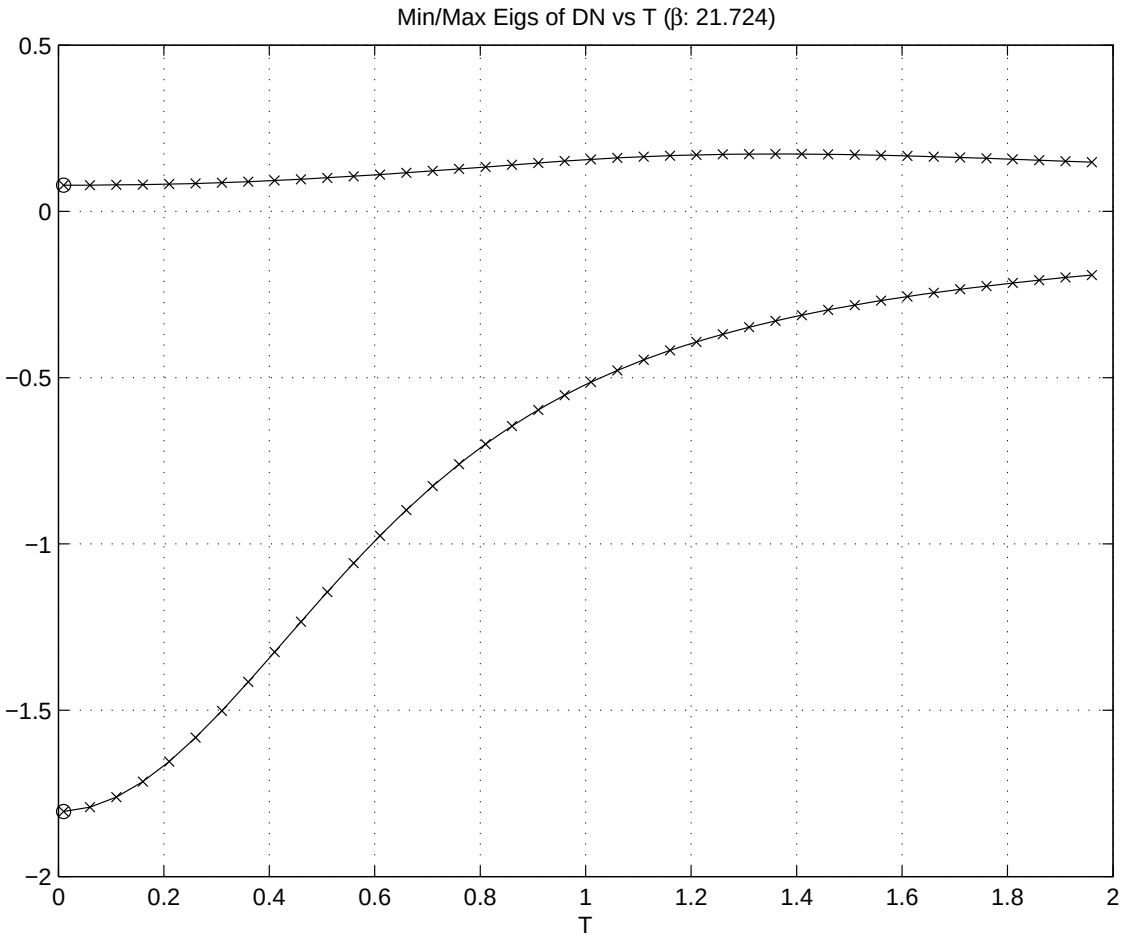


Figure 3.18: The maximum and minimum eigenvalues of $D\mathcal{N}_\alpha$ for 2.5445β are plotted. For the range shown, the smallest eigenvalue crosses -1 at $T = 0.595$ explaining why the fixed point iteration began to fail for $T < 0.595$.

First, define $(\mathcal{B}[\psi])(t)$ as follows

$$(\mathcal{B}[\psi])(t) = \int_0^1 g_\alpha(t,s) h_\alpha(s) \psi(s)\, ds \tag{3.24}$$

Note that $\gamma(t) = (\mathcal{B}[\psi])(t)$.

Because $\gamma(t)$ is a compact operator, we can approximate $\gamma(t)$ by a sequence of finite rank compact operators. Consider the following sequence of finite rank operators, $\gamma_n(s)$

$$\gamma_n(s) = (\mathcal{B}_n[\psi]) \left(\frac{2i-1}{2n} \right), \quad s \in \left(\frac{i-1}{n}, \frac{i}{n} \right) \tag{3.25}$$

$$= \sum_{j=1}^{n} g_\alpha \left(\frac{2i-1}{2n}, \frac{2j-1}{2n} \right) h_\alpha \left(\frac{2j-1}{2n} \right) \psi \left(\frac{2j-1}{2n} \right) \frac{1}{n} \tag{3.26}$$

$$= G_n H_n \psi_n \tag{3.27}$$

where $i = \lceil ns \rceil$.

Proposition 21. *The matrix $\mathcal{B}_n$ has real eigenvalues.*

Proof. Since $G_n = G_n^T > 0$, there exists a unique $W = W^T > 0$, such that $G_n = WW^T$. $B_n = G_n H_n$. Therefore, $W^{-1} B_n W = W^{-1} W W^T H_n W = W^T H_n W$. Hence B_n is similar to a symmetric matrix and therefore has real eigenvalues. □

3.7 Example of a Nonconstant Inner Arm Profile

Remember from section 3.2 that the inverted pendulum with odd period forcing has the general form

$$\ddot{\varphi} = \alpha^2 \sin\varphi + \beta\,\eta(t)\sin(\varphi - \theta(t))$$

where $\eta(t)$ and $\theta(t)$ are continuous functions that are even and (generalized) odd periodic of period 2, respectively, and $|\eta(t)| \leq 1$ for $t \in [0,1]$. For the sake of brevity, we will write the general form as

$$\ddot{\varphi} = \alpha^2 \sin\varphi + \beta\, f(\varphi, t)$$

where the function $f(\varphi,t) = \eta(t)\sin(\varphi - \theta(t))$ is has certain properties.

Let $\theta(\cdot) = \pi t - a\sin(2\pi t)$. Then, $\psi = \arctan(\ddot{\theta}/\dot{\theta}^2)$ and $a(t) = l_1/l\sqrt{(\dot{\theta}^4 + \ddot{\theta}^2)}$. Figures 3.19 and 3.20 illustrate $\theta(\cdot)$ and $\varphi(\cdot)$ with $\theta = \pi t - a\sin(2\pi t)$ as $0 < a < 1.0$. Figure 3.21 is a strobe of the pendubot maneuver taken at 20 equal time intervals. Figure 3.22 traces the tip of the outer link around the maneuver.

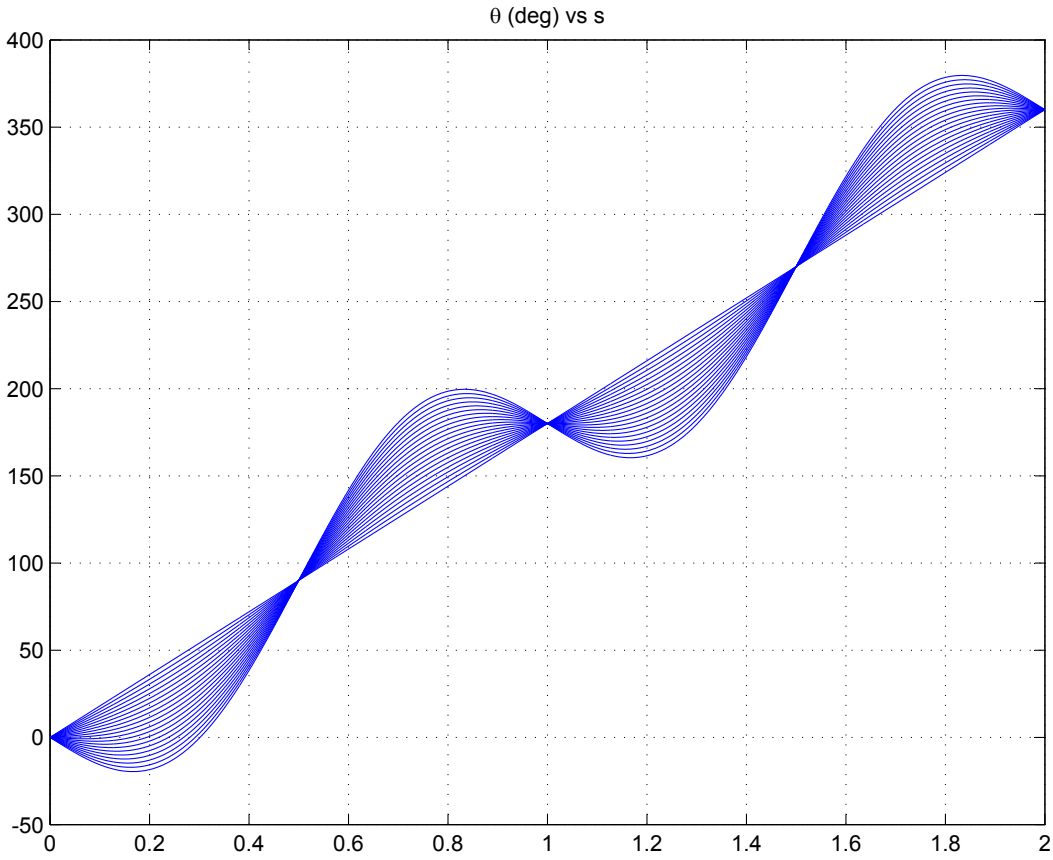


Figure 3.19: Plot of a non-constant inner arm velocity profile $\theta(\cdot) = \pi t - a\sin(2\pi t)\theta$ for $T = 1.0$ sec as a varies from 0.0 to 1.0 in increments of 0.05.

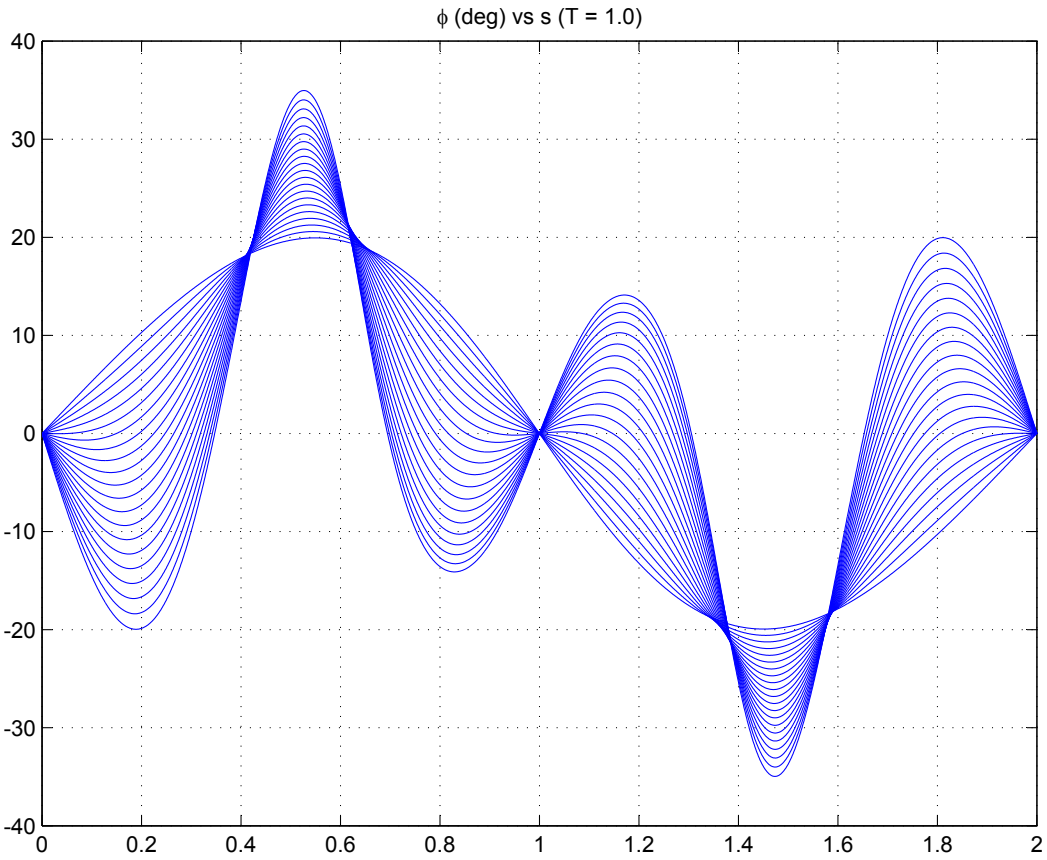


Figure 3.20: Plot of $\varphi(t)$ for a pendubot with a non-constant inner arm velocity profile $\theta(\cdot) = \pi t - a\sin(2\pi t)$ for $T = 1.0$ sec as a varies from 0.0 to 1.0 in increments of 0.05.

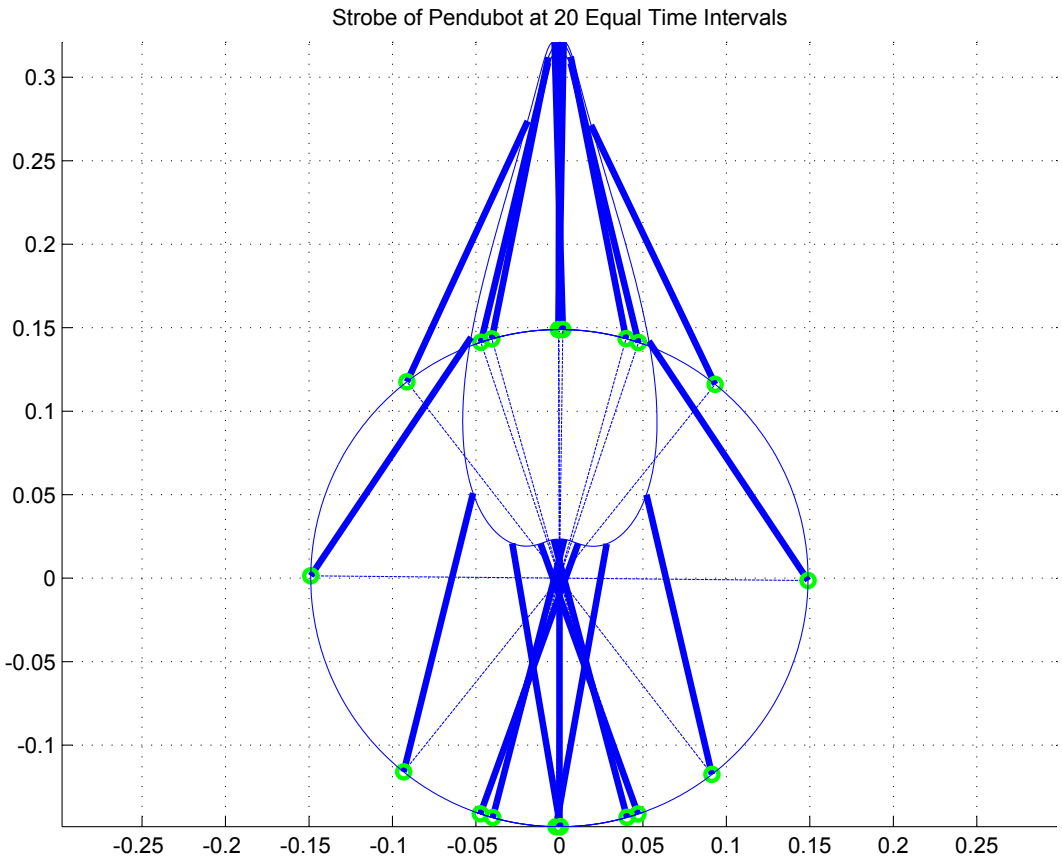


Figure 3.21: Strobe at twenty equal time intervals of the pendubot maneuver with non-constant inner arm velocity profile $\theta(\cdot) = \pi t - a\sin(2\pi t)$ for $T = 1.0$ sec and $a = 1.0$.

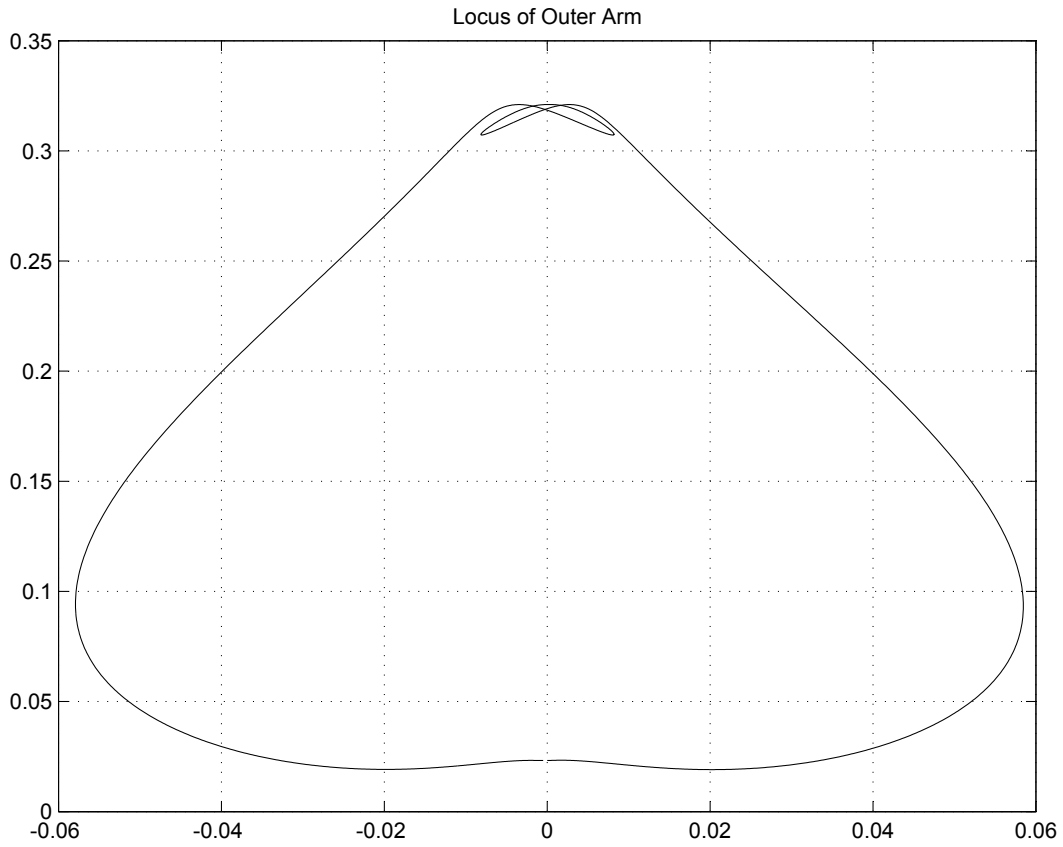


Figure 3.22: Locus of the Outer Link for $T = 1.0$ sec and $a = 1.0$.

Chapter 4

Non-Inverted Trajectory Exploration

In chapter 3, we examined inverted trajectories of the pendubot driven by odd-periodic forcing. Using the Schauder fixed point theorem, we then showed that the inverted pendulum with an odd periodic driving acceleration at the pivot **always** possesses an odd periodic solution. In this chapter, we study properties of non-inverted trajectories of the pendubot. The exponential dichotomy present in the inverted system isn't preserved in the non-inverted system as we go faster and faster. It turns out, using the Schauder fixed point theorem, that solutions always exists for an odd-periodic driving force. However, uniqueness is not guaranteed. In fact, for a sinusoidal driving force we demonstrate that we can find multiple solutions.

4.1 Driven Hanging Pendulum

The general form of a driven hanging pendulum as shown in Figure 4.1 with continuous forcing term, $f(t)$, can be written as

$$\ddot{\varphi} + g/l \sin \varphi = f(t) \ . \tag{4.1}$$

where l is the inertial length of the outer link and g is the gravitational constant. T-periodic solutions to the equation can be found by considering the corresponding periodic boundary value problem

$$\ddot{\varphi} + g/l \sin \varphi = f(t) \, , \quad \varphi(0) - \varphi(T) = 0 = \dot{\varphi}(0) - \dot{\varphi}(T) \tag{4.2}$$

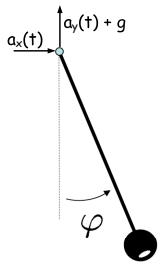


Figure 4.1: Driven hanging pendulum.

for $\varphi(t)$, $t \in [0, T]$. Note that the coordinate system used here is different than the one chosen in Chapters 2 and 3 even though we use the same variable names.

Again, for the pendubot, the inner arm trajectory $\theta(\cdot)$ may be chosen arbitrarily and imposed by an appropriate (state dependent) choice of $\tau(\cdot)$ giving

$$l\ddot{\varphi} = -g \sin \varphi - a_y(t) \sin \varphi - a_x(t) \cos \varphi \tag{4.3}$$

where the continuous acceleration functions, $a_x(t)$ and $a_y(t)$, are periodic (with common period T) and of the form

$$a_x(t) = l\Big(\ddot{\theta}(t) \cos \theta(t) - \dot{\theta}^2(t) \sin \theta(t)\Big)$$
$$a_x(t) = l\Big(\ddot{\theta}(t) \sin \theta(t) + \dot{\theta}^2(t) \sin \theta(t)\Big).$$

Defining $a(t) = (a_x^2(t) + (g + a_y)^2(t))^{1/2}$, we see that (4.3) is of the form

$$\ddot{\varphi} = -\frac{a(t)}{l} \sin(\varphi - \psi(t)) \tag{4.4}$$

where $\psi(t)$ satisfies $a_x(t) = -a(t) \sin \psi(t)$ and $a_y(t) = a(t) \cos \psi(t)$.

4.2 Existence

For $u \in \mathcal{C}[0, 1]$, define the average value as

$$\mu(u) = \frac{1}{T} \int_0^T u(t) dt \,. \tag{4.5}$$

It turns out, that when the average value of the forcing term, $f(t)$ in equation (4.2), is too big, then there will not be any solutions to the boundary value problem. [1], [13]

Theorem 22. *If there is a solution $\varphi : [0,T] \to \mathbb{R}$ to (4.1) that satisfies $\dot{\varphi}(0) = \dot{\varphi}(T)$, then $|\mu(f)| \leq g/l$.*

Proof. First write $\ddot{\varphi} = f(t) - g/l \sin\varphi$ and integrate both sides to get

$$\int_0^T \ddot{\varphi}(t)dt = \dot{\varphi}(T) - \dot{\varphi}(0) = 0 = \int_0^T f(t)dt - g/l \int_0^T \sin\varphi(t)dt$$

so that

$$T|\mu(f)| = \left|\int_0^T f(t)dt\right| = g/l \left|\int_0^T \sin\varphi(t)dt\right| \leq g/l \int_0^T |\sin\varphi(t)|\, dt \leq g/l\ T$$

completing the proof. □

Note that as the effective length, l, increases, g/l decreases imposing a stronger condition on the average value. Odd-periodic driving functions always satisfy this necessary condition for all l since the average value will be zero. It turns out that a solution always exists for odd-periodic driving functions as the following theorem from chapter 5 of [13] states.

Theorem 23. *Let $f : \mathbb{R} \to \mathbb{R}$ be an odd, T-periodic map f, for some $T > 0$. Then the forced pendulum equation (4.1) has an odd, T-periodic solution $\varphi : \mathbb{R} \to \mathbb{R}$.*

A proof is presented in chapter 5 of [13] and relies on the Schauder fixed point theorem and fact that $f(t) - g/l \sin\varphi$ has a bounded image. One of the keys to the analysis presented in [13] is the bounded image of $f(t) - g/l \sin\varphi$. Note that often we rely on the linearization of the differential equation to provide insights of the solutions. However, the linearization, in this case does not result in a bounded image and indicates that there is a resonance condition that results in an unbounded solution. Even in the analysis of the nonlinear system without a bounded image, the analysis becomes more complicated. It is the presence of the bounded image of $f(t) - g/l \sin\varphi$ that allows for a much simpler analysis and application of these types of fixed point theorems.

4.3 Nonlinear Least Squares Trajectory Exploration

We want to calculate periodic solutions of the outer arm (outer arm profiles) in a non-inverted position for a given set of periodic accelerations. As discussed above, we first view the double pendulum as a single pendulum being driven by the accelerations of the pivot point. For a given inner arm trajectory, the accelerations of the pivot point can be determined. Or, the accelerations may be specified directly. Then, using the acceleration profiles we are going to look for solutions which are consistent both with the accelerations at the pivot point and some additional constraints.

The driven pendulum is described by a periodic second order differential equation (with no control). We are seeking a periodic solution, $\varphi(\cdot)$, that satisfies the second order differential equation. There are several potential approaches to finding this solution. One approach is to use boundary value problem solver. This can be done numerically, for example, using the Matlab command `bvp4c`. A second approach is to use is to use optimal control.

Consider the problem for finding a trajectory of $\dot{x} = f(x, u)$ that is close to a specified curve $\xi_d = (x_d(\cdot), u_d(\cdot))$ in a weighted L_2 sense. In particular, given symmetric positive definite matrices Q, R, and P_1, we seek to (locally) minimize the least squares functional

$$h(\xi) = \int_0^T \|x(\tau) - x_d(\tau)\|_Q^2/2 + \|u(\tau) - u_d(\tau)\|_R^2/2 \; d\tau + \|x(T) - x_d(T)\|_{P_1}^2/2$$

over trajectories $\xi = (x(\cdot), u(\cdot)) \in \mathcal{T}$. For simplicity, we only require that the desired curve ξ_d be continuous on $[0, T]$. The dynamics for the driven pendulum system shown in Figure 4.1 are given by

$$\ddot{\varphi} = \frac{-(g + u_2)}{l} \sin\varphi - (1/l)\cos\varphi \; u_1$$

where the controls u_1 and u_2 are taken to be the pivot point lateral and vertical acceleration a_x and a_y, respectively. In state space form, we have

$$\begin{bmatrix} \dot{x}_1 \\ \dot{x}_2 \end{bmatrix} = \begin{bmatrix} f_1(x, u) \\ f_2(x, u) \end{bmatrix} = \begin{bmatrix} x_2 \\ \frac{-(g+u_2)}{l} \sin x_1 - (u_1/l)\cos x_1 \end{bmatrix}$$

The linearization about a trajectory $\xi = (x(\cdot), u(\cdot))$ is given by

$$\begin{bmatrix} \dot{z}_1 \\ \dot{z}_2 \end{bmatrix} = \begin{bmatrix} 0 & 1 \\ \frac{-(g+u_2)}{l}\cos x_1 + (u_1/l)\sin x_1 & 0 \end{bmatrix} \begin{bmatrix} z_1 \\ z_2 \end{bmatrix} + \begin{bmatrix} 0 & 0 \\ -(1/l)\cos x_1(t) & -(1/l)\sin x_1(t) \end{bmatrix} \begin{bmatrix} v_1 \\ v_2 \end{bmatrix}$$

defining $A(x(t), u(t))$ and $B(x(t), u(t))$. We will also make use of the second derivative of $f(\cdot, \cdot)$. Each $D^2 f_i(x, u)$ has a matrix representation: $D^2 f_1(x(t), u(t)) = 0_{4\times 4}$ and

$$D^2 f_2(x(t), u(t)) = \left[\begin{array}{cc|cc} \frac{(g+u_2)}{l}\sin x_1 + (u_1/l)\cos x_1 & 0 & (1/l)\sin x_1(t) & -(1/l)\cos x_1(t) \\ 0 & 0 & 0 & 0 \\ \hline (1/l)\sin x_1(t) & 0 & 0 & 0 \\ -(g/l)\cos x_1(t) - (1/l)\cos x_1(t) & 0 & 0 & 0 \end{array}\right].$$

A suitable $K(\cdot)$ for finite horizon regulation may be obtained by solving a linear quadratic optimal control problem. To wit, one may choose (with subscript r meaning regulator)

$$K_r(t) = -R_r^{-1} B(t)^T P_r(t)$$

where $P_r(\cdot)$ satisfies the Riccati equation

$$\dot{P}_r + A(t)^T P_r + P_r A(t) - P_r B(t) R_r^{-1} B(t)^T P_r + Q_r = 0, \;\; P_r(T) = P_{1r}, \tag{4.6}$$

or, equivalently,

$$\dot{P}_r + A(t)^T P_r + P_r A(t) - K_r(t)^T R_r K_r(t) + Q_r = 0, \;\; P_r(T) = P_{1r},$$

with $Q_r = Q_r^T > 0$, $R_r = R_r^T > 0$, and $P_{1r} = P_{1r}^T > 0$. (The matrices Q_r, R_r, and P_{1r} here need not be related to cost function above.) The terminal value P_{1r} is often chosen in a fashion to make it approximately compatible with Q_r and R_r and the linearized system dynamics. For instance,

suppose that $(x(T), u(T)) = (x_{eq}, u_{eq})$ is an equilibrium point, $f(x_{eq}, u_{eq}) = 0$, with controllable linearization (A_{eq}, B_{eq}) and let $P_{1r} = P_{1r}^T > 0$ be the stabilizing solution to the associated algebraic Riccati equation. Then the extension of $K_r(\cdot)$ (constant on $t \geq T$) stabilizes the corresponding extension of ξ (also constant on $t \geq T$). Naturally, these comments are also useful in the selection of P_1 for the least squares functional $h(\cdot)$ above.

Suppose now that we have obtained a $K(\cdot)$ and we wish to evaluate $\mathcal{P}(\xi)$ and $g(\xi) = h(\mathcal{P}(\xi))$ for some $\xi = (\alpha(\cdot), \mu(\cdot))$ that is not necessarily a trajectory. This is easily accomplished by integrating the augmented system

$$\begin{aligned} \dot{x} &= f(x,u) & x(0) = x_0, \\ u &= \mu(t) + K(t)\left[\alpha(t) - x\right] & \\ \dot{x}_{n+1} &= \|x - x_d(t)\|_Q^2/2 + \|u - u_d(t)\|_R^2/2 & x_{n+1} = 0 \end{aligned} \tag{4.7}$$

over $[0, T]$ and noting that

$$g(\xi) = h(\mathcal{P}(\xi)) = x_{n+1}(T) + \|x(T) - x_d(T)\|_{P_1}^2/2\,.$$

The system (4.7) can be implemented in `Matlab` using an S-function system with

- state (x, x_{n+1}),

- input $(\alpha(t), \mu(t), K(t), x_d(t), u_d(t))$, $t \in [0, T]$,

and

- output u.

4.4 Trajectory Exploration Odd-Periodic Driving Function

With odd-periodic forcing terms, we know there will always be a solution to 4.2 from the Schauder fixed point theorem. The Schauder fixed point theorem, however, does not guarantee uniqueness. In fact, once we find one solution to 4.2, we actually have an infinite number of solutions. For example, if $y(t)$ is a solution, then $y(t) + 2\pi k$ will be a solution for $k = 0, 1, 2, 3, ...$

However, it is possible to find solutions that are really different (i.e., differ by more than a constant). In this section, we provide some examples of trajectories we found during our trajectory exploration of the pendubot with the inner arm following a sinusoidal input.

Let $\theta = A \sin \omega t$. Figure 4.2 is a plot of the maximum angle the outer arm angle ($\varphi(\cdot)$ will achieve when driven by $\theta(t) = 30\,\pi/180 \sin\,\omega\, t$. We were able to find multiple T-periodic solutions for the same driving function for various ω as seen in Figures 4.3 and 4.5. Moreover, the difference between these solutions is not simply a constant function. Just looking at Figures 4.3 and 4.5 one might suspect that the resulting solutions for the outer arm are sinuisoids. This, however, is not the case. Clearly, the largest solution shown in Figure 4.5 is not a sinusoid. Also, the other solutions are not pure sinusoids. For example, Figure 4.4 shows the solution with maximum angle around 2.4 and $\omega = 5$ along with the first and third fourier components.

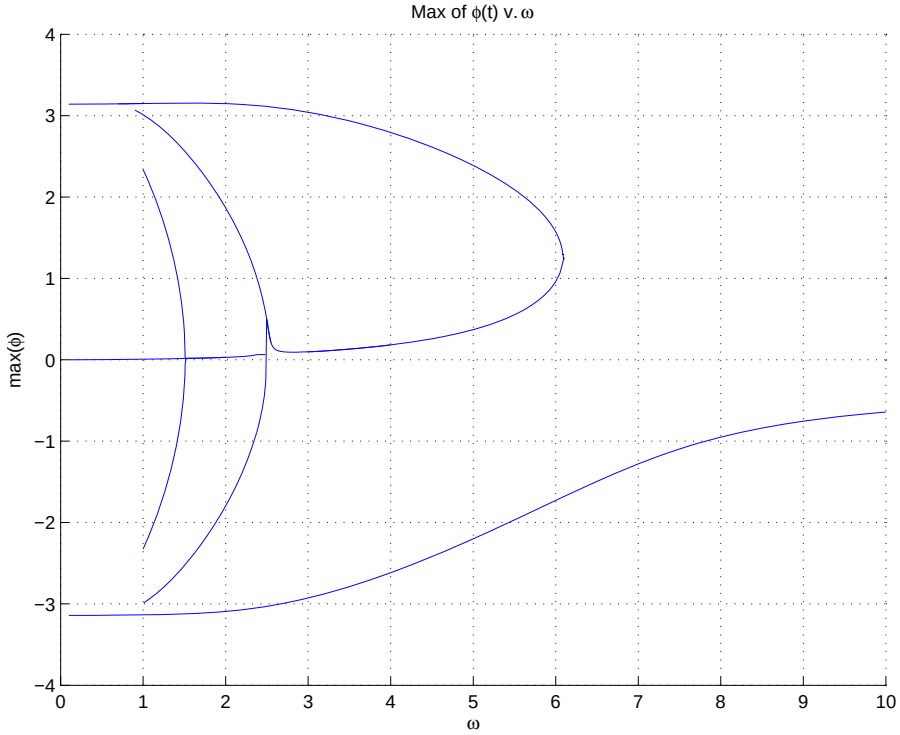


Figure 4.2: Plot of the maximum angle the outer arm will achieve driven by $\theta(t) = 30\,\pi/180 \sin\,\omega\,t$. We were able to find multiple solutions for the same driving function for various ω.

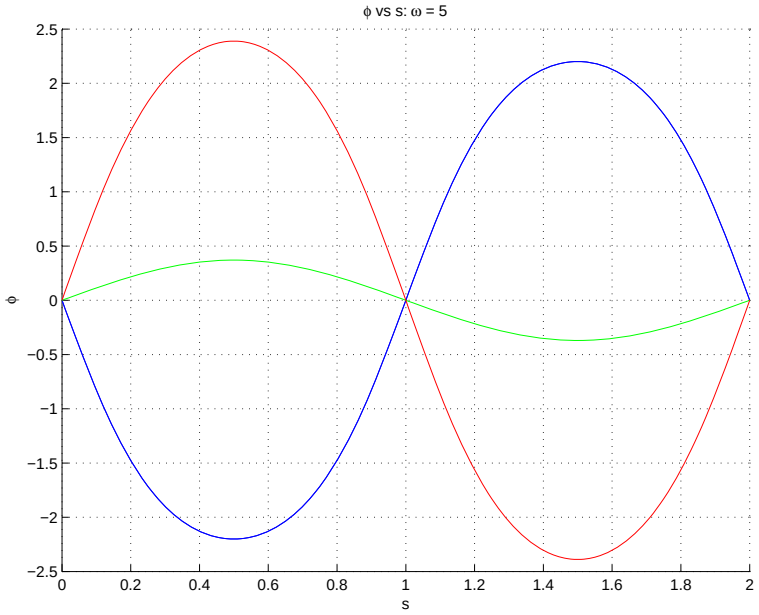


Figure 4.3: Plot of multiple, normalized, solutions when $\theta(t) = 30\,\pi/180 \sin\,5.0\,t$. In this case, we found three solutions for the same sinusoidal driving function when $\omega = 5.0$.

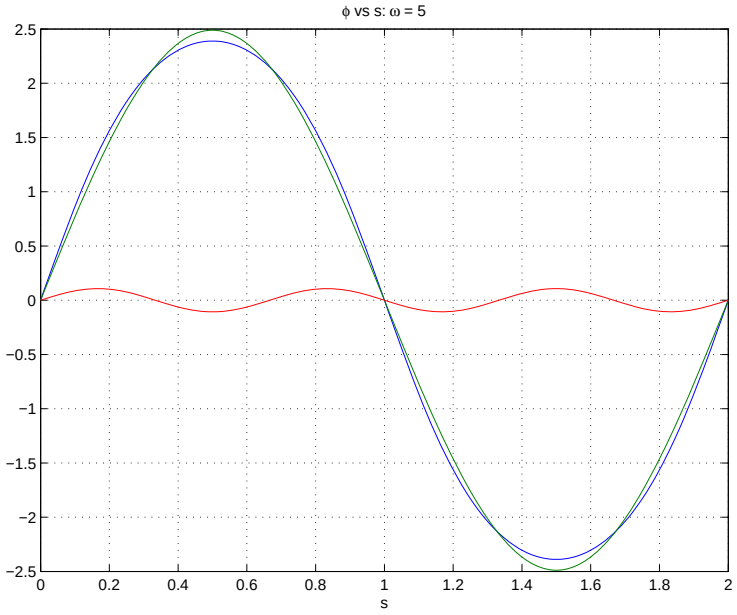


Figure 4.4: Plot of one of the solutions when $\theta(t) = 30\,\pi/180 \sin\, 5.0\,t$ along with the first and third fourier components. In this case, the sinusoidal driving function does not result in a pure sinusoid for the outer link.

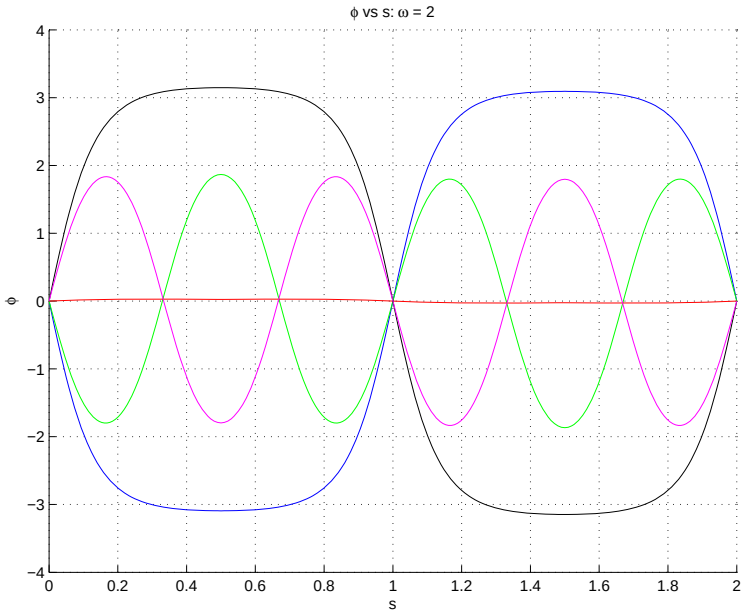


Figure 4.5: Plot of multiple, normalized, solutions when $\theta(t) = 30\,\pi/180 \sin\, 2.0\,t$. In this case, we found five solutions for the same sinusoidal driving function when $\omega = 2.0$.

Chapter 5

Maneuver Regulation

This chapter starts with an overview of some of the basic concepts of maneuver regulation. [9], [21], [22], Then, we demonstrate through simulation and/or physical implementation, the usefulness of maneuver regulation for provided orbital stabilization for the trajectories found in Chapters 3 and 4.

5.1 Overview

Nonlinear dynamics can impose nontrivial operating limitations on the operation of physical systems. In addition, all physical systems include some type of input saturations and dynamic limitations which can result in a decrease in the size of the domain of attraction. The input saturations and dynamic limitations of the pendubot imposes limits on the time parameterizations of feasible maneuvers. Given these types of limitations, maneuver regulation can prove useful in successfully defining and achieving control objectives.

Maneuver regulation has a type of local support property in that a significant local degradation of regulation is quickly forgiven and does not impact future performance. In contrast, trajectory tracking is globally affected by local degradation as the system tries to catch up in time. It is the forgiveness of significant local degradation by the maneuver regulation controller that makes it an ideal choice for implementing aggressive maneuvers. In the next few sections, we see that maneuver regulation relies on the construction of a suitable change of coordinates to write the dynamics in a new form. In particular, the new form lays bare a transverse structure of the system

while keeping exposed the differential equations to allow for regulation of the transverse dynamics. Then, we use able to use a **linear** control design to produce a **nonlinear** controller that results in a periodic orbit becoming attractive.

5.2 Longitudinal and transverse coordinates

Consider the nonlinear system

$$\dot{x} = f(x,u) \ , \tag{5.1}$$

with state $x \in \mathbb{R}^n$ and control $u \in \mathbb{R}^m$. Then, $(\alpha,\mu)(t) \in \mathbb{R}^n \times \mathbb{R}^m, t \in \mathbb{R}$, is a trajectory of 5.1 if for all $t \in \mathbb{R}$,

$$\alpha'(t) = f(\alpha(t),\mu(t))$$

where $\alpha'(\theta) = \frac{d}{d\theta}\alpha(\theta)$.

A maneuver is a curve in the state-control space that is independent of any parameterization and consistent with the system dynamics. For example,

$$\alpha'(\theta) = f(\alpha(\theta),\mu(\theta)), \quad \theta \in \mathbb{R}$$

Using an output map

$$y = h(x) \ , \tag{5.2}$$

where $y \in \mathbb{R}^p, p \leq n$, we can specify a desired trajectory that we would like to regulate the system to. Given the task $y_\xi(t)$, we assume that there exists a state-control trajectory $\xi(t) = (x_\xi(t), u_\xi(t))$ that satisfies

$$\begin{aligned} \dot{x}_\xi(t) &= f(x_\xi(t), u_\xi(t)) \\ y_\xi(t) &= h(x_\xi(t)) \quad . \end{aligned} \tag{5.3}$$

The trajectory y_ξ may be regarded as a regular curve in the output space $\mathbb{R}^p$ on which we can specify a new **parameterization**, i.e. a function

$$\begin{aligned} s_\xi(\cdot): \ \mathbb{R} &\rightarrow \mathbb{R} \\ t &\mapsto s_\xi(t) \end{aligned} \tag{5.4}$$

that is invertible and, at least, of class C^1. We denote the inverse of the parameterization as $\bar{t}_\xi(\cdot)$ giving $s_\xi(\bar{t}_\xi(\theta)) = \theta$. The time derivative of $s_\xi(t)$ defines a continuous function

$$\nu_\xi(t) := ds_\xi(t)/dt \tag{5.5}$$

that we refer to as the **velocity** along y_ξ. Such a quantity may also be expressed using the parameterization s_ξ, obtaining

$$\bar{\nu}_\xi(\theta) = \nu_\xi(\bar{t}_\xi(\theta)) \ .$$

We use a bar sign when a curve is expressed in the new parameterization. From equation(5.3), we see that $\bar{x}_\xi$ satisfies

$$\begin{aligned} \bar{x}'_\xi(\theta)\bar{v}_\xi(\theta) &= f(\bar{x}_\xi(\theta), \bar{u}_\xi(\theta)) \\ \bar{y}_\xi(\theta) &= h(\bar{x}_\xi(\theta)) \ , \end{aligned} \tag{5.6}$$

where $\bar{x}'_\xi(\theta)$ denotes the derivative with respect to θ. Around the curve $\bar{y}_\xi$ we define a set of local coordinates

$$(\theta, \rho) = \Phi(y), \ \theta \in \mathbb{R}, \ \rho \in \mathbb{R}^{p-1} \tag{5.7}$$

having the property that ρ vanishes if y belongs to the curve, that is $\Phi(\bar{y}_\xi(\theta)) = (\theta, 0)$. Denote $\phi_1, \ldots, \phi_p$ the components of Φ. The first component $\phi_1(y)$ will be also denoted $\pi : \mathbb{R}^p \to \mathbb{R}$ and we define it as

$$\pi(y) = \arg\min_{\theta \in \mathbb{R}} \|y - \bar{y}_\xi(\theta))\|^2 \ . \tag{5.8}$$

A set of **longitudinal coordinate**, s, and **transverse coordinates**, $w = (w_1, \ldots, w_{n-1})$, can be computed by taking the inverse of $\Phi(y)$ about the state space curve $\bar{x}_\xi(s)$, i.e.,

$$(s, w) = \Psi(x) \ . \tag{5.9}$$

The projection map $\pi(\cdot)$ defined in (5.8) provides the longitudinal coordinate by posing

$$s = \psi_1(x) = \pi(h(x)) \ . \tag{5.10}$$

The first $p-1$ transverse coordinates $w_1, \ldots, w_{p-1}$ of x are obtained combining the output function $h(\cdot)$ together with the functions $\phi_i(\cdot),\ i = 2, \ldots, p$, obtaining

$$w_{i-1} = \psi_i(x) = \phi_i(h(x)), \quad i = 2, \ldots, p. \tag{5.11}$$

The remaining coordinates are defined as

$$w_{i-1} = \psi_i(x) = n(x) - n(\bar{x}_\xi(\pi(h(x)))), \quad i = p+1, \ldots, n. \tag{5.12}$$

5.3 Transverse Form of the Dynamics

The transformation $x = \Psi(s, w)$ allows us to write the dynamics of the nonlinear system (5.1) using the longitudinal and transverse coordinates. Using the new set of coordinates we can analyze the system and infer important properties on the stability of the desired trajectory. The main result states the following:

Proposition 24. *The dynamics of the nonlinear system (5.1) on a neighborhood of the trajectory $\bar{x}_\xi$ has the form*

$$\begin{aligned} \dot{s} &= \bar{\nu}_\xi(s) + f_1(s, w, v) \\ \dot{w} &= A(s)w + B(s)v + f_2(s, w, v) \end{aligned} \tag{5.13}$$

where $v = u - \bar{u}_\xi(s)$ while $f_1(\cdot,\cdot,\cdot)$ and $f_2(\cdot,\cdot,\cdot)$ satisfy

$$f_1(s,0,0) = 0,\ f_2(s,0,0) = 0,\ \frac{\partial f_2(s,0,0)}{\partial w} = 0,\ \textit{and}\ \frac{\partial f_2(s,0,0)}{\partial v} = 0\ .$$

Proof: See, e.g., [9]

The differential equation (5.13) expressed in longitudinal and transverse coordinates is the **trasverse form** of the dynamics of the nonlinear system (5.1).

5.4 Transverse Linearization

Given the nonlinear system (5.1), a trajectory $\xi(t) = (x_\xi(t), u_\xi(t))$, and a parameterization $s_\xi(t)$, the dynamics of the nonlinear system can be written in transverse form. It is possible,

however, to rewrite the dynamics of the transverse coordinates w as a differential equation in the longitudinal coordinate s avoiding the explicit dependence from time t. Indeed, from [9], we have

Proposition 25. *For any trajectory $((s(t), w(t)), v(t))$ of the nonlinear system (5.13) for which $s(\cdot)$ is invertible (that is there exist $\bar{t}(\cdot)$ such that $s(\bar{t}(\theta)) = \theta$), the transverse coordinates expressed as a function of the longitudinal parameterization, i.e. $\bar{w}(\theta) = w(\bar{t}(\theta))$, satisfy*

$$\frac{d\bar{w}}{d\theta} = A_{\mathsf{T}}(\theta)\bar{w} + B_{\mathsf{T}}(\theta)\bar{v} + f_{\mathsf{T}}(\theta, \bar{w}, \bar{v}) \ , \tag{5.14}$$

where

$$A_{\mathsf{T}}(\theta) := \frac{A(\theta)}{\bar{\nu}_\xi(\theta)} \quad , \quad B_{\mathsf{T}}(\theta) := \frac{B(\theta)}{\bar{\nu}_\xi(\theta)}$$

while $f_{\mathsf{T}}(\cdot, \cdot, \cdot)$ is of higher order in $\bar{w}$ and $\bar{v}$, that is

$$f_{\mathsf{T}}(\theta, 0, 0) = 0, \ \frac{\partial f_{\mathsf{T}}}{\partial w}(\theta, 0, 0) = 0, \ \frac{\partial f_{\mathsf{T}}}{\partial v}(\theta, 0, 0) = 0 \ , \tag{5.15}$$

and where the input $\bar{v} = \bar{v}(\theta)$ is equal to $v(\bar{t}(\theta))$.

Writing the transverse dynamics as a differential equation in the coordinate s allows the design of control laws that regulate the transverse dynamics to zero without being an explicit function of time. With a slight abuse of notation, we will write (5.14) using the letter s in place of θ as

$$\frac{d\bar{w}}{ds} = A_{\mathsf{T}}(s)\bar{w} + B_{\mathsf{T}}(s)\bar{v} + f_{\mathsf{T}}(s, \bar{w}, \bar{v}) \ . \tag{5.16}$$

The transverse linearization of (5.13) can be written as

$$\frac{d\bar{w}}{ds} = A_{\mathsf{T}}(s)\bar{w} + B_{\mathsf{T}}(s)\bar{v} \ . \tag{5.17}$$

5.5 Driven Pendulum Example

Consider the driven pendulum system

$$\ddot{\varphi} - \sin\varphi = u$$

which can be written as

$$\begin{aligned}\dot{\varphi} &= \omega \\ \dot{\omega} &= \sin\varphi + u\ .\end{aligned}$$

Suppose now that we would like the system to follow a desired velocity profile $\tilde{\omega}(\varphi)$ where $\tilde{\omega}(\cdot) \in C^1$ is periodic and strictly positive. On the maneuver, $\omega = \tilde{\omega}(\varphi)$. To obtain $\omega = \tilde{\omega}(\varphi)$, we expect that $u = \tilde{u}(\varphi)$ as well. Indeed, applying $\dot{\varphi} = \omega$, we find that

$$\dot{\omega} = \tilde{\omega}'(\varphi)\dot{\varphi} = \tilde{\omega}'(\varphi) = \tilde{\omega}'(\varphi)\tilde{\omega}(\varphi)$$

so that

$$\tilde{u}(\varphi) = \tilde{\omega}'(\varphi)\tilde{\omega}(\varphi) - \sin\varphi$$

holds. To complete the specification of the maneuver, we choose s as the longitudinal coordinate so that $\dot{s} = 1$ on the maneuver. Integrating $\dot{\varphi} = \tilde{\omega}(\varphi)$, $\varphi(0) = 0$, to obtain $\varphi(t)$, $t \geq 0$, and set T to be the first time $t > 0$ gives $\varphi(t) = 0$.

Now, pick $\varphi = \bar{\varphi}(s)$. It is not hard to see that

$$\begin{aligned}\bar{\varphi}' &= \bar{\omega}(s) \\ \bar{\omega}' &= \sin\bar{\varphi} + \bar{u}(s)\end{aligned}$$

giving a maneuver of

$$[(\bar{\varphi}(s), \bar{\omega}(s), \bar{u}(s)], s \in S^1$$

Since $\dot{\varphi} = \bar{\varphi}'(s)\dot{s} = \omega = \bar{\omega}(s) + \rho$ and $u = \bar{u}(s) + v$, we get the following transverse dynamics

$$\begin{aligned}\dot{s} &= 1 + \tfrac{1}{\bar{\omega}(s)}\rho \\ \dot{\rho} &= -\left(\sin\bar{\varphi}(s) + \bar{u}(s)\right)\tfrac{1}{\bar{\omega}(s)}\rho + v\ .\end{aligned}$$

5.6 Maneuver Regulation Control Law

A linear feedback with gain matrix depending on the "current position" s along the maneuver is sufficient to make the transverse linearization (when stabilizable) uniformly exponentially stable. This result, obtained in the domain of the transverse coordinates without an explicit dependence

from time t may be restated for the nonlinear dynamics in the original coordinates and in the usual setting of a differential equation with respect to time. From [9], we have the following well-known result for maneuver regulation

Proposition 26. *Suppose that the feedback $\bar{v} = -K(s)\bar{w}$ makes the origin of the linear system*

$$\frac{d\bar{w}}{ds} = (A_{\mathsf{T}}(s) - B_{\mathsf{T}}(s)K(s))\bar{w} \tag{5.18}$$

(uniformly) exponentially stable. Then, the control law

$$u = \bar{u}_{\xi}(\pi(h(x))) - K(\pi(h(x))W(x) \tag{5.19}$$

applied to the nonlinear system (5.1) is such that $x(t) \to [x_{\xi}]$ (and consequently $y(t) \to [y_{\xi}]$) as $t \to \infty$, provided that the initial condition $x(0)$ is sufficiently close to the maneuver $[x_{\xi}]$.

Proof: By hypothesis, the closed loop time-varying matrix $A_c(s) := A_{\mathsf{T}}(s) - B_{\mathsf{T}}(s)K(s)$ is such that the origin of the linear system $\bar{w}' = A_c(s)\bar{w}$ is (uniformly) exponentially stable. This implies that, given a continuous, bounded, positive definite, symmetric matrix $Q(s) > c_1 I > 0$, with c_1 some constant, there exists a continuously differentiable, bounded, positive definite, symmetric matrix $P(s)$ that satisfies the time-varying Lyapunov equation

$$-P'(s) = A_c^T(s)P(s) + P(s)A_c(s) + Q(s)\ , \tag{5.20}$$

where $P'(s)$ denotes $(dP/ds)(s)$. We now show that

$$V(x) = W(x)^T P(\pi(h(x)))W(x) \tag{5.21}$$

is a Lyapunov function that proves the exponential stability of curve x_{ξ}. That is, on a neighborhood of x_{ξ}, $V(\cdot)$ satisfies

$$k_1\|x\|_{\xi}^2 \leq V(x) \leq k_2\|x\|_{\xi}^2$$

and

$$\|\frac{\partial V}{\partial x}\| \leq k_3\|x\|_{\xi}$$

and

$$\dot{V}(x) \leq -k_4 \|x\|_\xi^2$$

for some positive constants k_1, k_2, k_3, k_4, and

$$\|x\|_\xi := \inf_{s \in \mathbb{R}} \|x - \bar{x}_\xi(s)\| \ .$$

Clearly, this Lyapunov function is defined in a neighborhood of x_ξ and vanishes along the curve x_ξ. (Indeed, $W(x) = 0$ on x_ξ.) Moreover $V(\cdot)$ is quadratic in $\|x\|_\xi$ since $P(\cdot)$ is positive definite and continuous and, on a sufficiently small compact neighborhood of x_ξ,

$$l_1 \|x\|_\xi \leq \|W(x)\| \leq l_2 \|x\|_\xi$$

for some $l_1, l_2 > 0$. Differentiating $V(x)$ we have

$$\begin{aligned} \dot{V}(x) \ &= \ -w^T Q(s) \bar{\nu}_\xi(s) w + \\ & \qquad w^T P(s) f_2(s, w, -K(s)w) + \\ & \qquad w^T P'(s) f_1(s, w, -K(s)w) w \ . \end{aligned}$$

Since the last two terms are cubic in w and $\bar{\nu}_\xi(s)$ is positive and bounded away from zero, it is clear that $\dot{V}$ is locally negative definite and quadratic in $\|x\|_\xi$. $\square$

5.7 Maneuver Regulation about Non-Inverted Trajectories

In this section, we design a maneuver regulation controller for trajectories of the pendubot generated by driving the inner arm with an odd periodic signal (e.g., $\theta = a \sin \omega t$) and the outer arm is hanging down. We convert the desired trajectory to a maneuver of the system and define a local transverse coordinate system about the maneuver before designing an indexed varying gain which is implemented as a state feedback controller on the physical system.

5.7.1 Maneuver Regulation

In Chapter 4, we described one way of finding some interesting periodic orbits of the pendubot and we found multiple trajectories $\left(\theta, \dot{\theta}, \varphi, \dot{\varphi}, \tau\right)(\cdot)$ of the pendubot for the same odd-

periodic $\theta(\cdot)$. Defining a projection, $s = \pi(x)$, we can convert the trajectory to a maneuver $(\alpha(s), \mu(s))$. A maneuver is a curve in the state-control space that is consistent with the system dynamics. By selecting a feedback transformation to give a transverse maneuver coordinate system (s, ρ) which is local about $\alpha(\cdot)$. Specifically, $x \mapsto (\alpha(s), \mu(s))$, where $x \in \mathbb{R}^n$ and $s \in \mathbb{R}$. A transverse coordinate system is then defined where $x \mapsto (s, \rho)$ and the transverse component $\rho \in \mathbb{R}^{n-1}$ such that (s, ρ) forms a local set of coordinates around $\alpha(s)$. The choice of the transverse coordinate system defines the projection $\pi(\cdot)$.

In particular, we define a feedback transformation $z = \Phi(z), u = \mu(s) + v$ which gives rise to the following system

$$\dot{z} = D\Phi(\Psi(z)) f(\Psi(z), \mu(s) + v) \equiv \tilde{f}(z, v) \tag{5.22}$$

where $\Psi(z) \equiv \Phi^{-1}(x)$. Note, that (5.22) includes information about the control needed to flow along the maneuver since $\dot{z} = \tilde{f}(z, v)$ and maneuver where $v = 0$ and $z = (s, 0)$. From here explore the design of a control which stabilizes the transverse dynamics by computing the indexed linearization of the transverse system (5.22) to get

$$z' = A(s)z + B(s)v.$$

Then we compute an indexed varying gain, $k(s)$, which exponentially stabilizes the transverse dynamics, by solving an indexed varying LQR.

5.7.2 One Transverse Coordinate System

We want to design a maneuver regulation controller to follow the maneuver $\left(\theta, \varphi, \dot{\theta}, \dot{\varphi}, \tau\right)(\cdot)$. By specifying $\theta(t) = a \sin \omega t$, then $\dot{\theta}(t) = a\omega \sin \omega t$ and we can determine the other states and needed input as described in Chapter 4.

Let the transverse coordinate, s, be θ and the longitudinal coordinates be

$$\rho_1 = -\frac{2}{\pi} \tan\left(\frac{\pi}{2}\left(\frac{R(\theta, \dot{\theta}) - a}{a}\right)\right)$$

$$\rho_2 = \varphi - \bar{\varphi}$$

$$\rho_3 = \dot{\varphi} - \dot{\bar{\varphi}}$$

where $R(\theta, \dot{\theta}) = \sqrt{\theta^2 + \frac{\dot{\theta}^2}{\omega^2}}$.

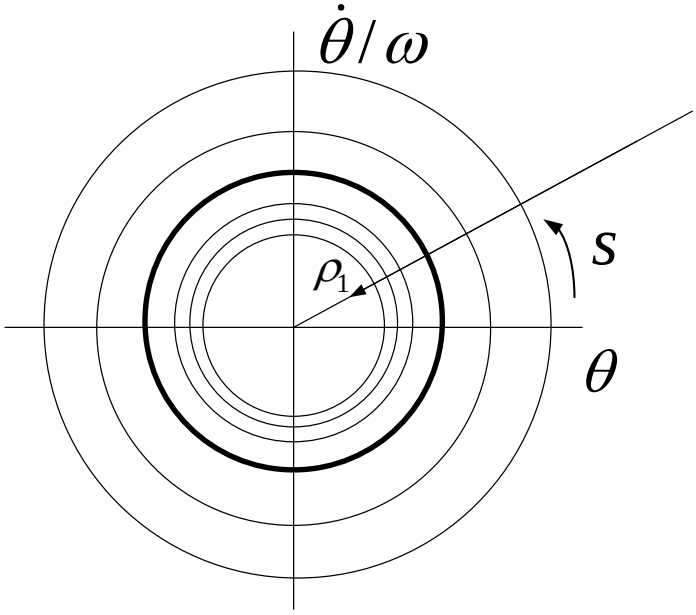


Figure 5.1: Phase plot of θ and $\dot{\theta}/\omega$ along with the local coordinate system (i.e., the transverse coordinate ρ_1 and longitudinal coordinate s).

Figure 5.1 shows a phase plot of θ and $\dot{\theta}/\omega$. Our choice of this transverse coordinate system was motivated by desiring a transformation which will look linear close to the orbit and increase quickly away from the orbit. In fact, for our choice we see that

$$R = 0 \quad w = \infty$$

$$R = 2a \quad w = -\infty$$

$$R = a \quad w = -\tfrac{2}{\pi}$$

We defined a map $\Psi : z \mapsto x$ as follows

$$x = \Psi(z) = \Psi(s, \rho) = \begin{bmatrix} r(\rho_1) \sin \omega s, \\ r(\rho_1)\omega \cos \omega s, \\ \bar{\varphi}(s) + \rho_2, \\ \dot{\bar{\varphi}}(s) + \rho_3 \end{bmatrix} \tag{5.23}$$

where $r(\rho_1) = a\left[-\frac{2}{\pi}\tan^{-1}\left(\frac{\pi}{2}\rho_1\right) + 1\right]$. This selection of $\Psi(z)$ implicitly defines the following inverse mapping $\Phi : x \mapsto z$,

$$\Phi : \begin{pmatrix} \theta \\ \dot{\theta} \\ \varphi \\ \dot{\varphi} \end{pmatrix} \mapsto \begin{pmatrix} s \\ \rho_1 \\ \rho_2 \\ \rho_3 \end{pmatrix} = \begin{pmatrix} \tan^{-1}\frac{\omega\theta}{\dot{\theta}} \\ -\frac{2}{\pi}\tan\left(\frac{\pi}{2}\left(\frac{\sqrt{\theta^2 + \frac{\dot{\theta}^2}{\omega^2}} - A}{A}\right)\right) \\ \varphi - \bar{\varphi}(\tan^{-1}\frac{\omega\theta}{\dot{\theta}}) \\ \dot{\varphi} - \dot{\bar{\varphi}}(\tan^{-1}\frac{\omega\theta}{\dot{\theta}}) \end{pmatrix}$$

Note that $z = \Phi(x)$. So, $x = \Phi^{-1}(z) \equiv \Psi(z)$. $A(s)$ and $B(s)$ may be computed as follows

$$A(s)\rho = D^2R(\alpha(s)) \cdot (f(\alpha(s), \mu(s)), Z(s)\rho) + DR(\Psi(s, 0)) \cdot D_1 f(\alpha(s), \mu(s)) \cdot Z(s)\rho$$

$$B(s)v = DR(\Psi(s, 0)) \cdot D_2 f(\alpha(s), \mu(s)) \cdot v$$

where

$$Z(s) \equiv \frac{\partial \Psi}{\partial \rho}(s, 0),$$

and

$$R(x) = (\psi_2(x), \psi_3(x), \psi_4(x))^T.$$

Following [9], $D^2R(\Psi(s, \rho))$ may be computed by defining

$$M(s, \rho)z \equiv DR(\Psi(s, \rho)) \cdot z$$

where z is a general perturbation and recalling that $\Psi(s,0) = \alpha(s)$. Then,

$$D^2R(\alpha(s)) \cdot (f(\alpha(s), \mu(s)), Z(s)\rho) = D_2M(s,0) \cdot \rho\alpha'(s)$$

resulting in

$$D\Psi(z) = \begin{bmatrix} \omega r(\rho_1)\cos(\omega s) & r'(\rho_1)\sin(\omega s) & 0 & 0 \\ -\omega^2 r(\rho_1)\sin(\omega s) & \omega r'(\rho_1)\cos(\omega s) & 0 & 0 \\ \bar{\varphi}'(s) & 0 & 1 & 0 \\ \dot{\bar{\varphi}}'(s) & 0 & 0 & 1 \end{bmatrix}$$

$$Z(s) = \begin{bmatrix} r'(0)\sin(\omega s) & 0 & 0 \\ \omega r'(0)\cos(\omega s) & 0 & 0 \\ 0 & 1 & 0 \\ 0 & 0 & 1 \end{bmatrix}$$

Note that $D\Phi(\Psi(z)) = [D\Psi(z)]^{-1}$ and $r(0) = r'(0) = a \neq 0$.

$$D\Phi(\Psi(z)) = \begin{bmatrix} \frac{1}{\omega r(\rho_1)}\cos(\omega s) & \frac{-1}{\omega^2 r(\rho_1)}\sin(\omega s) & 0 & 0 \\ \frac{1}{r'(\rho_1)}\sin(\omega s) & \frac{1}{\omega r'(\rho_1)}\cos(\omega s) & 0 & 0 \\ \frac{-\bar{\varphi}'(s)}{\omega r(\rho_1)}\cos(\omega s) & \frac{\bar{\varphi}'(s)}{\omega^2 r(\rho_1)}\sin(\omega s) & 1 & 0 \\ \frac{-\dot{\bar{\varphi}}'(s)}{\omega r(\rho_1)}\cos(\omega s) & \frac{\dot{\bar{\varphi}}'(s)}{\omega^2 r(\rho_1)}\sin(\omega s) & 0 & 1 \end{bmatrix}$$

and

$$DR(\Psi(z)) = \begin{bmatrix} \frac{1}{r'(\rho_1)}\sin(\omega s) & \frac{1}{\omega r'(\rho_1)}\cos(\omega s) & 0 & 0 \\ \frac{-\bar{\varphi}'(s)}{\omega r(\rho_1)}\cos(\omega s) & \frac{\bar{\varphi}'(s)}{\omega^2 r(\rho_1)}\sin(\omega s) & 1 & 0 \\ \frac{-\dot{\bar{\varphi}}'(s)}{\omega r(\rho_1)}\cos(\omega s) & \frac{\dot{\bar{\varphi}}'(s)}{\omega^2 r(\rho_1)}\sin(\omega s) & 0 & 1 \end{bmatrix}$$

Defining $M(s,\rho) = DR(\Psi(s,\rho))$, then

$$D_2M(s,0) \cdot \rho = \begin{bmatrix} 0 & 0 & 0 & 0 \\ \frac{-\bar{\varphi}'(s)}{\omega a}\cos(\omega s) & \frac{\bar{\varphi}'(s)}{a\omega^2}\sin(\omega s) & 1 & 0 \\ \frac{-\dot{\bar{\varphi}}'(s)}{\omega a}\cos(\omega s) & \frac{\dot{\bar{\varphi}}'(s)}{a\omega^2}\sin(\omega s) & 0 & 1 \end{bmatrix} \cdot \rho_1$$

$$[D_2 M(s,0)\cdot\rho]\,\alpha'(s) = -\rho_1 \begin{bmatrix} 0 \\ \bar{\varphi}'(s) \\ \dot{\bar{\varphi}}'(s) \end{bmatrix}$$

Finally giving,

$$A_{\mathsf{T}}(s) = \begin{bmatrix} 0 & 0 & 0 \\ -\bar{\varphi}'(s) & 0 & 0 \\ -\dot{\bar{\varphi}}'(s) & 0 & 0 \end{bmatrix} + DR(\Psi(s,0))\cdot D_1 f(\alpha(s),\mu(s))Z(s)$$

$$B_{\mathsf{T}}(s) = DR(\Psi(s,0))\cdot D_2 f(\alpha(s),\mu(s))\ .$$

5.7.3 Regulation of the Transverse Coordinates

As discussed above, using a linear feedback with an index varying gain, $K(s)$, which depends on the index s along the maneuver is sufficient to make the transverse linearization uniformly exponentially stable. To design an index varying gain, we choose to solve the Linear Quadratic Regulator (LQR) problem given by

$$min\frac{1}{2}\int_0^T \|\rho\|_Q^2 + \|v\|_R^2 ds$$

subject to

$$\rho' = A_{\mathsf{T}}(s)\rho + B_{\mathsf{T}}(s)v,\ \ \rho(0) = \rho_0$$

to give a linear state feedback of $v = -K(s)\rho$, where $K(s) = -R^{-1}B_{\mathsf{T}}^T P$. Thus, the maneuver regulation control law may be written as

$$v = \alpha(s) - K(s)\rho(s). \tag{5.24}$$

With the maneuver regulation control law in hand, we simulated and then successfully implemented several trajectories found in Chapter 4. For example, when

$$\theta(t) = \frac{40\pi}{180}\sin(\frac{2\pi}{0.5}t)$$

we solved the two point boundary value problem to find φ and τ as shown in Figures 5.2 and 5.3.

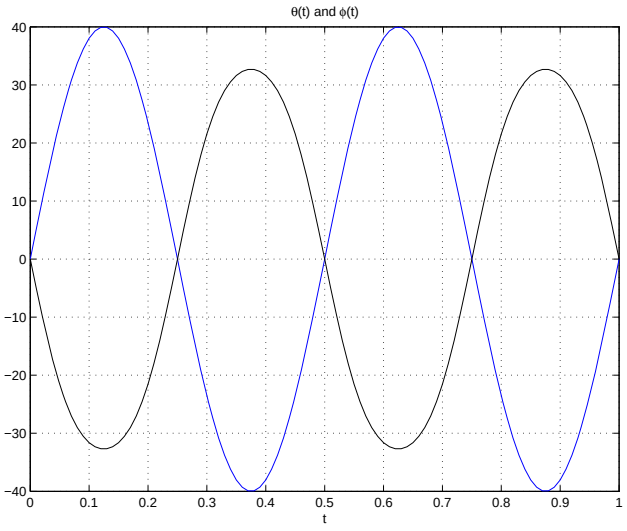


Figure 5.2: Plot of desired θ and φ. The driving function, $\theta(t)$, has an amplitude of 40 degrees and a period $T = 0.5$.

Figures 5.4 - 5.7 show the data collected from the physical system. In figures 5.4 and 5.5 show plots of θ vs $\dot{\theta}$ and φ vs $\dot{\varphi}$. In both plots, the circles represent the desired trajectory and the solid lines representing the data collected from the system. We see from these plots that the tracking is not perfect. The use of the estimator (or "dirty differentiator") contributes to the observed error in regulating the maneuver. In fact, these plots of the physical system data are showing the data collected from the dirty differentiator. In addition to the dirty differentiator, we are not able to effectively command the torque. We know from our experiments with the physical system that there is also a torque map that is slightly different than our model indicates. It is interesting to note that the physical system converges to a periodic maneuver of the system which is slightly perturbed from the desired maneuver.

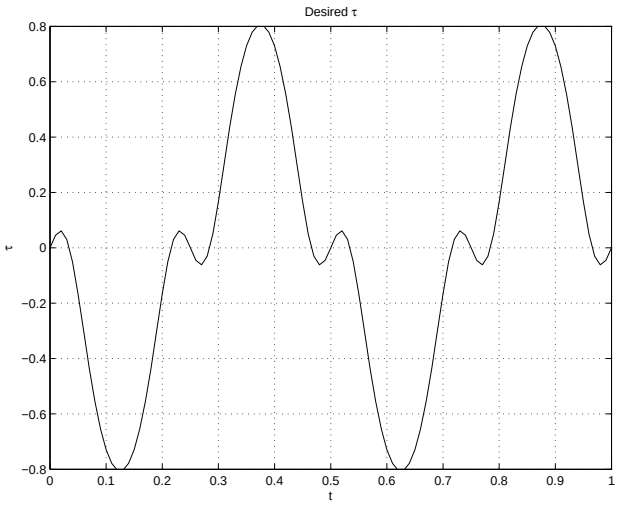


Figure 5.3: Plot of desired τ when a then inner arm of the pendubot is driven by the odd-periodic $\theta(t) = \frac{40\pi}{180}\sin(\frac{2\pi}{0.5}t)$.

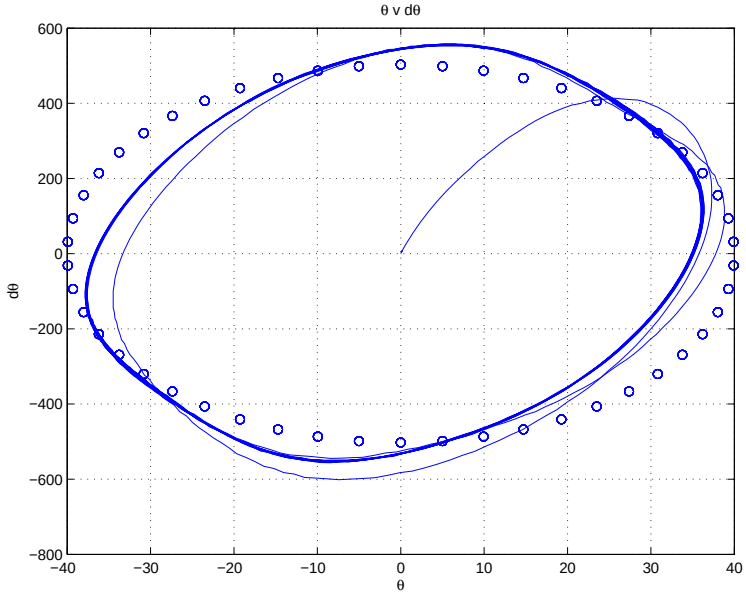


Figure 5.4: Plot of θ vs $\dot{\theta}$ where $\theta(t) = 40\ \pi/180\ \sin 4\pi t$. The circles represent the desired trajectory with solid line representing the data collected from the system.

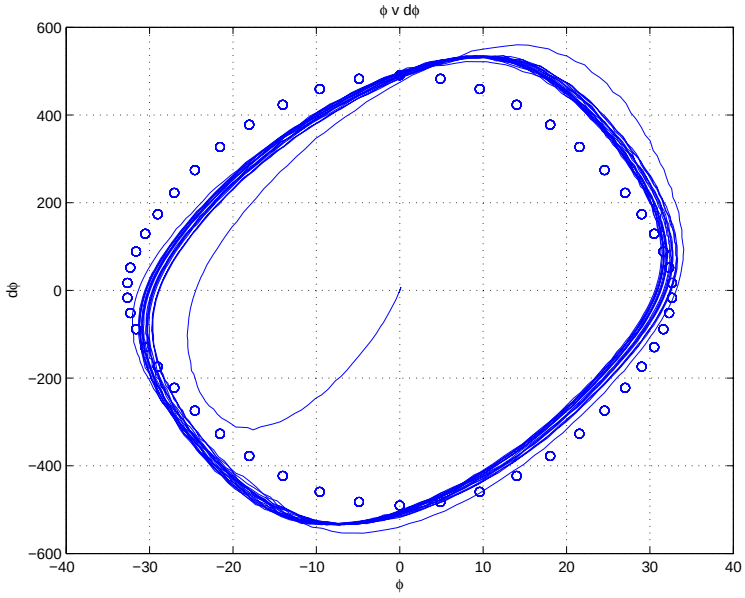


Figure 5.5: Plot of φ vs $\dot{\varphi}$ driven by $\theta(t) = 40\ \pi/180\ \sin 4\pi t$. The circles represent the desired trajectory with solid line representing the data collected from the system.

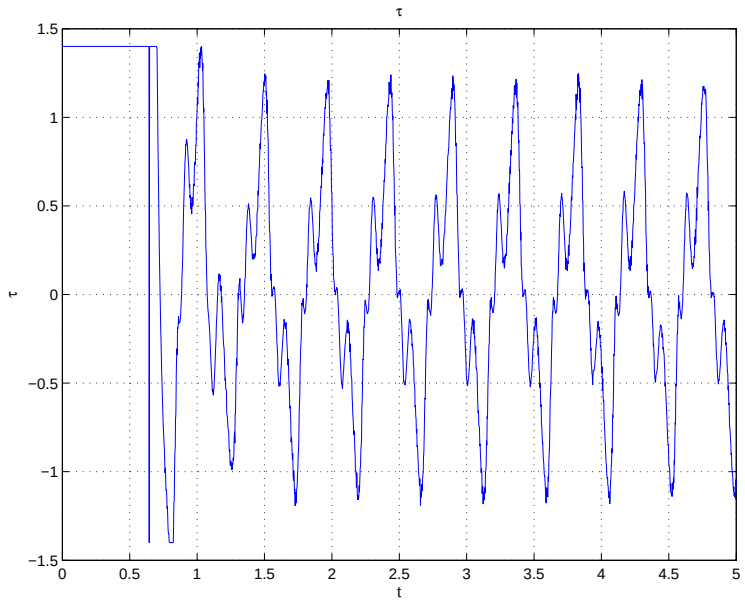


Figure 5.6: Plot of τ collected from physical system with the maneuver regulation controller.

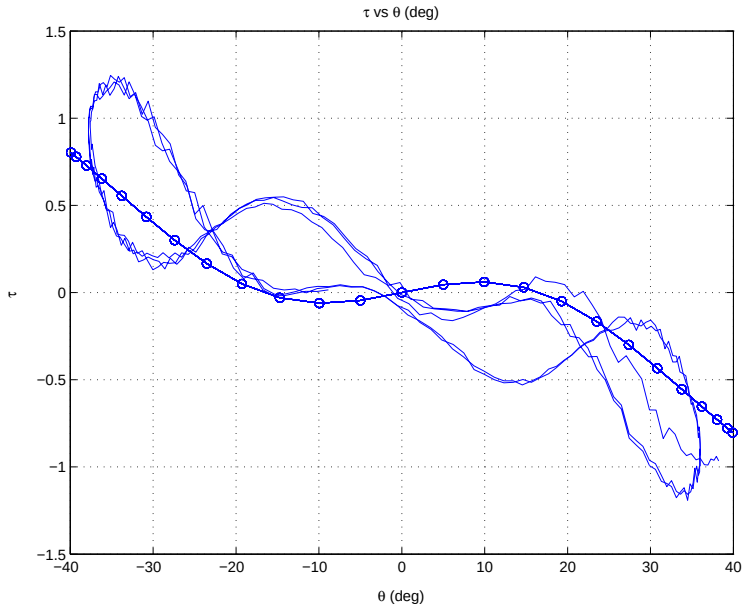


Figure 5.7: Plot of τ vs θ (in degrees). The circles indicate the desired curve while the lines show the τ measured from physical system during the maneuver.

5.8 Maneuver Regulation about Inverted Trajectories

In this section, we design a maneuver regulation controller for an inverted maneuver of the pendubot with a constant inner arm velocity and present some simulation results. In designing the transverse coordinate system for regulating about an inverted trajectory with a constant inner arm velocity, θ is always increasing. So, we let $s = \theta$. We chose the transverse coordinates to be

$$\rho_1 = \dot{\theta} - \dot{\bar{\theta}}(s)$$

$$\rho_2 = \varphi - \bar{\varphi}(s)$$

$$\rho_3 = \dot{\varphi} - \dot{\bar{\varphi}}(s)$$

After computing the transverse linearization, we designed a linear quadratic regulator controller to stabilize the transverse dynamics. The $K(s)$ is shown in Figure 5.8.

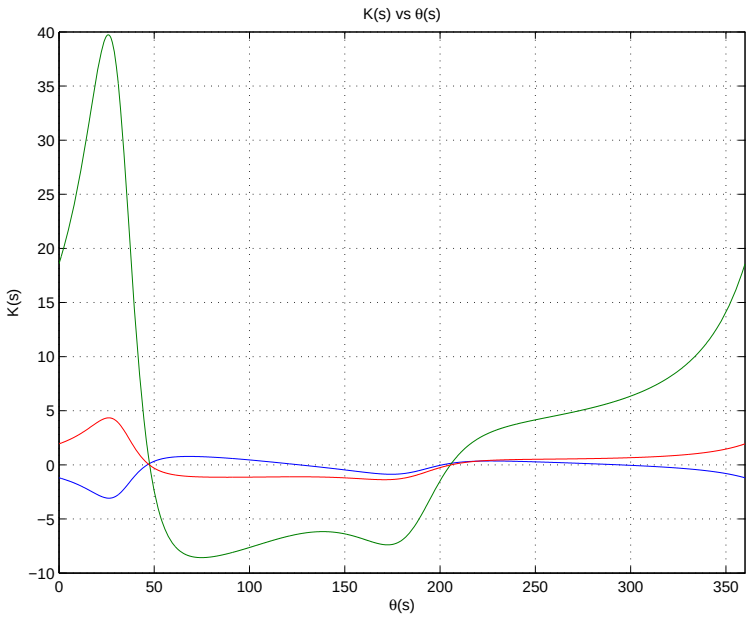


Figure 5.8: Plot of K(s) used for maneuver regulation about an inverted in inverted trajectory of the constant velocity pendubot with period $T = 1.0$.

For an inverted trajectory with a period of $T = 1.0$, the required torque is well within the range of those possible by the physical system. The maximum lean angle of φ is just under 20

degrees. Starting at rest with the inner arm hanging down (i.e., $\theta(0) = 0$) and the outer arm inverted (i.e., $\varphi(0) = 0$) the maneuver regulation controller was able to nicely regulate the system about the maneuver.

Adding the velocity estimators, the system was still able to regulate the system about the maneuver even when starting from rest. Figures 5.9-5.12 show the results of the simulation. We see that within a couple of periods the system has effectively converged to the desired periodic orbit.

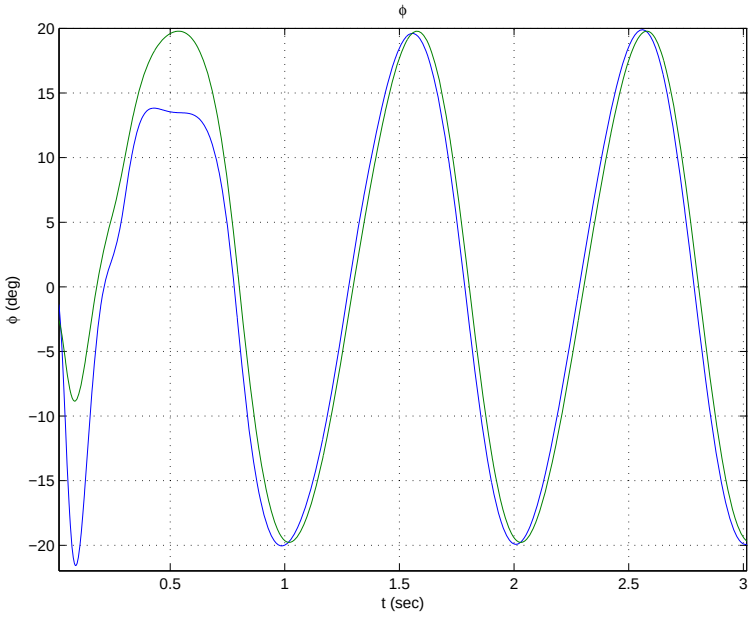


Figure 5.9: Plot of the desired φ and results from a simulation of the inverted trajectory using the maneuver regulation controller with velocity estimation.

While the initial design shows some promise, we haven't been able to successfully implement the controller on the physical system. Unlike the non-inverted trajectories, these desired maneuvers are naturally unstable making the system more unforgiving. We suspect that our ability to effectively command the torque and the torque ripple within the motor as being likely reasons for the current lack of success. The particular motor on the pendubot at CU was not meant for precision position control. To this end, a redesign of the system that includes direct measurements of the velocities and a better motor may be the most helpful. It is possible that a different transverse

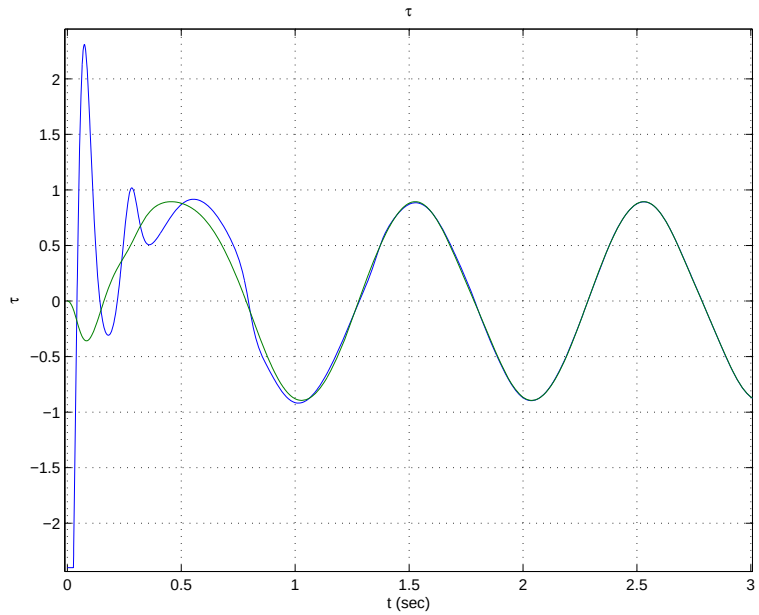


Figure 5.10: Plot of the desired torque and results from a simulation with velocity estimation of an inverted maneuver on the constant velocity pendubot.

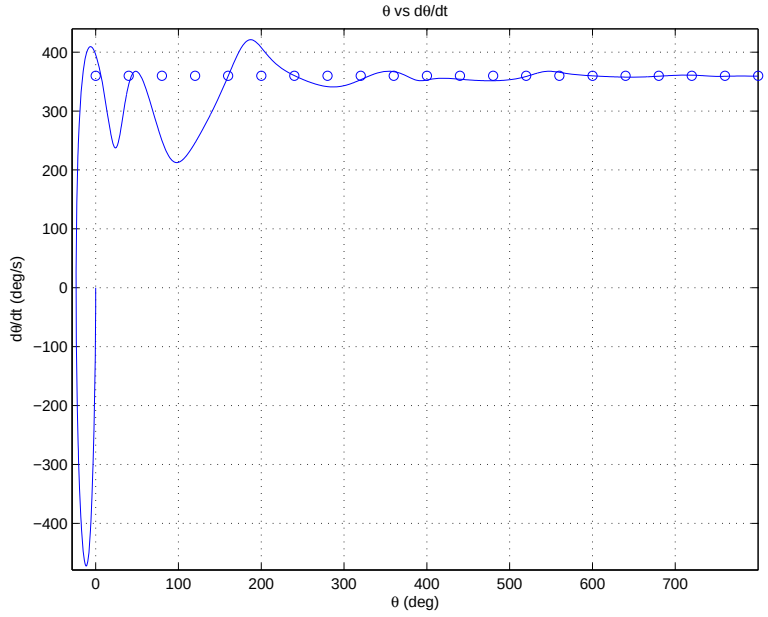


Figure 5.11: Plot of simulation results of θ vs. $d\theta/dt$ of an inverted maneuver on the constant velocity pendubot. The circles show the desired trajectory and the solid line shows the simulation results.

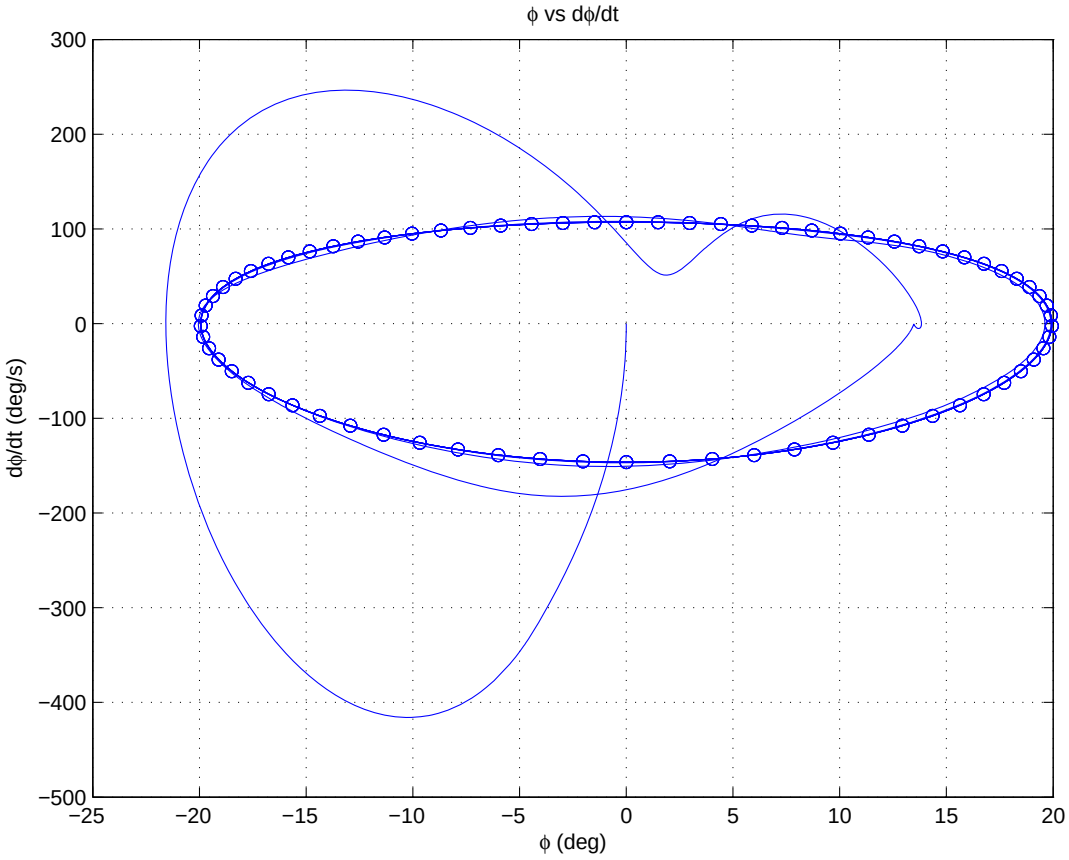


Figure 5.12: Plot of simulation results of φ vs. $d\varphi/dt$ of an inverted maneuver on the constant velocity pendubot. The circles show the desired trajectory and the solid line shows the simulation results.

coordinate system could reduce some of the sensitivities to the unmodelled dynamics.

Chapter 6

Conclusions

In this thesis, we studied equations that described a general driven pendulum. The equations also describe the under-actuated, double pendulum system called the pendubot. We studied both inverted pendulum in Chapter 3 and non-inverted pendulum in Chapter 4. Using the Schauder fixed point theorem, we were able to show that trajectories always exist for a pendubot driving by odd-perioidic forcing in both the inverted and non-inverted cases. We showed various methods for computing the trajectories. With the inverted and non-inverted trajectories in hand, we were able to demonstrate through simulation and/or physical implementation, the usefulness of maneuver regulation for provided orbital stabilization in Chapter 5.

For the inverted configuration, we first wrote the problem as a two point boundary value problem with Dirichlet boundary conditions. Then, we develop an equivalent linear operator $\mathcal{N}_\alpha^\beta$ that combines a Nemitski operator (or superposition operator) with the linear operator for the unstable harmonic oscillator. By exploring the properties of the Green's function for the unstable harmonic oscillator with Dirichlet boundary conditions, we developed bounds on various norms that prove useful for determining which parameter values will satisfy invariance and contraction conditions.

With a direct application of the Schauder fixed point theorem, we showed that equation our family of equations representing an inverted pendulum always possessed an odd periodic solution for all $\alpha > 0$ and $\beta > 0$. Using the Banach fixed point theorem we were able to ensure that there is a unique solution within an invariant region of the space of possible solution curves. When there

is a unique solution, successive approximations can be used to compute the solution trajectory. To illustrate the power and application of these ideas, we apply them to a pendubot with the inner arm moving at a constant velocity.

We then described larger sets on which the invariance and contraction condition are satisfied. In addition, both continuation methods and conjugate point theory were used to explore odd-periodic solutions when the family of equations has parameters that do not satisfy the contraction condition developed. We approximated the eigenvalues of the operator with a series of finite rank operators (matrices). Using these estimates we were able to seed the conjugate point problem to find the real eigenvalues of $D\mathcal{N}_\alpha^\beta$. The effectiveness of all of these techniques in providing useful estimates and in finding solutions was demonstrated in the case of a pendubot (with physically relevant parameters).

For β_{CU}, we have found that all of the eigenvalues of $D\mathcal{N}_\alpha^\beta[\varphi_\alpha(\cdot)]$ have magnitude strictly less than one, indicating that the fixed points $\varphi_\alpha(\cdot)$ are at least locally stable for the nonlinear map. For larger values of β (a longer inner arm), we demonstrated an eigenvalue can pass through -1.0 as T decreases, resulting in a loss of local stability of the map. In that case, the accumulation points of the infinite sequence appear to be fixed points of iterated versions of the map. The effectiveness of all of these methods in providing useful estimates and in finding solutions was demonstrated in the case of a pendubot (with physically relevant parameters) where the odd periodic driving is the result of constant inner arm velocity.

For the non-inverted trajectories of the pendubot, we presented a necessary condition for periodic trajectories to exist. For odd-periodic trajectories this condition is always satisfied. Moreover, for an odd-periodic driving function, an odd-periodic solution always exists even at resonance since the map has a bounded image. For a driving function of $A\sin(\omega t)$, we found multiple solutions for the outer link.

There remain several interesting directions for future research. For example, in this thesis we examined odd-periodic trajectories. An exploration of trajectories that are possible with more general periodic driving of the inner arm would be interesting. A natural extension to the inverted

and hanging trajectories that we examined would be to explore trajectories that switch between a hanging position and inverted position.

The physical implementation of an inverted trajectory would be interesting. To this end, understanding the effect of the choice of transverse coordinates and developing some design strategies for the maneuver regulation controllers may be useful. We also suspect that a redesign of the system may be helpful in this regard since the current motor was not meant for precision control at slow speeds and it was difficult to effectively command the torque. In addition, an analysis of the effect of uncertainties, time delays, quantization, sampling, observer design, and model mismatches would all be beneficial.

Bibliography

[1] J. Mahwin, "Seventy-five years of global analysis around the forced pendulum equation," EquaDiff Proceedings, pp. 115–145, 1997.

[2] K. Furuta and M. Yamakita, "Swing up control of inverted pendulum," In IECON'91, pp. 2193–2198, 1991.

[3] D. Block and M. Spong, "Mechanical design and control of the pendubot," 46th Annual Earthmoving Industry Conference, Peoria, IL, 1995.

[4] M. Spong, "Swing up control of the acrobot," IEEE Control Systems Magazine, Feb. 1995.

[5] N. Getz, "Control of balance for a nonlinear nonholonomic non-minimum phase model of a bicycle," American Control Conference, 1994.

[6] ——, "Dynamic inversion of nonlinear maps with applications to nonlinear control and robotics," Ph.D. dissertation, University of California at Berkeley, 1995.

[7] R. Frezza and A. Beghi, "Simulating a motorcycle driver," in New trends in Nonlinear Dynamics and Control and their Applications, W.Kang, M. Xiao, and C. Borges, Eds. Springer-Verlag, 2003, pp. 175–186.

[8] J. Hauser, A. Saccon, and R. Frezza, "Aggressive motorcycle trajectories," IFAC Symposium on Nonlinear Control Systems, 2004.

[9] A. Saccon, "Maneuver regulation of nonlinear systems: The challenge of motorcycle control," Ph.D. dissertation, Dept. Inf. Eng., Univ. Padova, Padova, Italy, 2006.

[10] Daniel J. Block, "Mechanical design and control of the pendubot," Department of General Engineering University of Illinois at Urbana-Champaign, Urbana, Illinois, 1996.

[11] J. Hauser, S. Sastry, and G. Meyer, "Nonlinear control design for slightly non-minimum phase systems: application to V/STOL aircraft," Automatica, vol. 28, pp. 665–679, 1992.

[12] J. Hauser, A. Saccon, and R. Frezza, "On the driven inverted pendulum," IEEE Conference on Decision and Control, 2005.

[13] R. F. Brown, A Topological Introduction to Nonlinear Analysis, 2nd ed. Boston: Birkhauser, 2004.

[14] S. Devasia and B. Paden, "Stable inversion for nonlinear nonminimum-phase time-varying systems," IEEE Transactions on Automatic Control, vol. 43, pp. 283–288, 1998.

[15] M. W. Spong and D. J. Block, "The pendubot: A mechatronic system for control research and education," Proc. 34th IEEE Conf. Decision Control.

[16] T. Albahkali, R. Mukherjee, T. Das, "Swing-Up Control of the Pendubot: An Impulse Momentum Approach," Robotics, IEEE Transactions on, vol.25, no.4, pp.975-982, Aug. 2009.

[17] I. Fantoni, R. Lozano, and M. W. Spong, "Energy based control of the pendubot," IEEE Trans. Automat. Contr. vol. 45.

[18] Xin Xin, S. Tanaka, Jin-Hua She, and T. Yamasaki, "Revisiting energy-based swing-up control for the Pendubot," Control Applications (CCA), 2010 IEEE International Conference on, vol., no., pp.1576-1581, 8-10 Sept. 2010.

[19] W. Li, K. Tanaka, and H. O. Wang, "Acrobatic control of a pendubot," IEEE Trans Fuzzy Systems, vol. 12, no. 4.

[20] L. Freidovicha, A. Robertssona, A. Shiriaeva, and R. Johansson, "Periodic motions of the pendubot via virtual holonomic constraints: Theory and experiments," Automatica 44.

[21] J. Hauser and R. Hindman, "Maneuver regulation from trajectory tracking: Feedback linearizable systems," In Proc. IFAC Symposium on Non-linear Control Systems Design, Lake Tahoe, CA, USA, pp. 2193–2198, 1995.

[22] A. Banaszuk and J. Hauser, "Feedback linearization of transverse dynamics for periodic orbits," Systems and Control Letters, 26, pp. 95–105, 1995.

[23] B. Francis, "The linear multivariable regulator problem," SIAM Journal of Control and Optimization, vol. 15, 1977.

[24] A. Isidori and C. Byrnes, "Output regulation of nonlinear systems," IEEE Transactions on Automatic Control, vol. 35, no. 2, pp. 131–140, 1990.

[25] Franz, R., and Hauser, J., "Optimization Based Parameter Identification of the Caltech Ducted Fan," American Control Conference, Denver, June, 2003.

[26] Gautier, M., and Khalil, W., "On the Identification of the Inertial Parameters of Robots," Proceedings of 27th IEEE CDC, pp. 2264-2269, 1988.

[27] Zhang and Tarn, "Hybrid control of the pendubot," IEEE-ASME TRANSACTIONS ON MECHATRONICS Volume: 7 Issue: 1.

[28] Cruz-Villar, Alvarez-Gallegos, and Villarreal-Cervantes, "Parametric redesign of the pendubot for vertical positioning in minimum time," REVISTA IBEROAMERICANA DE AUTOMATICA E INFORMATICA INDUSTRIAL Volume: 5 Issue: 1.

[29] M. W. Spong, "Partial feedback linearization of underactuated mechanical systems," In Proceedings of the international conference on intelligent robots and systems.

[30] Spong and Block, "Pendubot user manual," University of Illinois, Urbana-Champaign, IL.

[31] Y. Orlov, L. T. Aguilar, and L. Acho, "Model orbit stabilization (mors) of pendubot with application to swing up control," In Proceedings of the 44th conference decision and control/European control conference, Seville, Spain.

[32] A. S. Shiriaev, O. Kolesnichenko, and L. Paramonov, "How to redistribute energy between different links of the pendubot," In Proceedings of the 15th IFAC World congress, Barcelona, Spain.

[33] J. Alvarez-Gallegos and H. Gonzalez-Hernandez, "Analysis of the dynamics of an underactuated robot: the forced pendubot," Proceedings of the 36th IEEE Conference on Decision and Control, Volume 2.

[34] P. Herman, "A controller of the pendubot using quasi-velocities," Control and Automation, 2008 16th Mediterranean Conference on.

[35] E. B. Davies, Linear Operators and their Spectra, Cambridge University Press, 2007

[36] J. B. Reade, Eigenvalues of Positive Definite Kernels, SIAM J. MATH. ANAL., Vol. 14, No. 1, pp. 152-157, January 1983.

[37] P. M. Anselone, Collectively Compact Operator Approximation Theory and Applications to Integral Equations, Prentice-Hall, 1971.

[38] F. Isabelle and L. Rogelio, "Stabilization of the furuta pendulum around its homoclinic orbit," International Journal of Control, Vol. 75 Issue 6, pp. 390–398, 2002.

[39] K. J. Astrom and K. Furuta, "Swinging up a pendulum by energy control," Automatica, Vol. 36 Issue 2, pp. 287–295, 2000.

[40] K. G. Eltohamy and C. Y. Kou, "Nonlinear optimal control of a triple link inverted pendulum with single control input," International Journal of Control, Vol. 69 Issue 2, pp. 239–256, 1998.

[41] F. Y. Cheng, G. M. Zhong, Y. S. Li, and Z. M. Xu, "Fuzzy control of a double inverted pendulum." Fuzzy Sets and Systems, Vol. 79 Issue 3, pp. 315–321, 1996.

[42] T. Albahkali, R. Mukherjee, and T. Das, "Swing-up control of the pendubot: An impulse–momentum approach," IEEE Transactions on Robotics, To Be Published.

[43] J. Mawhin, "The forced pendulum: A paradigm for nonlinear analysis and dynamical systems," Expo. Math., 6, pp. 271–287, 1998.

[44] J. Mawhin and M. Willem, "Multiple solutions of the periodic boundary value problem for some forced pendulum-type equations," J. Differential Equations 52, pp. 264–287, 1984.

[45] R. Ortega, "Counting periodic solutions of the forced pendulum equation," Nonlinear Analysis Volume 42, Issue 6, pp. 1055–1062, 2000.

[46] ——, "A forced pendulum equation with many periodic solutions," Rocky Mountain J. Math. 27, pp. 861–876, 1997.

[47] M. Berkemeier and R. Fearing, "Tracking fast inverted trajectories of the underactuated acrobot," IEEE TRANSACTIONS ON ROBOTICS AND AUTOMATION Volume: 15 Issue: 4, pp. 740–750, 1999.

[48] C. Kao, A. Megretski, and U. Jonsson, "A cutting plane algorithm for robustness analysis of periodically time-varying systems," IEEE TRANSACTIONS ON AUTOMATIC CONTROL Volume: 46 Issue: 4, pp. 579–592, 2001.

[49] U. Jonsson, C. Kao, and A. Megretski, "Robustness of periodic trajectories," IEEE TRANSACTIONS ON AUTOMATIC CONTROL Volume: 47 Issue: 11, pp. 1842–1856, 2002.

[50] D. Alonso, E. Paolini, and J. Moiola, "Global bifurcation analysis of a controlled underactuated mechanical system," NONLINEAR DYNAMICS Volume: 40 Issue: 3, pp. 205–225, 2005.